

**Development of Specific Electrochemical Sensors
for Detection of a Few Food Additives with a
Portable Measuring Interface**

Thesis submitted

By

Shreya Nag

Doctor of Philosophy (Engineering)

**Department of Instrumentation and Electronics Engineering
Faculty Council of Engineering & Technology
Jadavpur University, Kolkata, India**

2023

JADAVPUR UNIVERSITY

KOLKATA- 700032

INDIA

INDEX NO. D-7/E/88/2020

Title of the Thesis **Development of Specific Electrochemical Sensors
for Detection of a Few Food Additives with a
Portable Measuring Interface**

Name, Designation
& Institution of the
Supervisor

Dr. Runu Banerjee Roy

Professor

*Dept. of Instrumentation and Electronics Engineering
Jadavpur University, Salt Lake Campus, Sector-III,
Block-LB, Plot-8, Kolkata-700106, India.*

Phone: 08240235742

Fax: 03323357254

Papers Published in International Journals

- [1] S. Nag, S. Pradhan, H. Naskar, R. B. Roy, B. Tudu, P. Pramanik, and R. Bandyopadhyay, "A simple nano cerium oxide modified graphite electrode for electrochemical detection of formaldehyde in mushroom," *IEEE Sens. J.*, vol. 21, pp. 12019 – 12026, 2021.
- [2] S. Nag, H. Naskar, S. Pradhan, R. Chatterjee, V. Sharma, B. Tudu and R. B. Roy, "Formalin Detection using Platinum Electrode-Based Electrochemical System", *Journal of The Institution of Engineers (India): Series B*, vol. 103, pp. 1159-1165, 2022.
- [3] S. Nag, S. Pradhan, D. Das, B. Tudu, R. Bandyopadhyay, and R. B. Roy, "Fabrication of A Molecular Imprinted Polyacrylonitrile Engraved Graphite Electrode for Detection of Formalin in Food Extracts," *IEEE Sens. J.*, vol. 22, pp. 42–49, 2022.
- [4] S. Nag, D. Das, H. Naskar, B. Tudu, R. Bandyopadhyay, and R. B. Roy, "Detection of Metanil Yellow Adulteration in Turmeric Powder Using Nano Nickel Cobalt Oxide Modified Graphite Electrode," *IEEE Sens. J.*, vol.22, pp. 12515-12521, 2022.
- [5] S. Nag, D. Das, and R. B. Roy, "Voltammetry application of molecularly imprinted polyacrylamide as vanillin receptor in desserts," *IEEE Sens. J.*, vol.23, 3446-3452, 2023.
- [6] S. Nag, D. Das, H. Naskar, B. Tudu, R. Bandyopadhyay, and R. B. Roy, "A Novel Molecular Imprinted Polymethacrylic Acid Decorated Graphite Electrochemical Sensor for Analyzing Metanil Yellow Adulteration in Food," *IEEE Sens. J.*, vol.23, pp. 20951-20958, 2023.

Papers Published in International Conference Proceedings

- [1] S. Nag, D. Das, S. Bhowmik, B. Tudu, R. Bandyopadhyay and R. B. Roy, "An assessment of Metanil Yellow Adulteration in Pigeon Pea using NIR Spectroscopy," 2022 IEEE Second International Conference on Emerging Technologies (ICEFEET), August 2022.
- [2] S. Nag, D. Das, B. Tudu and R. B. Roy, "Multivariate Analysis of Formalin Using UV-Vis Spectroscopy," 2021 IEEE Second International Conference on Control, Measurement and Instrumentation (CMI), pp. 133-137, 2021.

- [3] S. Nag, D. Das, H. Naskar, R. B. Roy, B. Tudu and R. Bandyopadhyay, "Estimation of Theophylline in Black Tea Using NIR Spectroscopy," 2020 International Conference on Emerging Frontiers in Electrical and Electronic Technologies (ICEFEET), pp. 1-3, 2020.
- [4] S. Nag, R. Chatterjee, V. Sharma, R. Banerjee Roy, B. Tudu, and R. Bandyopadhyay, "Electrochemical Detection of Formalin using Carbon Paste Electrode," MSSND, 2019

List of Patent Published

- [1] "A novel molecular imprinted polymer based electrochemical sensor for the selective and sensitive detection of metanil yellow adulteration in food," Shreya Nag, Debangana Das, Hemanta Naskar, Runu Banerjee Roy, Bipan Tudu, Rajib Bandyopadhyay, Application no. 202231071419, 2022.

List of Presentations at International Conferences/ Workshops

- [1] 2022 IEEE Second International Conference on Emerging Technologies (ICEFEET), August 2022
- [2] 2021 IEEE Second International Conference on Control, Measurement, and Instrumentation (CMI), 2021
- [3] 2020 International Conference on Emerging Frontiers in Electrical and Electronic Technologies (ICEFEET)
- [4] MSSND, 2019
- [5] UEMCOS, 2020 (Best paper)

List of Book Chapter Published

- [1] S. Nag, D. Das, and R. B. Roy, "Assay of Molecular Imprinted Polymers as Food Additive Detectors," Impactful Technologies Transforming the Food Industry, pp. 255-267, IGI Global, 2023.

Other Publications in International Journals

- [1] D. Das, S. Nag, S. De, A. Hazarika, S. Sabhapondit, B. Tudu, R. Bandopadhyay, P. Pramanik and R. B. Roy, "Electrochemical Detection of Epicatechin in Green Tea Using Quercetin-Imprinted Polymer Graphite Electrode," *IEEE Sensors Journal*, vol. 21, no. 23, pp. 26526-26533, 2021.
- [2] D. Das, S. Nag, S. Acharya, S. Barik, S. Sabhapondit, B. Tudu, R. Bandopadhyay, and R. B. Roy, "Discrimination of Tea using Caffeine-Sensitive Sensor by Employing different Classifiers and various Data Analysis Techniques", *Journal of The Institution of Engineers (India): Series B*, vol. 102, no. 5, pp. 939–946, 2021.
- [3] D. Das, S. Nag, A. Adval, A. Hazarika, S. Sabhapondit, A. R. Bhattacharya, B. Tudu, R. Bandopadhyay, and R. B. Roy, "Amine Functionalized MWCNTs Modified MIP- based Electrode for Detection of Epicatechin in Tea," in *IEEE Sensors Journal*, vol.22, pp.10323 – 10330, 2022
- [4] S. Roy, S. Nag, M. Bhattacharyya Banerjee, S. Dasgupta, P. Pramanik, and R. Bandyopadhyay, "Detection of Geraniol in Palmarosa Essential oil using Silicone Sealant as molecularly imprinted polymer in a QCM sensor", *Journal of Materials NanoScience*, vol. 9, 120–124, 2022.
- [5] D. Bandyopadhyay, S. Nag, D. Das, S. Acharya, B. Tudu, P. Pramanik, R. Bandyopadhyay and R. B. Roy, "Voltammetric Detection of Inositol Using a Platinum Based Electrode", *Nano LIFE*, vol. 12, pp. 2250004, 2022.

Other Publications in International Conference Proceedings

- [1] D. Das, S. Nag, U. Saha, B. Tudu and R. B. Roy, "Development of Molecularly Engraved Polymer Based Sensor for Detection of Theobromine in Tea," 2021 IEEE Second International Conference on Control, Measurement and Instrumentation (CMI), pp. 144-148, 2021.
- [2] D. Das, S. Nag, H. Naskar, A. K. Hazarika, R. B. Roy, S. Sabhapondit, B. Tudu, and R. Bandyopadhyay "Discrimination of Various Clones of Black Tea Using NIR Spectroscopy," 2020 International Conference on Emerging Frontiers in Electrical and Electronic Technologies (ICEFEET), pp. 1-3, 2020.
- [3] H. Naskar, S. S. Ali, A.H.M. Toufique Ahmed, D. Das S. Nag and Tudu, B. Tudu, R. Bandyopadhyay, "Detection of Curcumin using a Simple and Sensitive Molecularly Imprinted Polymer (MIP) Embedded Graphite Electrode Based Electrochemical Sensor," 2020 International Conference on Emerging Frontiers in Electrical and Electronic Technologies (ICEFEET), pp. 1-4, 2020.
- [4] J. Dei, H. Naskar, S. Dasgupta, S. Nag, B. Behera, B. Tudu, R. B. Roy, and R. Bandyopadhyay, "Fish Freshness Assessment using NIR spectroscopy," 2020 International Conference on Emerging Frontiers in Electrical and Electronic Technologies (ICEFEET), 2020,

pp. 1-3, doi: 10.1109/ICEFEET49149.2020.9187016.

[5] D. Bandyopadhyay; S. Nag; R. B. Roy, Quantification of Syringic Acid in Real Samples Based on UV-Vis Spectroscopy; 2022 IEEE Silchar Subsection Conference (SILCON); 31st January 2023. M, Moulick, S. Nag, D. Das, B. Tudu, R. Bandyopadhyay and R. B. Roy, "Detection of Tannic Acid using Nd₂O₃ Modified Graphite Electrode," 2022 IEEE Second International Conference on Emerging Technologies (ICEFEET), August 2022.

[6] A.H.M. Toufique Ahmed; S. Nag, D. Das, H. Naskar, R. B. Roy, R. Bandyopadhyay; Bipan Tudu, "Detection of Andrographolide Using Platinum Electrode Based Electrochemical System," 2022 IEEE Second International Conference on Emerging Technologies (ICEFEET), August 2022.

[7] S. Banerjee, H. Naskar, B. Ghatak, S. Banerjee, S. Nag, D. Das, R. B. Roy, N. Das, B. Tudu, R. Bandyopadhyay, "Sensitive Electrochemical Detection of Carvacrol using Carbon Paste Electrode," 2022 IEEE Second International Conference on Emerging Technologies (ICEFEET), August 2022.

[8] S. Dasgupta, S. Nag, R. B. Roy, R. Bandyopadhyay, B. Tudu, "Malachite Green Detection Using Carbon Paste Electrode Based on Voltammetry," 2022 IEEE Second International Conference on Emerging Technologies (ICEFEET), August 2022.

Other Patent Filed

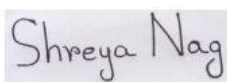
[1] "A formulation of eco e-paint for flexible electronics," Application no. 202231044198, 2022

Statement of Originality

I, Shreya Nag, registered on 3rd March, 2020 do hereby declare that this thesis entitled “Development of Specific Electrochemical Sensors for Detection of a Few Food Additives with a Portable Measuring Interface” contains a literature survey and original research work done by the undersigned candidate as part of Doctoral studies.

All information in this thesis has been obtained and presented in accordance with existing academic rules and ethical conduct. I declare that, as required by these rules and conduct, I have fully cited and referred all materials and results that are not original to this work.

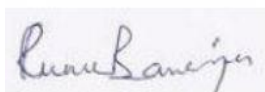
I also declare that I have checked this thesis as per the “Policy on Anti Plagiarism, Jadavpur University, 2019”, and the level of similarity as checked by iThenticate software is 7 %.



Shreya Nag

Index No. D-7/E/88/2020

Date: 24, February, 2023



Professor
Dept. of Instrumentation & Electronics Engg
Jadavpur University
Saltlake, 2nd Campus
Kolkata-700 106

Prof. Runu Banerjee Roy

Professor

*Dept. of Instrumentation
And Electronics Engineering*

Jadavpur University, Salt

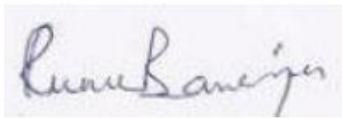
Lake Campus, Kolkata-

700106. India

Certificate from the Supervisor

Date: 24.02.2023

This is to certify that the thesis entitled “Development of Specific Electrochemical Sensors for Detection of a Few Food Additives with a Portable Measuring Interface” submitted by Shreya Nag, who got her name registered on 3rd March 2020 for the award of Ph.D. (Engineering) degree of Jadavpur University, is absolutely based upon her own work under the supervision of Prof. Runu Banerjee Roy, and that neither her thesis nor any part of the thesis has been submitted for any degree/diploma or any other academic award anywhere before.



Professor
Dept. of Instrumentation & Electronics Engg
Jadavpur University
Saltlake, 2nd Campus
Kolkata-700 106

Prof. Runu Banerjee Roy
Professor
Dept. of Instrumentation
And Electronics Engineering
Jadavpur University, Salt
Lake Campus, Kolkata-
700106. India

विद्या प्रशस्यते लोकैः विद्या सर्वत्र गौरवा ।
विद्यया लभते सर्वं विद्वान सर्वत्र पूज्यते ।।

Knowledge is extolled by everyone, knowledge is considered great everywhere, one can attain everything with the help of knowledge, and the person is respected everywhere.

This thesis is dedicated to my parents

Sri Sudhindranath Nag and Smt. Chandra Nag

For their endless love, support, and encouragement

Acknowledgements

It all started with the realization that in order to have a successful career as a researcher, I need a PhD degree! I would like to acknowledge the invaluable contributions and indispensable advice of those individuals who have inspired me on my journey towards doctorate of philosophy. I express my gratitude to the State Government Research Scheme, Jadavpur University for providing a Senior Research Fellowship. As a student at this university, I have been extremely fortunate to have access to the facilities and infrastructure provided by the Department of Instrumentation and Electronics Engineering (IEE), Jadavpur University.

I express a deep sense of gratitude to my supervisor Prof. Runu Banerjee Roy, for her unwavering motivation, assistance, and support in conducting the research. It is with great gratitude that I am writing to express my sincere thanks to Prof. Rajib Bandyopadhyay and Prof. Bipan Tudu of the Department of Instrumentation & Electronic Engineering at Jadavpur University for their immense support throughout the process. A friendly environment was provided to meet their expectations. My thesis was beautifully crafted by their great patience and flexibility in choosing research areas. I would like to offer my heartfelt appreciation for their firm integration. I pray for their blessings to pursue my ambitions even further.

I owe a great deal of gratitude to Dr. Panchanan Pramanik, retired professor from the Department of Chemistry at IIT Kharagpur, who helped me with my research, particularly the chemistry-related work for my thesis.

I sincerely thank the following for their technical assistance: Dr. Dipankar Mandal, Institute of Nano Science and Technology, Mohali, FTIR analysis; Dr. Ramdhan Majhi, Indian Institute of Chemical Biology, Kolkata, HPLC analysis; Department of Physics, Jadavpur University, Kolkata, FESEM and FTIR analysis; UGC DAE Consortium, Kolkata Centre for XRD amenities. The IEE department's technical and non-technical employees gave me invaluable assistance in conducting my study. I want to express my sincere appreciation in particular to Mrs. Ruma De, who was never far away when I needed her.

I want to express my appreciation and thanks to all of my seniors, contemporary lab mates, and juniors Mrs. Susmita Pradhan, Ms. Debangana Das, Mrs. Mahuya Bhattacharya, Mrs. Samhita

Dasgupta, Mrs. Madhurima Moulick, Ms. Swatilekha Roy, Mr. Hemanta Naskar, Mr. Sourav Bagchi, Mr. Diganta Mondal, Mr. Nilabha Debabhuti, Mr. Dipan Bandyopadhyay, Mr. Srikanta Acharya, Mr. Deepam Ganguly, technical and non-technical staff in the Instrumentation & Electronics Engineering department of Jadavpur University, Dr. Sudip Biswas, Postdoctoral Associate, Yangzhou City, Jiangsu, China, the faculty members, for their help whenever I needed it.

I would also like to extend my sincere thanks to Prof. Subhajit Chatterjee, University of Engineering and Management Kolkata, who has showered his unconditional support during this study endeavor. The adage that having a supportive family is essential for success is undoubtedly true. God is to be praised for giving me such a supportive family. I want to express my gratitude to my parents for their support throughout all of my difficult times and for having faith in my talents. I also wish to thank my grandmother Mrs. Bimala Nandi for encouraging me in every way she could.

Abstract

Food has always been the primary source of nourishment at all times. Given the significance of consuming food that is safe, we must assure adequate quality to achieve the goal. Unfortunately, very few measures are taken in the food quality evaluation business to preserve quality at that. As a result, it is absolutely necessary to establish approaches for estimating the quality of food items. The goal of this thesis study is to rapidly detect some food additives that serve as quality attributes and health concerns. In this thesis, three distinct food additives formalin (FAL), metanil yellow (MY), and vanillin (VNL) have been selected as targets analytes. Metal oxides, and molecularly imprinted polymer (MIP) based electrodes are presented to explain the selective determination of FAL, MY, and VNL. With the support of Fourier transform infrared (FTIR) spectroscope, a field emission scanning electron microscope (FESEM), and an ultraviolet visible (UV-Vis.) spectroscope, characterization of the molecule size, intermediary varieties, and morphological characteristics of the imprinted electrodes were reported. Firstly, an electrochemical sensor system has been implemented as a novel and simple approach for food preservative formalin detection. In the proposed work, a low cost, rapid electrochemical detection system of formalin (FAL) using a platinum (Pt) working electrode has been fabricated. The electrochemical performances were recorded using a three-electrode system and a potentiostat device. The responses obtained have been analyzed by means of voltammetry along with chemometrics. Next, a rare earth metal cerium oxide nanoparticle-modified graphite electrode ($\text{CeO}_2\text{@GP}$) has been prepared for electrochemical detection of formalin (FAL) in mushrooms. The prepared electrode provided a wide linear range of 25 μM -1 mM with a low detection limit of 1 μM . The next work has been intended to discuss the synthesis of MIP electrode dedicated for the detection of noxious food additive FAL. The electrode studied in this work exhibited a wide linearity range from 10 μM to 1000 μM with a limit of detection of 0.63 μM under optimized experimental conditions. In addition, the electrode has been applied to study the FAL content in real food extracts like mushroom and fish with accuracy compared to the reference HPLC method. In the second study, electrochemical detection of food colour metanil yellow (MY) in turmeric powder samples using nickel cobalt oxide (NiCo_2O_4) nano crystallites cast over graphite paste has been demonstrated. An electrode made of nickel cobalt oxide modified graphite paste ($\text{NiCo}_2\text{O}_4\text{@GP}$) demonstrated excellent electrochemical performance and a wide linear characterization range.

Next a sensitive, specific, and accurate molecular imprinted polymer based electrode with an electrochemically induced approach for detecting MY, was developed and is next presented. The sensor also excelled in terms of lower detection limit 0.67 nM for MY with a wide linear range 1 nM to 1000 μ M. In addition, MIP analysis efficiently detected the different quantities of MY in real turmeric powder and pigeon pea samples and the responses were validated with the results from HPLC analysis. The third study includes an electrochemical approach to detect and measure food flavour vanillin (VNL) in food using graphite paste electrodes decorated with molecularly imprinted polymer. The electrodes were studied using differential pulse voltammetry (DPV) and cyclic voltammetry (CV). Additionally, the performance of the developed sensor was studied in real samples for VNL trace discrimination. In the end, recently an approach toward the development of a low-cost, portable food quality assessment device has been developed based on App-based display. The system is capable to detect specific target analytes in food and beverage samples. The system comprises of Arduino UNO-based function generator (1KHz in our system) with a signal conditioning unit, a potentiostat circuit, Arduino Nano-based output response sampler, a data acquisition, and a display through a user interface.

Contents

List of publications	v
Certificate of supervisor	xi
Acknowledgements	xv
Abstract	xvii
List of figures	xxv
List of tables	xxxii
List of abbreviations	xxxiii
Chapter 1: Introduction and scope of the thesis	1-36
1.1. Introduction	3
1.2. Electrochemical techniques	6
1.2.1. Types of electrochemical techniques	7
a) Coulometry	7
b) Potentiometry	8
c) Voltammetry	8
i) Linear sweep voltammetry (LSV)	11
ii) Cyclic voltammetry (CV)	11
iii) Pulse voltammetry (PV)	12
Normal pulse voltammetry (NPV)	12
Differential pulse voltammetry (DPV)	13
Square wave voltammetry (SWV)	13
iv) Stripping voltammetry (SV)	14
1.3. Molecular imprinted polymer (MIP) technique	14
1.3.1. Types of imprinting techniques	16
1.3.1.1 Covalent imprinting	16
a) Imprinting with readily reversible covalent bond	17
b) Covalent imprinting with boronate esters	17
c) Covalent imprinting with Schiff's bases	18
d) Covalent imprinting with acetals and ketals	18
1.3.1.2. Non-covalent imprinting	18
a) Non-covalent imprinting with a single functional monomer	19
b) Non-covalent imprinting with combination of monomers	20
1.3.1.3. Semicovalent imprinting	21
1.3.1.4. Imprinting with sacrificial spacers	21
1.4. Literature survey on MIP based sensors	22
1.5. Objectives and scope	26
References	29

Chapter 2: Fabrication of electrochemical sensors towards the detection of food preservative: Formalin **37-84**

2.1. Introduction	39
2.2. Formalin detection using platinum electrode-based electrochemical System	40
2.2.1. Experimental	41
2.2.1.1. Chemicals and reagents	41
2.2.1.2. Apparatus and Instruments	41
2.2.1.3. Experimental set-up	41
2.2.1.4. Data analysis	42
2.2.2. Results and Discussions	42
2.2.2.1. Electrochemical behaviour of Pt working electrode	42
2.2.2.2. Outcome for different scan rate variation	43
2.2.2.3. Effect of concentration variation	44
2.2.2.4. Principal component analysis	44
2.2.2.5. Partial least square regression (PLSR)	45
2.2.2.6. Principal component regression (PCR)	46
2.2.3. Summary	47
2.3. Development of cerium oxide nanoparticles decorated graphite paste electrode for formaldehyde detection in mushroom	47
2.3.1. Experimental process	49
2.3.1.1. Chemical and reagents	49
2.3.1.2. Synthesis of cerium oxide nanoparticles	49
2.3.1.3. Characterization techniques	50
2.3.1.4. Fabrication of CeO ₂ @GP electrode	51
2.3.1.5. Real sample preparation	51
2.3.2. Results and discussion	51
2.3.2.1. Study of X-ray diffraction characteristics of CeO ₂	51
2.3.2.2. Study of TEM analysis of CeO ₂	52
2.3.2.3. Electrocatalytic behaviour of CeO ₂ @GP electrode	53
2.3.2.4. Influence of scan rate variation	54
2.3.2.5. Determination of formalin	56
2.3.2.6. Study of repeatability, reproducibility, and stability	58
2.3.2.7. Interference study	60
2.3.2.8. Investigation of real sample	60
2.3.3. Summary	61
2.4. Fabrication of a molecular imprinted polyacrylonitrile engraved graphite electrode for detection of formalin in food extracts	62
2.4.1. Experimental	64
2.4.1.1. Reagents and standards	64
2.4.1.2. Methods and measurement	64
2.4.1.3. Synthesis of molecular imprinted polymer	64
2.4.1.4. Fabrication of electrode	65
2.4.1.5. Real sample analysis	65
2.4.2. Results and discussion	66
2.4.2.1. Monomer optimization	66
2.4.2.2. Characterization of the synthesized material	66

1. FTIR analysis	66
2. UV-Vis spectroscopy	67
2.4.2.3. SEM measurements	68
2.4.2.4. Detection principle of FAL using MiPAN@GP	68
2.4.2.5. Electrochemical performance of MiPAN@GP electrode	69
2.4.2.6. Effect of scan rate variation	70
2.4.2.7. Calibration curve and detection limit	71
2.4.2.8. Study of repeatability, reproducibility, and stability	73
2.4.2.9. Interference and Selectivity Study	74
2.4.2.10. Detection of FAL in real samples	75
2.4.3. Summary	76
2.5. Conclusion	77
References	78

Chapter 3: Fabrication of electrochemical sensors towards the detection of food colourant: Metanil Yellow **85-116**

3.1. Introduction	87
3.2. Detection of metanil yellow adulteration in turmeric powder using nano nickel cobalt oxide modified graphite electrode	88
3.2.1. Experimental	89
3.2.1.1. Chemicals and reagents	89
3.2.1.2. Synthesis of nickel-cobalt oxide nanoparticles	89
3.2.1.3. Characterization techniques	89
3.2.1.4. Fabrication of NiCo ₂ O ₄ @GP electrode	90
3.2.2. Results and discussion	90
3.2.2.1. Study of X-ray diffraction characteristics of NiCo ₂ O ₄	90
3.2.2.2. Study of SEM analysis of NiCo ₂ O ₄	91
3.2.2.3. Study of FTIR analysis of NiCo ₂ O ₄	91
3.2.2.4. Electrocatalytic behaviour of NiCo ₂ O ₄ @GP electrode	92
3.2.2.5. Influence of scan rate variation	94
3.2.2.6. Determination of metanil yellow	95
3.2.2.7. Study of repeatability, reproducibility, and stability	96
3.2.2.8. Study of selectivity	97
3.2.2.9. Investigation of real sample	98
3.2.3. Summary	99
3.3. A novel molecular imprinted polymethacrylic acid decorated graphite electrochemical sensor for analyzing metanil yellow adulteration in food	99
3.3.1. Experimental	101
3.3.1.1. Reagents and standards	101
3.3.1.2. Methods and measurement	101
3.3.1.3. Synthesis of molecular imprinted polymer	101
3.3.1.4. Fabrication of electrode	102
3.3.2. Results and discussion	102
3.3.2.1. Monomer optimization	102
3.3.2.2. Characterization of the synthesized material	103
1. FTIR analysis	103

2. UV-Vis spectroscopy	103
3.3.2.3. SEM measurements	104
3.3.2.4. Electrochemical performance of MIP electrode	104
3.3.2.5. Effect of scan rate variation	106
3.3.2.6. Calibration curve and detection limit	107
3.3.2.7. Study of repeatability, reproducibility and stability	109
3.3.2.8. Interference study	110
3.3.2.9. Detection of MY in real samples	110
3.3.3. Summary	111
3.5. Conclusion	112
References	113

Chapter 4: Fabrication of electrochemical sensors towards the detection of food flavourant: Vanillin **117-134**

4.1. Introduction	
4.2. Voltammetry application of molecularly imprinted polyacrylamide as vanillin receptor in desserts	119
4.2.1. Experimental	121
4.2.1.1. Chemicals and reagents	121
4.2.1.2. Apparatus and techniques	121
4.2.1.3. Synthesis of molecular imprinted polymer	122
4.2.1.4. Fabrication of electrode	122
4.2.1.5. Real sample analysis	122
4.2.2. Results and discussion	123
4.2.2.1. Monomer optimization	123
4.2.2.2. Material characterization	123
4.2.2.3. SEM measurements	125
4.2.2.4. Electrochemical performance of MIPAM/GP electrode	125
4.2.2.5. Effect of scan rate variation	126
4.2.2.6. Calibration curve and detection limit	127
4.2.2.7. Repeatability, reproducibility, and stability analysis	129
4.2.2.8. Interference and selectivity study	129
4.2.2.9. Detection of VNL in real samples	130
4.3. Conclusion	131
References	132

Chapter 5: Towards the development of an App based low cost, portable food quality assessment device **135-146**

5.1. Background of the work	137
5.2. Objective of the work	138
5.2.1. Illustration of hardware	138
5.2.1.1. Function generator and filter circuit	138
5.2.1.2. Potentiostat circuit	139
5.2.1.3. Response sampler	140
5.2.1.4. Control, user interface	143
5.3. Brief description of the device	144

5.4. Summary	145
References	146
Chapter 6: Conclusions and future scopes	147-155
6.1. Introduction	149
6.2. Summary of findings	150
6.3. Recommendations	153
6.4. Future scopes of research	153
6.5. Conclusion	154
References	155

List of figures

Figure No.	Figure Caption	Page No.
Fig. 1.1.	Voltammetric setups for a configuration with three electrodes	9
Fig. 1.2.	(a) Connections on the Auto Lab PGSTAT101 cell wires that correlate to the correct colour codes; (b) A diagram showing the three-electrode configuration	10
Fig. 1.3.	An electrical potentiostat's basic circuitry	10
Fig. 1.4.	(a) Waveform for cyclic voltammetry; (b) Parameters for a reversible reaction is shown on a typical cyclic voltammogram	12
Fig. 1.5.	(a) Differential pulse voltammetry's excitation potential waveform; (b) A common differential pulse voltammetry	13
Fig. 1.6.	The schematic of a basic MIP process	15
Fig. 1.7.	Schematic explaining the covalent imprinting process	17
Fig. 1.8.	Schematic explaining the mechanism of non covalent imprinting	19
Fig.2.1.	An illustration of the experimental setup.	42
Fig. 2.2.	CV outcome of working electrode (Pt) with and without FAL in 0.1 M NaOH.	43
Fig.2.3.	(a) CV outcome of varying peak current with different scan rate from 10 to 100 mV/s, (b) linear regression scheme of peak current vs. scan rate in 0.1M NaOH.	43
Fig. 2.4.	DPV outcome for formaldehyde by means of Pt electrode within 0.1 M NaOH. (a)100-1000 μ M.(b) Linear regression plot for peak current vs. different concentration.	44
Fig. 2.5.	Graphical illustration of DPV response analysis by PCA.	45
Fig. 2.6.	Schematic of CeO ₂ nanoparticles synthesis, electrode fabrication, and measurement using three electrode set-up.	49
Fig. 2.7.	Effect of various electrolyte compositions and pH over DPV measurements at the CeO ₂ @GP electrode.	51
Fig. 2.8.	X-ray diffraction pattern of synthesized CeO ₂ nano crystallites.	52

Fig. 2.9.	(a)TEM image; the inset shows the particle size distribution graph and (b)SAED pattern of synthesized CeO ₂ nanoparticle.	53
Fig. 2.10.	CV response of CeO ₂ @GP electrode in 0.1 M NaOH (a) with and without FAL (b) comparative performance with bare GP.	54
Fig. 2.11.	CV response of CeO ₂ @GP electrode in 0.1 M NaOH (a) variation of peak current with scan rate variation (b) linear plot of peak current vs scan rate (c) maximum peak potential vs log of scan rate.	55
Fig. 2.12.	DPV measurements for FAL using CeO ₂ @GP electrode in 0.1 M NaOH (a) Concentration variation of 25, 50, 120, 300, 500, 700, 900, 1000 μM (b) linear plot of peak current vs concentration.	57
Fig. 2.13.	DPV measurements of the CeO ₂ @GP electrode in 0.1 M NaOH (a) five consecutive measurements in 50 μM FAL (b) in 400 μM FAL (c) five electrode response in 50 μM FAL (d) in 400 μM FAL.	59
Fig. 2.14.	DPV measurements of the CeO ₂ @GP electrode in 0.1 M NaOH (a) Four measurements over a period of 1 month in 50 μM FAL (b) in 400 μM FAL (c) bar graph with peak current measure in 50 μM FAL (d) in 400 μM FAL.	59
Fig. 2.15.	Influence of interferences to voltammetry peak current responses of 50 μM FA in 0.1 M NaOH with the relative signal changes at the CeO ₂ @GP electrode.	60
Fig. 2.16.	Schematic representation of MiPAN@GP synthesis to evaluate the electrode responses to FAL in mushroom.	63
Fig. 2.17.	CV response of different monomers in the presence of 0.1M NaOH.	66
Fig. 2.18.	FTIR spectra of MIP (a) before template extraction (b) after template extraction.	67
Fig. 2.19.	UV-Vis spectra of MIP before and after template extraction.	67
Fig. 2.20.	SEM images of (a) MIP (b) NIP synthesized material.	68
Fig. 2.21.	The detection principle of FAL using MiPAN@GP electrode.	68
Fig. 2.22.	CV response of MiPAN@GP electrode and NiPAN@GP electrode in 0.1M NaOH.	69
Fig. 2.23.	(a) Effect of various electrolyte compositions (b) effect of FAL presence over DPV measurements at the MiPAN@GP electrode.	70
Fig. 2.24.	CV response of MiPAN@GP electrode in 0.1M NaOH (a) variation of peak current with scan rate variation (b) linear plot of peak current vs peak current (c) maximum peak potential vs log of scan rate.	71

Fig. 2.25.	DPV measurements for FAL using MiPAN@GP electrode in 0.1M NaOH (a) Concentration variation (b) linear plot of peak current vs concentration.	72
Fig. 2.26.	Analytical characteristics of the MiPAN@GP electrode in 0.1M NaOH (a) repeatability (b) reproducibility (c) stability.	74
Fig. 2.27.	Influence of interferences to voltammetry peak current responses of 200 μ M FA in 0.1M NaOH at MiPAN@GP electrode.	75
Fig. 2.28.	Study of selectivity to different analytes in 0.1M NaOH at MiPAN@GP electrode.	75
Fig. 3.1.	X-ray diffraction pattern of (a) synthesized NiCo ₂ O ₄ nano crystallites (b) Graphite (c) NiCo ₂ O ₄ modified graphite.	91
Fig.3 2.	SEM image of (a) synthesized NiCo ₂ O ₄ nanoparticles (b) pure graphite.	91
Fig. 3.3.	FTIR pattern of synthesized NiCo ₂ O ₄ nano crystallites	92
Fig. 3.4.	(a) Comparative performance of NiCo ₂ O ₄ @GP electrode with bare GP (b) Bar plot of modifier to graphite ratio vs peak current.	93
Fig. 3.5.	(a) Plot of peak current vs pH value (b) CV response of NiCo ₂ O ₄ @GP electrode in PBS 6 with and without MY (c) peak potential vs pH value.	94
Fig. 3.6.	CV response of NiCo ₂ O ₄ electrode (a) variation of peak current with scan rate variation (b) linear plot of peak current vs scan rate (c) maximum peak potential vs log of scan rate.	95
Fig. 3.7.	DPV measurements for MY using NiCo ₂ O ₄ @GP electrode (a) Concentration variation of 5 to 1000 μ M (b) linear plot of peak current vs concentration.	96
Fig. 3.8.	Analytical characteristics of the NiCo ₂ O ₄ @GP electrode (a) repeatability(b) reproducibility(c) stability.	97
Fig.3.9.	Influence of interferences to voltammetry peak current responses of MY at NiCo ₂ O ₄ @GP electrode.	98
Fig. 3.10.	Schematic representation of MIP synthesis to evaluate the electrode responses to MY in pigeon pea and turmeric powder.	100
Fig. 3.11.	CV response of different monomers in the presence of 100 μ M MY in 0.1M PBS6.	103
Fig. 3.12.	FTIR spectra of the MIP (a) before (b) after template removal.	103
Fig. 3.13.	UV-Vis spectra of MIP before and after template extraction.	104
Fig. 3.14.	SEM images of synthesized (a) MIP and (b) NIP material.	104

Fig. 3.15.	CV response of (a) MIP and NIP electrodes (b) MIP electrode with and without the presence of 100 μ M MY in 0.1M PBS6.	105
Fig. 3.16.	(a) Influence of different supporting electrolyte compositions (b) influence of phosphate supporting electrolyte with different pH on the peak current in the presence of 100 μ M MY.	105
Fig. 3.17.	CV measurements of MIP electrode in 0.1M PBS6 (a) peak current variation with scan rate (b) linear plot for the peak current vs scan rate (c) maximum peak potential vs log of scan rate.	107
Fig. 3.18.	DPV response of MY using MIP electrode in 0.1M PBS6 (a) Variation of concentration (b) linear plot of the peak current vs concentration.	108
Fig. 3.19.	Analytical characteristics of the MIP electrode (a) repeatability (b) reproducibility (c) stability.	109
Fig. 3.20.	Impact of various interferences on the voltammetry response of 100 μ M MY in 0.1M PBS6 at MIP electrode.	110
Fig. 4.1.	CV response for monomer optimization in 100 μ M VNL at 0.1M PBS 5.	123
Fig. 4.2.	FTIR spectra of MIP before and after template removal.	124
Fig. 4.3.	UV-Vis spectra of MIP before and after template removal.	124
Fig. 4.4.	SEM pictures of (a) MIP (b) NIP.	125
Fig. 4.5.	CV response of (a) MIP and NIP electrode (b) with and without VNL molecule in 0.1M PBS 5.	125
Fig. 4.6.	Plot of (a) peak current vs supporting electrolytes (b) peak current vs pH in 100 μ M VNL.	126
Fig. 4.7.	MIPAM/GP electrode CV response to 100 μ M VNL in 0.1M PBS 5 (a) current varying with scan rate (b) peak current plot against scan rate (c) peak potential plot against the log of scan rate.	127
Fig. 4.8.	VNL DPV response (a) Concentration variance (b) Peak current plot against concentration by MIPAM/GP electrode in 0.1M PBS 5.	128
Fig. 4.9.	Sensory characteristics of the MIPAM/GP electrode showing (a) reproducibility (b) repeatability and (c) stability.	129
Fig. 4.10.	Sensory characteristics of the MIPAM/GP electrode showing interference study.	130
Fig.5.1.	The circuit design comprising filter and potentiostat circuit.	140

Fig.5.2.	Timing diagram of protocol signals assuming the input triangular wave is generated in 3 steps.	142
Fig.5.3.	Schematic diagram of the system.	143
Fig.5.4.	Raspberry pi GUI.	144
Fig.5.5.	The proposed experimental setup.	144

List of tables

Table No.	Table Title	Page No.
Table 1.1.	Comparison between MIP sensors with natural biomolecule-based sensors	16
Table 1.2.	An overview of the literature on the MIP-based electrochemical transduction methods	22
Table 2.1.	An evaluation for the actual, predicted levels of formalin based on PLSR	46
Table 2.2.	An evaluation of the actual and predicted levels of formalin based on PCR	46
Table 2.3.	Comparison of electron transfer kinetics at proposed CeO ₂ @GP with different electrodes	56
Table 2.4.	Comparison of proposed CeO ₂ @GP performance with the previous reports	58
Table 2.5.	Determination of FAL in fresh mushroom extract using CeO ₂ @GP electrode	61
Table 2.6.	Comparison of proposed MiPAN@GP performance with the previous reports	73
Table 2.7.	Detection of FAL using MiPAN@GP electrode	76
Table 3.1.	Comparison of proposed NiCo ₂ O ₄ @GP performance with the previous reports	96
Table 3.2.	Determination of MY in turmeric using NiCo ₂ O ₄ @GP electrode	98
Table 3.3.	Comparison of proposed MIP performance with the previous reports	108
Table 3.4.	Detection of MY using MIP electrode (m=3)	111
Table 4.1.	Comparison of MIPAM/GP behaviour with the preceding reports	128
Table 4.2.	Detection of VNL using MIPAM/GP electrode	131
Table 6.1.	Major findings of the thesis	152

List of abbreviations

WHO	World health organization
IARC	International agency for research on cancer
FAL	Formalin
MY	Metanil yellow
VNL	Vanillin
HPLC	High performance liquid chromatography
GCMS	Gas chromatography mass spectrometry
MIP	Molecular imprinted polymer
FTIR	Fourier transforms infra-red
FESEM	Field emission scanning electron microscope
SEM	Scanning electron microscope
UV-Vis.	Ultra- Violet visible spectroscopy
SCE	Saturated calomel reference electrode
CE	Counter electrode
RE	Reference electrode
WE	Working electrode
CA	Control amplifier
CF	Current follower
LSV	Linear sweep voltammetry
CV	Cyclic voltammetry
PV	Pulse voltammetry
NPV	Normal pulse voltammetry
DPV	Differential pulse voltammetry
SWV	Square wave voltammetry
SV	Stripping voltammetry
ASV	Anodic stripping voltammetry

CSV	Catodic stripping voltammetry
BHT	Butylated hydroxytoluene
EGDMA	Ethylene glycol dimethacrylate
MAA	Methacrylic acid
AIBN	2,2'-Azobisisobutyronitrile
TBHQ	Tertiary butylhydroquinone
BHA	Butylated hydroxyanisole
AM	Acrylamide
EPA	Environmental protection agency
PFA	Prevention of food adulteration act of india
PCR	Principal component regression
PLSR	Partial least square regression
PCA	Principal component analysis
CF	Correlation factor
RMSEV	Root mean square error of validation
RMSEP	Root mean square error of prediction
CPE	Carbon paste electrode
SPE	Screen printed electrode
POs-EA	Os(bpy) ₂ -poly(vinylpyridine)
FDH	Formaldehyde dehydrogenase
AuNPS	Gold nanoparticles
[EMIM][OTF] trifluoromethanesulfonate	1-ethyl-3-methylimidazolium
CHIT	Chitosan
MWCNT	Multiwalled carbon nanotube
NIP	Non imprinted polymer
MIP	Molecular imprinted polymer
Px	P-xylylenediamine
Pt	Platinum nanoparticles

PAN	Polyaniline
EG	Expanded graphite
Pd	Palladium nanoparticles
GCE	Glassy carbon electrode
CNTs	Carbon nanotubes
GO	Graphene oxide
CeO ₂ @GP electrode	Cerium oxide nanoparticle modified graphite
HRTEM	High-resolution transmission electron microscope
QCM	Quartz crystal microbalances
LOD	Limit of detection
BP	benzoyl peroxide
PBS	phosphate buffer solution
Ag/AgCl	Silver/Silver chloride
Au	Gold
CuO	Copper oxide
PHT	phthalate
ACT	acetate
PHP	phosphate
XRD	X-ray diffraction
PMMA	Polymethylmethacrylate
EIS	Electrochemical impedance spectroscopy
MiPAN@GP	Polyacrylonitrile based molecular imprinted polymer infused in graphite
AN	Acrylonitrile
AA	Acrylamide
NiPAN@GP	Non imprinted graphite based polyacrylonitrile
PVDF	Polyvinylidene fluoride

CQDs/GCE	Carbon quantum dots modified glassy carbon electrodes
Calix8/Au NPs/GCE	Glassy carbon electrodes modified with calixarene and gold nanoparticles
NiCo ₂ O ₄ @GP	NiCo ₂ O ₄ modified graphite electrode
Bare GP	Bare graphite electrode
PDA	Polydopamine
MIPAM/GP	Molecular imprinted polymer based on polyacrylamide



Introduction and scope of the thesis

The aim of this thesis is exemplified in this chapter. The importance of food additives in our day-to-day life has been discussed, as well as the impact they have on our health. Several conventional methods are also described, as well as their advantages and disadvantages, for measuring several food additives. A discussion of the distinct transduction mechanisms follows. An overview of the scope and goals of the study is provided at the end of the chapter.

Chapter 1

Introduction and scope of the thesis

1.1. Introduction

In modern era, food safety has become a major cause of concern around the globe. A good number of additives such as salt, spices, and sulphites have been used to preserve and enhance the taste of foods since ancient times. A rise in food processing necessitated more use of food additives. In general, food additives are a variety of chemical substances which are added to the food to preserve its flavour as well as to enhance its taste, appearance, or other qualities. Additives to food can be categorized into four categories: nutritional additives, processing agents, preservatives, and sensory agents. Dairy and cereal products are fortified with vitamin A and D; flour, cereals, baked goods are fortified with several B vitamins, and fruit beverages and confectioneries are fortified with vitamin C. Processing agents are added to foods in order to sustain the desired consistency of the product. Preservatives may be of two types namely antioxidants and antimicrobials. As a result of oxidative mechanisms, antioxidants prevent foods from deteriorating. Microorganisms that cause food spoilage and pathogens can be inhibited by antimicrobial agents. Examples of antioxidants are ascorbic acid, butylated hydroxytoluene (BHT), butylated hydroxyanisole (BHA), tertiary butylhydroquinone (TBHQ), citric acid, sulphites. Products with low pH include acetic, benzoic, propionic, and sorbic acids as antimicrobials. Hams and bacon are cured using nitrates and nitrites to prevent clostridium botulinum bacteria from growing. Wines, fruit juices, and dried fruits are treated with sulfur dioxide and sulphites to prevent spoilage. Microorganisms produce the preservatives nisin and natamycin. Nisin is effective against moulds and yeasts, whereas nisin inhibits the development of certain bacteria. One such chemical preservative which has major influence in fish industries is formalin (37% formaldehyde). Since fish is a highly perishable commodity, traders supply formalin treated fish to prevent spoilage and increase shelf life. India is the second largest producer of fish in the world. Further, the annual growth rate in fish consumption in India is increasing day by day due to population growth. Since it has been identified by the International Agency for Research on Cancer (IARC) as a Group 1 human carcinogen, formaldehyde is

regarded as a dangerous element. [1]. Formaldehyde builds up in the body and has a negative impact on longevity. It is also responsible for various health hazards like abdominal pain, vomiting, renal injury, burning sensations of eyes, nose and throat ($>0.1\text{ppm}$ in air), skin irritation, nausea, coughing, wheezing. Recently, there was lots of report of formalin use in fish preservation in different states of India *viz.* Assam, West Bengal, Odisha, Andhra Pradesh and Goa. The Occupational Safety and Health Administration and Environmental Protection Agency have set limits on exposure to and health risks from this hazardous material. The United States Environmental Protection Agency (EPA) states that the formaldehyde maximum daily dosage reference is 0.2 mg/kg bw/day [1]. Tolerable daily intake 0.15 mg/kg body weight per day is approved by world health organization (WHO) [2]. To adhere to these regulations, formaldehyde levels must be precisely monitored. A common malpractice among several traders in India is adulteration of food with an illicit synthetic dye called metanil yellow. Such a toxic food dye is prohibited by the food regulatory authorities but still the use is widely prevalent among various food merchandises. A review on a number of food products was conducted such as turmeric, besan, and laddoo in the state of West Bengal, which revealed 36.21% of the trials comprised metanil yellow at a level below the tolerable limit of 100 mg kg^{-1} while 63.79% of the adulterated samples comprised metanil yellow above the maximum permissible limit according to prevention of food adulteration act of India (PFA, 2008) [3]. Vanilla occupies a prominent place in modern food culture among a variety of natural flavours used in diverse foods, such as confectionery, beverages, pharmaceuticals, food, and perfumery [4]. Vanillin (4-hydroxy-3-methoxybenzaldehyde) in vanilla is the main aromatic component ($1.0\text{--}2.0\text{ weight \%}$) among more than 200 compounds in natural vanilla, which are responsible for the desirable flavour and aroma [4]. The natural vanillin in vanilla has antimicrobial, anticarcinogenic, and antimutagenic properties which attributes to the benefits for human health [1]. As well as suppressing UV and X-ray-induced chromosomal aberrations, it functions as a DNA-PK inhibitor that assists in DNA strand repair and prevents mutations at the CD59 locus on human chromosomes [4]. A mere 0.2% of the market demand is covered by natural vanillin made from vanilla, while the remaining 98% is synthetic vanillin obtained via chemical or biochemical means. While synthetic vanillin is widely used due to its lower price and availability, extensive research shows that excessive consumption can trigger headaches, nausea, and vomiting, as well as cause kidney and liver damage [4-6]. In food science, medicine, and pharmacology, it is increasingly

important to develop simple, accurate, and economical techniques for the measurement and quality control of vanillin.

Recently several techniques over formaldehyde contaminations found in various common foods, including seafood, vegetables, fruits, meat and dried mushrooms etc. have been reported [7]. For determining formaldehyde concentration levels in the lab, several traditional techniques are available, including gas chromatography-mass spectrometry (GC-MS), high-performance liquid chromatography (HPLC), fluorimetry, Nash test, and gravimetric methods [8,9]. Although these methods showed sufficient sensitivity towards formalin detection but they suffer from certain limitations. Similarly, a number of non-destructive methods, including Fourier transform raman spectroscopy (FT-Raman) and Fourier transform infrared spectroscopy (FT-IR), can be used to recognize metanil yellow within turmeric samples [10,11]. Metanil yellow content as low as 1% and 5% has been detected using these methods. A study has reported the separation of pure turmeric from contaminated turmeric by means of NIR spectroscopy paired with principal component regression (PCR) along with partial least square regression (PLSR) [12]. Measuring natural vanillin in various food samples or vanilla extracts has been performed using a wide diversity of chemical practices, like thin layer chromatography, gas chromatography, UV spectrophotometry, high-performance liquid chromatography, capillary electrophoresis, and micellar electrokinetic chromatography, among others [13-20]. As a result, these methods are hardly suitable for the recognition of vanillin away from a laboratory environment due to their high cost and complicated and time-consuming procedures aimed at the pretreatment of samples. All of these traditional techniques use risky chemicals and are prone to interferences, which cause false positive results. Additionally, these methods are impracticable for real-time measurements because of the required high end equipment and skilled technicians. The challenges faced with these methods include the need for specialized personnel, the high equipment costs, and the laboratory based instrument setups. As a consequence, investors are now favouring the development of simple, cost-effective, portable devices that would meet the same precision, selectivity, robustness, sensitivity, no-potential-power requirements, reproducibility and less measurement time specifications as the expensive high-end instruments. Currently, electrochemical sensors offer a new analytical tool that enhances performance in terms of selectivity and sensitivity.

In this regard, electrochemical techniques have become an ideal alternative because they are sensitive, accurate, simple to use, quick, and portable for food safety determination. In addition, they offer a potential solution to the electrode fouling effect that hampers traditional methods. A deep insight into literature survey indicates that there are few reports for electrochemical detection of food additives. Therefore, in the current scenario, the emphasis will be on developing inexpensive, highly sensitive and ready-to-use electrochemical sensors for detecting food additives in real-time. Online analysis, high sensitivity, high selectivity, field application, and quick response are all advantages of these electrochemical sensors. A key aspect of product quality control and safety may be to use electrochemical sensors, which are much cheaper and easier to miniaturize.

This thesis describes three distinct works for the selective determination of three different food additives (a) preservative: formalin (FAL), (b) colourant: metanil yellow (MY), and (c) flavourant: vanillin (VNL) using specifically designed metal oxide and molecularly imprinted polymers (MIP). The electrodes' morphological modifications were studied using a Fourier transform infrared (FTIR) spectroscope, a field emission scanning electron microscope (FESEM), and an ultraviolet visible (UV-Vis) spectroscope, respectively. This thesis examines all the electrodes' analytical characteristics. The voltammetry method was used to measure real-time food quality parameters.

In the remaining section of this thesis, the information is organized in the following way. Voltammetric techniques are briefly discussed in relation to electrochemical principles of sense. In the following section, we discuss different methods of molecular imprinting and how they can be used to fabricate MIP sensors. The purpose and scope of the thesis are presented after a detailed literature review.

1.2. Electrochemical techniques

Volatile and non-volatile compounds can be quantified using electrochemical transduction mechanisms. Through the use of the redox reaction process, one can obtain information regarding the sample by observing the currents corresponding to the target species and the potential differences between the electrodes, which assist in quantifying the sample to a

quantitative level. Electrochemical techniques are commonly used in practice owing to their low cost, stability, sensitivity, ease of recovery, and less interference [21], [22].

1.2.1. Types of electrochemical techniques

Electrochemical reactions are governed by potential, current, charge, and time. Electrochemical techniques have several indistinguishable characteristics, which are listed below:

- i) Analyte form at the electrode surface is determined by the potential of the electrode
- ii) In addition to conventional oxidation and reduction, the analyte may undergo other reactions
- iii) Current measures the oxidation and reduction rate of the analyte
- iv) Potential and current cannot be controlled at the same time

The following categories of electrochemical methods may be made based on the excitation signal and the resultant response.

a) Coulometry

A certain quantity of electricity (Coulomb) is required for a chemical to change into a new oxidation state, in this form of electro analytical method. The first law of electrolysis by Faraday serves as the method's guiding concept [36]. The following Eq. (1.1), which takes Q Coulomb charge transfer into account, can be used to determine the weight of the material (w) created or consumed in electrolysis.

$$w = \frac{MQ}{96487n} \quad (1.1)$$

where n is the reaction electron number and M is the molecular mass of the substance freed or consumed. The two generalised approaches of potentiostatic (controlled potential) and amperostatic (controlled current) coulometry are often employed for coulometric analysis. The working potential of the electrode is maintained constant in a regulated potential situation. Without the involvement of less reactive species in the sample or the solvent, the analyte might be oxidised or reduced. On the other hand, controlled current type coulometry allows for the

measurement of the signal in terms of current until the reaction is complete. Furthermore, by measuring the current's strength and its duration, the amount of the output charge may be determined.

b) Potentiometry

Potentiometry is a technique that measures an electrochemical cell's potential without using a significant amount of current. An indicator electrode (measuring electrode) and a reference electrode make up the two electrode system. By dipping the measuring electrode into the solution containing the target analyte and comparing it to a set of reference electrode, the potential signal may be acquired. Direct potentiometry and potentiometric titrations are additional divisions of the potentiometry technology. The concentration of the active chemical species is related to the cell potential through potentiometry, which also affects the cell potential. The cell potential is calculated as a component of the reagent volume in potentiometric titrations [23].

c) Voltammetry

The voltammetry concept, which measures the current across the electrode within a changeable potential window, is employed most frequently in electrochemical methods [23], [24]. To maintain the electroactive chemical species at the working electrode surface, the voltage is changed within a predetermined range. The peak current generated due to adsorption of analyte at the working electrode surface might be utilized for determination of the quantitative information about the target species.

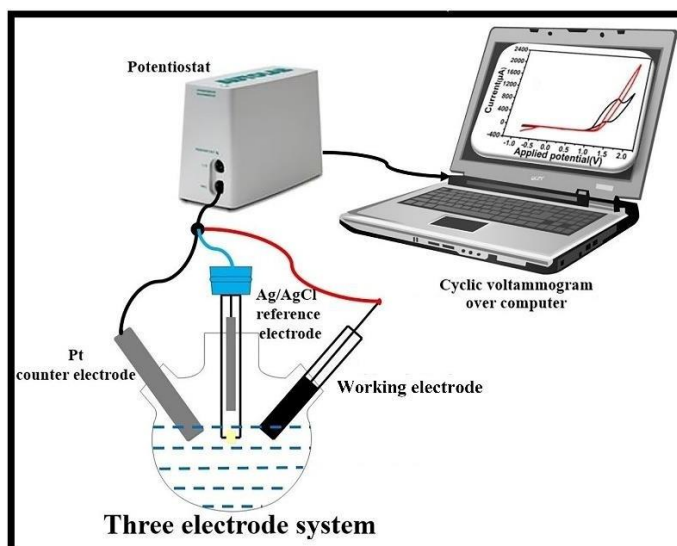


Fig. 1.1 Voltammetric setups for a configuration with three electrodes.

A three-electrode electrochemical cell is shown in fig. 1.1. It consists of a reference electrode—such as an Ag/AgCl electrode or a saturated calomel reference electrode (SCE)—a counter electrode, and a working or measuring electrode. In contrast to potentiometry, the reference electrode is used to keep a reference potential in relation to the working electrode using a power source or potentiostat. The regulated voltage source in an electrical system is comparable to the potentiostat. It generates current by causing redox reactions at the electrode interface, which monitors and regulates the voltage applied across the working electrode. The produced current, which travels between the working electrode and the counter electrode, carries numerical data on the electrochemical characteristics and the reaction kinetics of a system. Fig. 1.1 [24] depicts the three electrode configuration and electrochemical linkages. In fig. 1.2 (b), the arrangement of three electrodes; a counter electrode (CE), a reference electrode (RE), and a working electrode (WE) is shown. The flow of current in this instance is between the CE and WE. On the other hand, the WE and CE connections are in charge of the potential difference, which is measured between the RE and sense (S) connections. In order to eliminate the solution resistance, it is noteworthy that the RE is positioned extremely close to the WE. WE is maintained at a constant, stable voltage with the correct connection to S in order to regulate the polarisation of the CE. The developed potential between the RE and WE, on the other hand, is time independent.

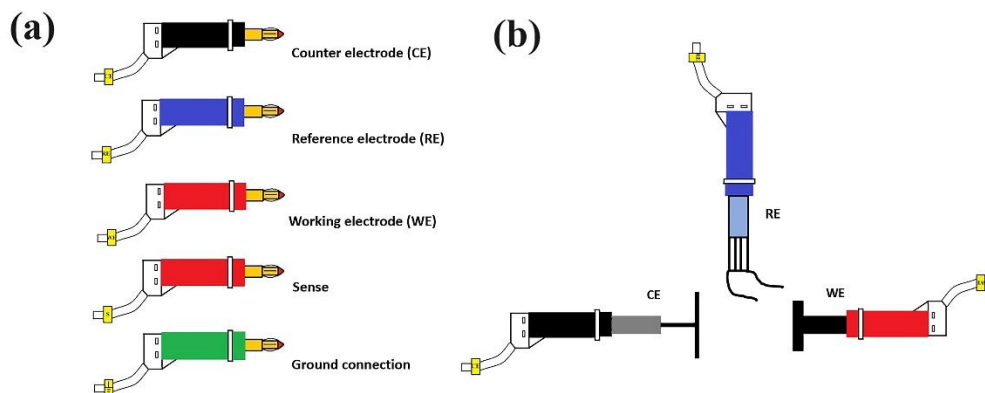


Fig. 1.2 (a) Connections on the Auto Lab PGSTAT101 cell wires that correlate to the correct colour codes; (b) A diagram showing the three-electrode configuration.

The potentiostat's fundamental electrical circuit is depicted in fig. 1.3 [24]. The CE is linked to a control amplifier (CA) block, which obstructs the electrochemical cell's ability to conduct current. Conversely, WE are linked to the low current follower (Low CF) circuit. For low and high currents, respectively, the corresponding value of the current is measured using a low CF or a shunt. The potential difference between RE and S is determined by the use of a differential amplifier. The resulting signal is supplied to the summation point, which serves as an input to CA together with the waveform created by the digital to analog converter (E_{in}). The output potential and current are denoted as E_{out} and I_{out} , respectively.

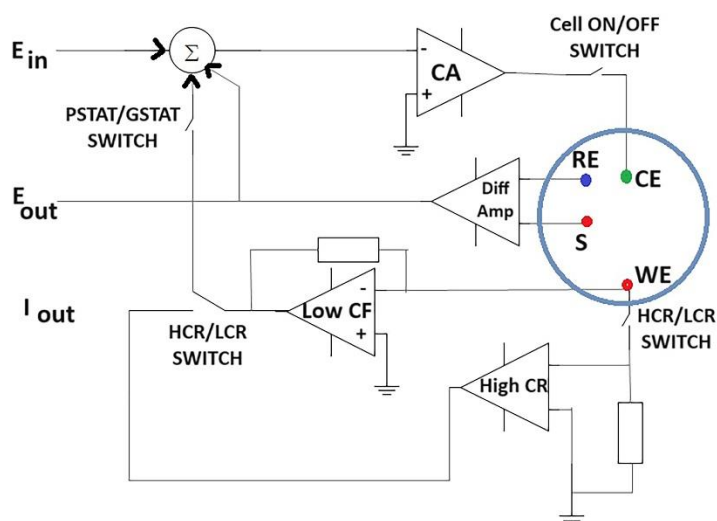


Fig. 1.3 An electrical potentiostat's basic circuitry.

Voltammetric measurements are typically conducted in one of the following ways:

i) Linear sweep voltammetry (LSV)

Electrochemical cells produce current when the potential between WE and RE linearly varies over time. LSV is characterized primarily by the following features [25]

- The rate at which electrons are transferred
- Species that are electroactive have chemical reactivity
- Scan rate of voltage

Due to this, the capacitive current generated can't be compensated electrochemically when the scan rate increases. Due to this, it might not be possible to achieve a lower detection limit.

ii) Cyclic voltammetry (CV)

Electrochemical potentiodynamic measurements are most commonly performed via CV, in which WE potential is linearly changed over time [25]. Once the working electrode reaches the saturation potential, its potential ramps in reverse for a short time before returning to its initial value. Fig. 1.4 (a) and (b) illustrate a typical cyclic voltammogram displaying the cathodic (i_{pc}) and anodic (i_{pa}) current responses to different time intervals corresponding to oxidation and reduction processes. The triangular pulse initiates the reaction as shown in fig. 1.4. Current increases with an increase in input potential during the forward scan (t_0 - t_1). Due to the significant amount of reactants present, oxidation occurs rapidly at this point. Next time, the voltage is applied, the availability of these reactants decreases and the value of the current becomes constant or lower. The cathodic peak is observed on the reverse sweep (t_1 to t_2) by reducing oxidized species.

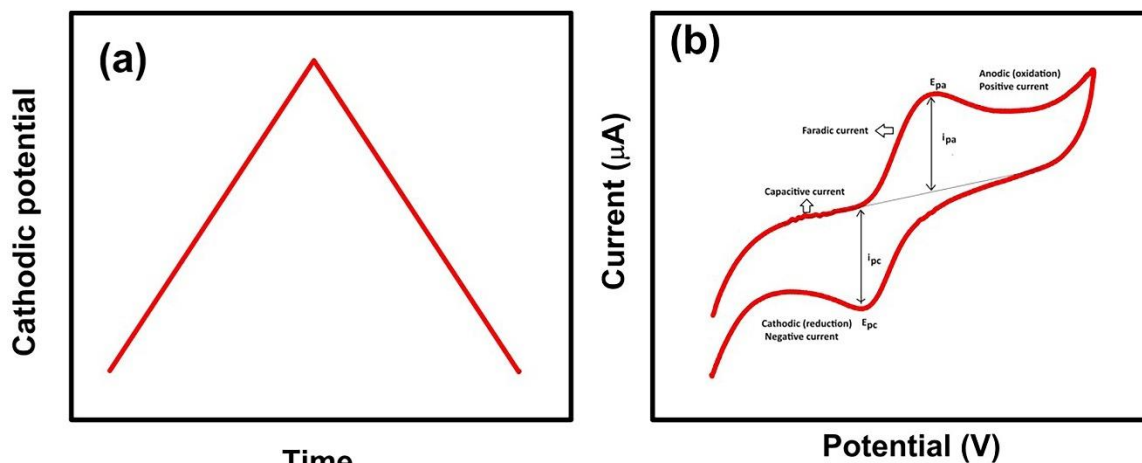


Fig. 1.4 (a) Waveform for cyclic voltammetry; (b) Parameters for a reversible reaction is shown on a typical cyclic voltammogram.

iii) Pulse voltammetry (PV)

The operational principle of pulse voltammetry is based on a potential pulse on the difference in the decay rates of the charging and Faradic currents. The charging current degrades exponentially whereas the faradaic current decays as a function of $1/(\text{time})^{1/2}$. The decline of the faradaic current occurs gradually than the charging current. By using this voltammetry approach, which Barker and Jenkin created [26], it is feasible to detect an analyte at concentrations up to 10^{-8} M. PV is categorized as follows based on the applied potential waveform and the related current profile:

➤ Normal pulse voltammetry (NPV)

Here, the output current is activated at the conclusion of each pulse in a sequence of monotonically rising potential pulses, giving the charging current time to drop between pulses. The pulse time (t) ranges from 1 to 100 ms in response to the potential (E_i), and the corresponding interval is 0.1 to 5 s. The sampled current is shown on the vertical axis and the voltammogram is shown as a stepped pulse on the horizontal axis.

➤ *Differential pulse voltammetry (DPV)*

A typical DPV approach is depicted in fig. 1.5. There are some similarities between the NPV and DPV. The difference is in the shape and incrementally increased amplitude of the applied potential. The baseline potential is maintained after each change in the application of successive pulses for a predetermined amount of time before the application of the next pulse, and the corresponding sequential current is sampled both before and after the pulse [27]. For a quantitative examination of the target analyte, the resultant difference between these two values of sampling current is further recorded.

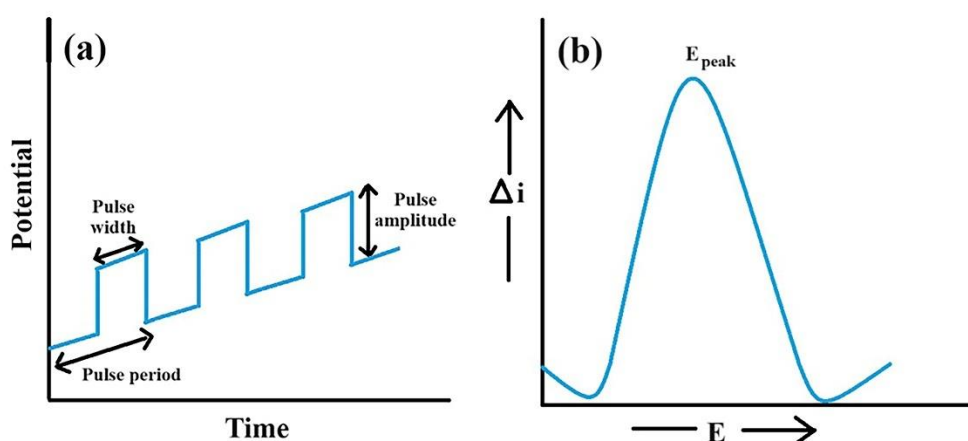


Fig. 1.5 (a) Differential pulse voltammetry's excitation potential waveform; (b) A common differential pulse voltammetry.

As a result, when compared to other types of PVs, DPV appears to be the most sensitive approach with a lower limit of detection.

➤ *Square wave voltammetry (SWV)*

The series of symmetrical square wave pulses of amplitude E_{sw} is overlaid on a staircase waveform in such a manner that the square wave's forward pulse matches the staircase's phase [25]. The resultant current, which is centred on the redox potential, is calculated from the difference between the forward and reverse currents. The lower detection limit is up to the order of 0.1 nM, and the amplitude of the peak and the concentration of the electroactive species are linearly related to one another.

iv) Stripping voltammetry (SV)

Sensitive SV method is mostly used to detect tiny amounts of metals in solutions. [25]. The three steps listed below make up the methodology:

- In order to cause the target metal ions to deposit on the electrode's active surface, a particular voltage is first given to the electrode. The solution is continuously stirred to increase the amount of metal ions available for deposition.
- The stirring action is stopped after the deposition of ions has settled on the electrode surface.
- The next stage, known as the stripping state, involves removing the deposited metal ions from the electrode by scanning the potential. The resultant current is proportional to the concentration of the metal in the solution.

Depending on whether the stripping process uses a positive potential scan or a negative potential scan, there are two main forms of stripping voltammetry. Cathodic stripping voltammetry (CSV) and anodic stripping voltammetry (ASV) are the two names for these techniques.

1.3. Molecular imprinted polymer (MIP) technique

A molecularly imprinted polymer is an effective method for creating a sensitive and selective sensor. Target molecules and functional monomers that are gathered and cross-linked to one another around a template are used to manufacture the MIP materials (target molecule). The functional monomers, which have been arranged around the template molecule, are polymerized to create an imprinted matrix by the interaction between functional groups on the template and monomers. The target particle is then removed from the structure under specific circumstances, giving up a pit integral that plays nicely with the scheme. The active binding region of the enzyme has a particular geometric configuration that is particularly suitable for a substrate. A poorly formed molecule that does not fit the binding site is not recognized, whereas a substrate that has a shape that corresponds to the site is recognized by preferentially attaching to the enzyme. Dickey conducted the first molecular imprinting studies in the 1940s and 1950s [28, 29], establishing the silica gel's affinity for dye molecules in conjunction with Linus Pauling's hypothesis [30]. The fundamental diagram of a MIP procedure [31] is shown in fig.1.6.

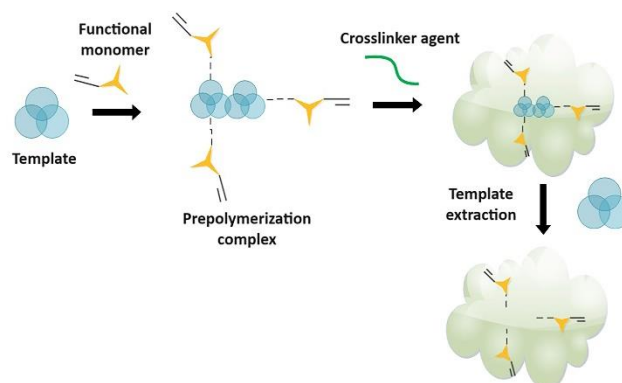


Fig. 1.6 The schematic of a basic MIP process.

The following three stages [32] can be used to sum up the process of synthesizing a MIP:

- a) **Association:** Covalent and non-covalent binding are used to assemble the target molecule and monomers.
- b) **Polymerization:** Different types of polymerization techniques are used, resulting in the creation of cross-linked copolymers that trap the template molecules.
- c) **Elution:** By using the right elution agent, template molecules trapped inside the polymer network are released. As a result, cavities with similar fit are created, which is necessary for molecular identification.
- d) There are two elements that help to shape the fundamental ideas that underlie molecular recognition [33]. These include;
 - The template-mediated pre-organization of the polymer's complementary functional groups.
 - Imprinting of a complementary shape-selective cavity to the template.

Because of their extreme flexibility, adaptability, and exceptional mechanical stability, MIPs are useful. Additionally, MIP sensors that are suitable to any target analyte may be efficiently generated due to the extensive accessibility of the practical monomers. Additionally, the MIP approach may be used in biosensors to replace unstable biological molecules like antibodies and enzymes. Table 1.1 lists the benefits of MIP sensors over organic biomolecules [32].

Table 1.1 Comparison between MIP sensors with natural biomolecule-based sensors

Sl. No.	Sensor based on natural biomolecules	MIP sensors
1	Poor stability	With low or high pH, MIP sensor stability is quite high
2	Receptors and enzymes are pricey	It is inexpensive and simple to use
3	Perform badly in media that aren't water	In organic solvents, they can react
4	Different natural biomolecules require various conditions to function (pH, ionic strength, temperature, substrate)	Different target-specific polymers might react in the same particular environment
5	Natural receptors and enzymes are absent for several significant analytes, making the production of antibodies impossible	Almost any chemical might be used with polymers
6	A lack of compatibility with miniaturisation and micromachining	Polymers and micromachining technologies are completely compatible

Any polymer matrix can develop active sites through a variety of chemical processes such as imprinting with sacrificial spacers, non-covalent imprinting, semi-covalent imprinting, and imprinting with covalent bonds. The following subsections expand on the many types of imprinting forms.

1.3.1. Types of imprinting techniques

1.3.1.1. Covalent imprinting

Covalent imprinting is an imprinting technique in which the template and at least one polymerizable unit are linked by reversible covalent bonds to generate a template monomer complex by a chemical procedure that is independent of the creation of polymers. Here, a pre-polymerization is used to create a derivative from the monomer and the template, and the polymerization process is then carried out. The covalent bond between the polymer and the template is broken upon the ejection of the template from the polymer after polymerization. Rebinding the template atom inside MIP results in another agreement on a similar connection [34]. The removal of the template molecule created during polymerization is the key selling point of this method. Fig. 1.7 shows a schematic of the covalent imprinting procedure [35].

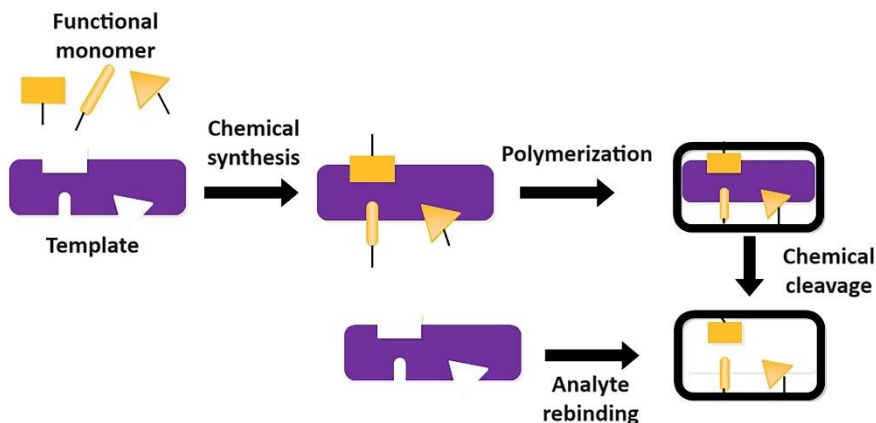


Fig. 1.7 Schematic explaining the covalent imprinting process.

a) *Imprinting with readily reversible covalent bonds*

This type of covalent bonding exclusively uses techniques for quickly reversible binding reactions, such as boronate ester, ketal/acetal, and Schiff's base development, to accelerate the design of the template-monomer binds. The hydrolysis of the organisation molecule from the polymer under sensitive liquid conditions is necessary for the enhancement of these binds. The number of configurations that may be imprinted is certainly constrained by the unique assistant requirements of covalent methods, namely 1,2- and 1,3-diols (boronate ester and ketal/acetal), aldehyde (acetal and Schiff's base), ketone (ketal), and amine (Schiff's base). The fact that the bounce back state is indeterminate from the as-prepared polymer, in which each coupling site almost resembles one another, is unquestionably one of the strategy's main goals. As the amount of monomer decreases, ambiguous confining may also completely decrease. However, the requirement for the organisation monomer to be combined is seen as a barrier to any covalent etching technique, and moreover, this type of format monomer may be sensitive to the proximity of water. Additionally, additional steric requirements are imposed by the processes in the imprinted polymer areas, ruining the system for swapping the template particle.

b) *Covalent imprinting with boronate esters*

The imprinting of carbohydrate or starch subsidiary makes the boronate ester strategy one of the finest reversible covalent techniques. This approach, which was originally put into practise by Gunter Wulff et al., contains formats for the imprinting process, including glyceric acid,

subordinates of mannose, galactose, and fructose, sialic acid, castasterone, and L-Dopamin (L-DOPA) [36]-[40]. Numerous studies have shown how to combine boronate esters to create MIPs for fluorescent detection [41]–[43], imprinted polyelectrolyte hydrogels [44], functionalized polyaniline coatings for microtitre plates [45], and more. They have also shown how to combine amino acids in an enantioselective manner. Additionally, this technique has been expanded to allow for the engraving of monoalcohol forms and those with spatially segregated distinct hydroxyl groupings thanks to the use of boron ophthalide-based monomers [46], [47]. The polymers structured using this method have also succeeded in specific derivatization of sterols by polymeric securing bunches [48].

c) Covalent imprinting with Schiff's bases

The chemistry of Schiff's base (imine) includes the accumulation of an essential amine and a carbonyl molecule (generally an aldehyde). This makes it a possibly beneficial method for imprinting amine- or aldehyde-bearing templates. Additionally, this method has been successfully used to imprint amino acid derivatives [49], however exchange with the resulting enantio selective polymers is frequently excessively delayed for application in chromatographic separations.

d) Covalent imprinting with acetals and ketals

Shea et al. [50]–[52] conducted a thorough analysis of the mono- and di-ketone templates in which a polymerizable diol was used as the binding group for the MIP's readiness. It has also been investigated if a series of cyclic hemi-acetals may serve as monoalcohol restricting groups [53].

1.3.1.2. Non-covalent imprinting

This method overcomes the limitations brought on by covalent imprinting. Non-covalent contact has been used since the early reports of imprinting in silica frame works, but Mosbach's group popularised it in the 1980s and developed it into a workable method for engineering imprinted receptors in engineered polymers [54]. Fig. 1.8 [55] depicts a schematic of the noncovalent engraving procedure. According to various interaction forces, template-monomer complexes are formed in the appropriate soluble solvents in this approach. The template is

thrown out of the polymerized test and is capable of rebounding using the same interaction forces. Dipole-dipole interactions and Van der Waals forces cause the atoms to be attracted to one another, resulting in useful monomers in arrangement and layout adducts.

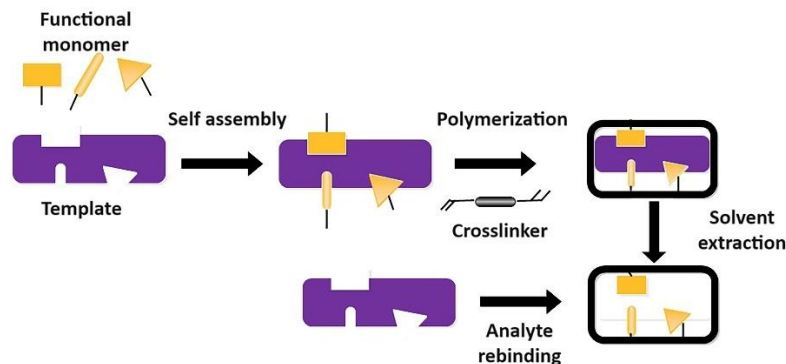


Fig. 1.8 Schematic explaining the mechanism of non covalent imprinting.

Non-covalent imprinting is one of the most widely utilised methods today because it allows for flexibility in terms of the features of a template that may be targeted. It is generally considered that in this process, little segments of polymer structure with various functional groupings start to fold over the template particle following the establishment of a pre-polymerization complex between the required template or target and practical monomers. Therefore, because of the different interactions than those that would have occurred in the case of single monomer-template associations, a mutual influence is produced. Depending on the amount of monomer used, these structures continue to form and alter as the polymerization process progresses. As a result, the target molecule's affinity for the receptor site increases until a completely framed polymerized network is formed. One monomer or a combination of monomers can be used for the non-covalent imprinting technique.

a) Non-covalent imprinting with a single functional monomer

The simplest approach is this method. It is the original and most extensively used strategy that has been demonstrated to be effective. It is necessary to consider the concept of the existing polymerization complex as well as the suitable bandings between the template and the monomer with the crosslinkers. This is because the monomer has the ability to change the equilibrium from the ideal template-monomer complexes, but the template may play a key role in describing or

improving usable receptors. There may be issues because of the monomer's propensity for self-association. For instance, there is a strong propensity for dimerise in carboxylic acids. Further, as they are frequently present (at least initially) at a fixation like the template's, possible interactions with the initiator should also be taken into account. Although vinylbenzoic acid can also be considered a desirable option due to its large bulk and aromatic ring's π electron configuration, it often has low reactivity proportions with popular (meth) acrylate cross-linkers and as a consequence causes problematic interactions with template molecules. The utilisation of phosphates and phosphate derivatives in imprinting, however, depends on how well they can bind to metal particles. The monomer vinyl pyridine interacts strongly with the aromatic rings that have insufficient numbers of electrons and the electron-rich π -electron ring network in their fundamental structure. These monomers are recognised as being extraordinarily productive in imprinting because they are commonly observed to significantly interact with templates. These helpful monomers might occasionally end up being detrimental because they produce strong π - π exchanges throughout template rebinding in aqueous circumstances, placing a heavy strain on the large amounts of non-specific binding sites. As a result, the template molecule exhibits the same affinity for both the imprinting and non-imprinting polymers. Tertiary amino monomers are among the other necessary monomers. Despite the fact that they are occasionally viable, the reaction is often less favourable than that of acidic monomers. This is likely due to their better chain flexibility, the growing distance between the amine activity and the polymer backbone.

b) Non-covalent imprinting with a combination of monomers

From the outside, it seems intriguing to combine the unique interface possibilities of several different monomers for a certain project. In actuality, it is predicated on the idea that a pre-polymerization mixture has a sizable number of equilibria. When the cross linker is correctly functionalized, Spivak's exciting ongoing research has shown that the monomers are not necessary to achieve optimal imprinting [57]. In order for the bonds formed between the template and the helpful monomers to be effective, they must be stronger than interactions between them. Additionally, mixing imprinting strategies that worked effectively in the tests were anticipated by computational virtual imprinting.

1.3.1.3. Semicovalent imprinting

As was seen in the preceding sections, in order for covalent imprinting to occur, the template molecule needs to be artificially altered with the functional monomer and evacuated by the breaking of the covalent bonds that are structured in that way. However, the non-covalent approach is more practical since it uses relatively weak forces of attraction, such as electrostatic contacts, hydrogen bonds, covalent bonds, hydrophobic interactions, etc., to achieve the desired goal of attaching the template to the monomer. This approach addresses the drawbacks of covalent imprinting by including covalent attachment during polymerization and hydrogen bond formation during recognition. Semi-covalent imprinting is a combination of covalent and non-covalent imprinting, in which the functional monomer and template are covalently bound together during polymerization and the rebinding process, respectively. As an example, the mixture created by the blending of the monomers is co-polymerized with a (meth) acrylate ester of the template. Because of the interface of the template's hydroxyl (s) with (meth) acrylic acid binders familiarized into the imprinted location, the template is released by hydrolysis and then rebinds to the polymer. However, due to the lack of direct template hydrolysis and the disparity in steric requirements of an acid and liquid in hydrogen bonding contact from the corresponding ester, this type of imprinting is not acknowledged.

1.3.1.4. Imprinting with sacrificial spacers

Few confines of the semi-covalent imprinting method can be alleviated by using a cross linker group amid the template element and the functional monomer, which is lost during template evacuation. The linker group serves two functions during polymer formation: it connects the template to the appropriate monomer and acts as a spacer between the template and the polymer-bound functionality to avoid flocking all through the noncovalent rebinding procedure [58]-[61]. Salicylate (2 hydroxybenzionate) was also utilized as a spacer group between the main amine of the template and the residue of polymerizable methacrylic acid [62]. The phenyl methacrylate ester splits more readily than the amide due to intramolecular hydrogen-bonding that maintains a tight contact between the ester oxygen and amide hydrogen during the noncovalent binding stage.

1.4. Literature survey on MIP based sensors

The MIP-based detection advancements in this section are described according to target analyte and different application areas. This is due to the fact that the transduction system has a great deal of influence on the progress of the polymerization process and the selection of monomers. The following Table 1.2 summarizes a significant number of research activities related to electrochemical transduction in the MIP strategy.

Table 1.2 An overview of the literature on the MIP-based electrochemical transduction methods

Sl. No.	Target analyte	Components of MIP	Polymerization method	Principle of operation	Ref.
1	Curcumin	Monomer: MAA Crosslinker: EGDMA Initiator: 2,2'-AIBN	Thermally induced Precipitation polymerization	CV	[63]
2	Melatonin	Monomer: 4-amino-3-hydroxy-1-naphthalenesulfonicacid (AHNSA) and melamine (MM)	Electropolymerization	CV, SWV	[64]
3	Emodin	Monomer: Allobarbitol Crosslinker: EGDMA Initiator: AIBN	In -Situ photopolymerization	CV, DPV	[65]
4	Rutin	Monomer: Acrylamide (AM) Crosslinker: EGDMA Initiator: 2,2'-AIBN	One-step solvothermal method	CV, DPV	[66]
5	Bisphenol A	Monomer: Ferrocenylmethyl methacrylate (FMMA) Crosslinker: EGDMA Initiator: 2, 2' Azobis(2-methylpropionit-rile) AIBN	MIPs synthesized with scCO ₂ technology	DPV	[67]
6	Tyrosine	Monomer: Pyrrole	Electropolymerization	CV, SWV	[68]
7	Colchicine	Monomer: MAA Crosslinker: EGDMA Initiator: AIBN	In situ polymerization	CV, DPV	[69]
8	6-Benzylamino urine	Monomer: 1-Vinyl-3-Butylimidazolium tetrafluoroborate Crosslinker: 1,4-butanediyl-3, 3'-bis-1-vinylimidazolium dibromide	-	CV, DPV	[70]
9	Amoxicillin	Monomer: MAA Crosslinker: EGDMA, Initiator: AIBN	-	CV, DPV	[71]
10	Mephedrone	Monomer: Tyramine	Sol-gel process	CV	[72]
11	Mitoxantrone	Monomer: β -CD	Electrochemical polymerization	CV, DPV	[73]
12	Hemoglobin	Monomer: Tetraethoxysilane	Magnetic molecularly imprinted process	CV, DPV	[74]
13	Trazosin	Monomer: MAA Crosslinker: EGDMA Initiator: 2,2'-AIBN	-	CV, DPV	[75]

Sl. No.	Target analyte	Components of MIP	Polymerization method	Principle of operation	Ref.
14	4-nonylphenol	Monomer: P-aminothio-phenol	Electrodepositing molecularly imprinted	CV, DPV	[76]
15	Lead ions	Monomer: Acrylamide Crosslinker: N,N'-Methylene-bis-acrylamide Initiator: AIBN	Ion-imprinting process	CV, DPV	[77]
16	Cyclophosphamide	Monomer: O-aminophenol	-	CV	[78]
17	Glucose	Monomer: MAA Crosslinker: EGDMA Initiator: AIBN	-	CV	[79]
18	Diphenylamine	Monomer: MAA Crosslinker: EGDMA Initiator: AIBN	-	DPV	[80]
19	Chlorpyrifos	Monomer: p Aminothiophenol	Photoelectrochemical process	CV	[81]
20	Manganese (II) ions	Monomer: MAA Crosslinker: EGDMA Initiator: 2,2'-azobisisobutyronitrile (AIBN)	-	SWASV	[82]
21	Thiamethoxam	Monomer: p-vinylbenzoic acid Crosslinker: EGDMA Initiator: AIBN	-	CV	[83]
22	Patulin	Monomer: p-Aminothiophenol	Electropolymerization	CV, DPV	[84]
23	Sunset Yellow	Monomer: MAA Crosslinker: EGDMA Initiator: AIBN	Precipitation polymerization	CV	[85]
24	Estrone 3-sulfate sodium salt	Monomer: Acrylamide Crosslinker: EGDMA Initiator: AIBN	-	CV	[86]
25	Quercetin	Monomer: aminobenzoic acid	Electropolymerization process	CV, DPV, EIS	[87]
26	Naloxone	Monomer: 4 aminobenzoic acid (4-ABA)	Electropolymerization process	CV, DPV	[88]
27	Loratadine	Monomr: MAA Crosslinker: EGDMA Initiator: AIBN	Bulk polymerization technique	CV, DPV, EIS	[89]
28	17-beta-Estradio	Monomer: Aniline	Electropolymerization process	CV, DPV, EIS	[90]
29	2,4 dichlorophenol	Monomr: MAA Crosslinker: EGDMA Initiator: AIBN	-	CV, DPV	[91]
30	Atrazine	Monomr: MAA Crosslinker: EGDMA Initiator: AIBN	Polymerization by means of UV light	CV	[92]
31	Sulfaguanidine	Monomr: Acrylamide Crosslinker: N, N-methylenebisacrylamide (NNMBA)	Electropolymerization process	DPV, EIS	[93]

The MIP-CPE, which is highly sensitive, was developed by Zhou et al. [63] for the detection of curcumin using a modified carbon glue cathode MIP (MIP-CPE). In order to prepare curcumin MIP (CUR-MIP), thermally actuated precipitation polymerization was used, with curcumin (CUR) as a template molecule, 2,20-azodiisobutyronitrile (AIBN) as the initiator, methacrylic acid (MAA) as the monomer, and ethylene glycol dimethacrylate (EDGMA) as the crosslinker. Electrochemical studies predicted that CUR exhibited a particular oxidation peak (E_{pa}) at 0.434 V (in comparison with SCE) in the pH 3.06 phosphate buffer solution. In this study, peak currents are 4-5 times greater than those observed with bare CPE. In this study, 10.1 nM was observed as the detection limit. Thus, CUR can be directly determined. It was found that 90.77–99.7% of the CUR in food substances could be recovered using this technique.

MIP sensors have been used to measure melatonin by Pankaj et al. [64]. The sensor synthesized using graphene (GR) and 4-amino-3-hydroxy-1-naphthalenesulfonic acid (AHNSA) and melamine (MM). Electro-polymerization of AHNSA and MM in the presence of melatonin was performed to synthesize the MIP. The linear range was observed to be 0.05 to 100 mM L⁻¹. The lowest detection limit was found to be 60×10^{-10} mol L⁻¹.

An innovative electrochemical sensor for the detection of rutin was proposed by Yang et al. [66]. The ternary combination of graphene oxide (rGO), magnetite (Fe₃O₄), and silver nanoparticle (Ag), which was made using the one-step solvothermal process, was used to create the sensor. The screen printed electrode was modified to allow for the detection of rutin using this ternary MIP composite. RT particles were captivated on the rGO/Fe₃O₄/Ag surface owing to the electrostatic force. A polymerization procedure was used to complete the MIP after that. The synthesised rGO/Fe₃O₄/Ag-MIP electrode provided a highly sensitive detection for rutin under optimal circumstances. The sensor was discovered to be linear between 1.0×10^{-2} and 10.0 μM and between 10.0 and 3.0×10^3 μM. The suggested sensor's detection limit was discovered to be as low as 4.2×10^{-3} μM. The sensor produced satisfactory results for the detection and measurement of rutin in pharmaceutical samples.

Tyrosine was demonstrated to be detected by Nihal et al. [68]. The molecularly imprinted polypyrrole film, which was utilised at the gold electrode for tyrosine detection, was used by the authors to apply the molecularly imprinted polymer approach (Tyr). Tyr served as the template molecule in this instance and was polymerized in the presence of pyrrole, the designated

monomer. An alternate polymer surface was also created for comparative purposes, although it did not contain the template molecule. In comparison to other essentially equivalent particles, the imprinted polypyrrole sensor demonstrated excellent selectivity for tyrosine.

In their work, Bai et al. [69] suggested a unique method for the MIP technology based detection of colchicines in pharmaceuticals and serum. Methacrylic acid was employed as the functional monomer in the development of an electrochemical sensor based on composite materials of graphene/Au nanoparticles (G@AuNPs) and modified glass carbon electrodes (GCEs). By in situ polymerization of membranes imprinted with colchicines, the film was created on the G@AuNPs modified GCE. The electrode's conductivity rose as a result of the gold nanoparticles' alteration of the sensor, which raised the sensor's selectivity. Additionally, an increase in electrode surface area and sensor catalytic efficiency was seen. As a catalyst, the imprinted membrane ensured exceptional selectivity and a high potential for anti-interference.

In the study by Sebastian et al. [77], a multiwalled carbon nanotube was used as the base material to create a sensitive electrochemical sensor to detect the lead ions. For the highly selective detection of lead ions, the recognition sites for lead particles were etched on MWCNTs (MWCNT-IIP) using lead particles as templates and NNMBA-crosslinked polyacrylamide as a strong matrix. Ion imprinted polymers (IIP) and non-imprinted polymers (NIP) without MWCNT were also tested to determine the MWCNT's intended use. The ion imprinted polymer shown strong lead ion selectivity in both systems. The electrochemical characteristics of the sensor with regard to lead ion detection were examined using CV and DPV.

Chlorpyris (CPF) detection employing MIP-based technology was suggested in the paper put out by Sun et al. [81] for its sensitive and effective detection. A molecularly imprinted polymer (MIP)-modified titanium dioxide nanorod (TiO₂ NR)-based photo electrochemical (PEC) sensor was created. TiO₂ NRs were created hydrothermally on a tin oxide substrate with fluorine doping. Hydrogen bonds formed during the electropolymerization process used to prepare MIP. The photocurrent response has an inverse relationship with the CPF concentration because of the insulating layer that prevents light from being harvested. The devised sensor was very stable and selective for the detection of CPF in the existence of other pesticides.

Another imprinted electrochemical sensor for distinguishing particularly sunset yellow was created by Qin et al. [85] utilising a glassy carbon cathode (GCE) that has been modified by graphene oxide and embellished with silver nanoparticles-MIP (GO/AgNPs-MIPs). By employing bulk polymerization techniques, MIP was created using different ratios and combinations of monomer, template, and cross linker. The amount of the imprinting factor by the choice of reagent (methanol and water) was evaluated in order to obtain satisfactory results in waste water tests. The polymer used in the methanol experiment did not show strong selectivity for atrazine. According to Scatchard analysis, the MIP was dependent on low levels of atrazine fixation (up to 40 mg/L), as the cavities that were formed in the MIP showed the influence of the cavities.

1.5. Objectives and scope of the thesis

The current study is concentrated on the use of the MIP approach for the individual measurement of a few food additive molecules, namely formalin, metanil yellow, and vanillin. With regard to the development of the sensors, several exploratory factors have been thoroughly examined, including the effects of pH, buffer, and scan rate. The following summarises the goals of this thesis work:

- The identification of monomers, crosslinkers, and initiators is necessary for the development of MIP sensors for formalin, vanillin, and metanil yellow.
- Identification of the sensor materials' size, structural, and morphological differences.
- Optimization of the experimental setup and investigation of the electrodes' electrocatalytic characteristics.
- Analyze the electro-analytical characteristics of different electrodes.

The entire thesis has been organized into five chapters in light of the aforementioned goals. Below is a quick chapter-by-chapter dissection of the thesis.

Chapter 1 describes the cause of the problem and exemplifies the goals of this thesis study. The distinct transduction mechanisms are then presented in the chapter. It also focuses on the numerous conventional techniques used recently for several food additive determinations as well their benefits and drawbacks. It was followed by a description of how MIP-based recognition systems may be used to overcome the challenges posed by conventional electrochemical

identification techniques. Here, a brief literature review of MIP-based sensing utilizing conventional approaches is presented after a brief description of the MIP method. The chapter concludes with a summary of the work's goals and scope.

Chapter 2 discusses the rapid electrochemical detection of noxious food additive formalin in the current study using three different approaches. Firstly, voltammetry responses performed in formalin with a noble metal Pt electrode reflected an extensive linearity. An index of high separability was achieved in successful data clustering using PCA. Furthermore, two regression models, the PLSR and the PCR, provided high prediction accuracies. In addition to their cost and lack of molecule selectivity, noble metal electrodes provided satisfactory analytical results. Hence, in the following work the metal oxide modification of the carbon paste was implemented to enhance electrode efficacy. Owing to its exceptional characteristics, CeO₂ nanocomposites over graphite were considered to achieve formalin detection with excellent electroanalytical features. Furthermore, the CeO₂@GP electrode provided moderately good electroanalytical characteristics over a period of time. The electrode also exhibited excellent performance over mushroom extracts. There were several challenges from the previous work, including limited linear range of operation, a limited detection limit, and a limited ability to recognize specific template molecules. Thus, inexpensive polymers with recognition cavities played a solution to selective electrocatalytic activities. Molecular imprinted acrylonitrile polymer (MIP) based electrochemical sensor was explored as a constructive solution. This MiPAN@GP electrode exhibited reasonably good selectivity and stable behaviour providing much improved performance in terms of linear range as well as LOD compared to the previous works. The electrode demonstrated accurate actual sample analysis in fish and mushroom extracts when the results were compared to the HPLC approach.

Chapter 3 presents the two different approaches being used in the present study to learn about the rapid electrochemical detection of food additive metanil yellow. As a first step, we analyzed voltammetry responses in metanil yellow while modifying the carbon paste with metal oxides to increase electrode efficacy. The electroanalytical features of NiCo₂O₄ nanocomposites over graphite are considered excellent due to their exceptional characteristics. Moreover, the NiCo₂O₄@GP electrode over time demonstrated moderate electroanalytical properties. Furthermore, the electrode performed well against turmeric powder. The linear range of operation, the detection limit, and the capacity to identify particular template molecules were all

constrained till the earlier research. A solution to selective electrocatalytic activity was therefore found in inexpensive polymers with recognition cavities. Electrochemical sensors based on molecule imprinted methacrylic acid polymer (MIP) were investigated as a possible solution. Compared to the previous work, this MIP electrode demonstrated reasonable selectivity and stable behavior, significantly improving linear range and LOD. Compared to HPLC technique, the electrode also demonstrated highly accurate analysis of turmeric powder and pigeon pea extracts.

Chapter 4 presents a MIP based sensor for estimation of vanillin in desserts. Here also, a monomer, EGDMA as a crosslinker and benzoyl peroxide as an initiator were used for the synthesis of specific vanillin sensor. Ultraviolet – Visible (UV-Vis.) spectroscopy has been used for characterization of the MIP material before and after removing the template molecule. The comparative study with other research reports of vanillin determination has been presented in this chapter.

Chapter 5 proposes a concept towards fabrication of a low-cost, portable food quality assessment device that has been developed based on App-based display. The system setup comprises of a) the specifically developed molecular imprinted (MIP) electrochemical sensors for target analytes and b) the quality assessment instrumentation interface. The system comprises of Arduino UNO-based function generator with a signal conditioning unit, a potentiostat circuit, Arduino Nano-based output response sampler, a data acquisition, and a display through a user interface.

Chapter 6 shows a general outline of the work done and highlights the finishing up comments. The important points and weaknesses of the proposed framework have been examined here with certain suggestions and a few proposals are presented which may be taken up later.

References

- [1] Md. Sazedul Hoquea, Liesbeth Jacxsensb, Bruno De Meulenaerb and AKM Nowsad Alamc, “Quantitative risk assessment for formalin treatment in fish preservation: food safety concern in local market of Bangladesh,” *Procedia Food Science*, vol. 6, pp. 151 – 158, 2016.
- [2] R.G. Liteplo, R. Beauchamp, M.E. Meek, R. Chénier, “FORMALDEHYDE,” World Health Organization, Geneva, 2002.
- [3] P. Nath, P. Sarkar, K. Tarafder, P. Mondal, M. Das, K., and G. Paul, “Practice of using metanil yellow as food colour to process food in unorganized sector of West Bengal - A case study,” *Int. Food Res. J.*, vol. 22, pp. 1424-1428, 2015.
- [4] L. Chen, K. Chaisiwamongkhol, Y. Chen, and R. G. Compton, “Rapid electrochemical detection of vanillin in natural vanilla,” *Electroanalysis*, vol. 31, pp. 1067–1074, 2019.
- [5] A. Sharma, S. C. Verma, N. Saxena, N. Chadda, N. P. Singh, A. K. Sinha, “Microwave- and ultrasound-assisted extraction of vanillin and its quantification by high-performance liquid chromatography in *Vanilla planifolia*,” *J. Sep. Sci.*, vol. 29, pp. 613–619, 2006.
- [6] E. Anklam, S. Gaglione, A. Muller, “Oxidation behaviour of vanillin in dairy products,” *Food Chem.*, vol. 60, pp. 43–51, 1997.
- [7] Supatinee Kongkaewa, Proespichaya Kanatharana, Panote Thavarungkula, Warakorn Limbuta, “A preparation of homogeneous distribution of palladium nanoparticle on poly (acrylic acid)-functionalized graphene oxide modified electrode for formalin oxidation,” *Electrochimica Acta*, vol 247, pp. 229–240, 2017.
- [8] Gabriel F. Pinto, Diogo L. Rocha, Eduardo M. Richter, Rodrigo A. A. Muñoz, and Sidnei G. da Silva “A Multicommuted Flow System for Spectrophotometric Determination of Formaldehyde in Mushroom,” *J. Braz. Chem. Soc.*, vol. 29, pp. 1400-1405, 2018.
- [9] P. Wahed, Md.A. Razzaq, S. Dharmapuri, M. Corrales, “Determination of formaldehyde in food and feed by an in-house validated HPLC method,” *Food Chem.*, vol 202, pp. 476–483, 2016.
- [10] S. Bonan, G. Fedrizzi, S. Menotta, and C. Elisabetta, “Simultaneous determination of synthetic dyes in foodstuffs and beverages by high-performance liquid chromatography coupled with diode-array detector,” *Dyes and Pigments*, vol. 99, pp. 36–40, 2013.
- [11] S. Dhakal, K. Chao, W. Schmidt, J. Qin, M. Kim, and D. Chan, “Evaluation of Turmeric Powder Adulterated with Metanil Yellow Using FT-Raman and FT-IR Spectroscopy,” *Foods*, vol. 5, 2016.

Chapter 1: Introduction and scope of the thesis

- [12] S. Kar, B. Tudu, A.K. Bag, and R. Bandyopadhyay, "Application of Near-Infrared Spectroscopy for the Detection of Metanil Yellow in Turmeric Powder," *Food Anal. Methods.*, vol. 11, pp. 1–12, 2017.
- [13] G. Lamprecht, F. Pichlmayer, and E.R. Schmidt, "Determination of the authenticity of vanilla extracts by stable isotope ratio analysis and component analysis by HPLC," *J. Agric. Food Chem.*, vol. 42, pp. 1722–1727, 1994.
- [14] K.N. Waliszewski, V.T. Pardio, and S.L. Ovando, "A simple and rapid HPLC technique for vanillin determination in alcohol extract," *Food Chem.*, vol. 101, pp. 1059–1062, 2006.
- [15] Y. Shen, C. Han, B. Liu, Z.F. Lin, X.J. Zhou, C.J. Wang, and Z.O. Zhu Z, "Determination of vanillin, ethyl vanillin, and coumarin in infant formula by liquid chromatography-quadrupole linear ion trap mass spectrometry," *J. Dairy Sci.*, vol. 97, pp. 679–686, 2014.
- [16] T. Sostaric, M.C. Boyce, and E.E.J. Spickett, "Analysis of the volatile components in vanilla extracts and flavorings by solid-phase microextraction and gas chromatography," *J. Agric. Food Chem.*, vol. 48, pp. 5802–5807, 2000.
- [17] D.L. Jager, G.A. Perfetti, and G.W. Diachenko, "Comparison of headspace-SPME-GC-MS and LC-MS for the detection and quantification of coumarin, vanillin, and ethyl vanillin in vanilla extract products," *Food Chem.*, vol. 107, pp. 1701–1709, 2008.
- [18] M.C. Boyce, P.R. Haddad, and T. Sostaric, "Determination of flavour components in natural vanilla extracts and synthetic flavourings by mixed micellar electrokinetic capillary chromatography," *Anal. Chim. Acta.*, vol. 485, pp. 179–186, 2003.
- [19] M. Ohashi, H. Omae, M. Hashida, Y. Sowa, and S. Imai, "Determination of vanillin and related flavor compounds in cocoa drink by capillary electrophoresis," *J. Chromatogr.*, vol. A 1138, pp. 262–267, 2007.
- [20] A. Longares-Patron, and M.P. Canizares-Macias, "Focused microwave-assisted extraction and simultaneous spectrophotometric determination of vanillin and p-hydroxybenzaldehyde from vanilla fragans," *Talanta*, vol. 69, pp. 882–887, 2006.
- [21] M. Palit, B. Tudu, P. K. Dutta, A. Dutta, A. Jana, J. K. Roy, N. Bhattacharyya, R. Bandyopadhyay, A. Chatterjee, "Classification of black tea taste and correlation with tea taster's mark using voltammetric electronic tongue," *IEEE Trans. Instrum. Meas.*, vol. 59, pp. 2230–2239, 2010.
- [22] B. J. Privett, J. H. Shin, M. H. Schoenfisch, *Electrochemical sensors*, *Anal. Chem.*, vol. 80, pp. 4499–4517, 2008.
- [23] F. Scholz, "Voltammetric techniques of analysis: the essentials," *Chem Texts*, vol 1, pp.1-24, 2015.
- [24] Autolab application note EC08, Basic overview of the working principle of a potentiostat/galvanostat (PGSTAT)-Electrochemical cell setup, pp.1-3, 2011.

- [25] F. Scholz, "Voltammetric techniques of analysis: the essentials," Chem Texts, vol.1, pp. 1-24, 2015.
- [26] H. H. Willard, Jr. L. L. Merrit, J. A. Dean, Jr. F. A. Settle, "Instrumental methods of analysis," 6th Edn. D. Van Nostrand, Princeton, 1981.
- [27] https://www.basinc.com/manuals/EC_epsilon/Techniques/Pulse/pulse
- [28] F. H. Dickey, "The preparation of specific adsorbents," Proc. Natl. Acad. Sci. U.S.A. vol. 35, 227-229, 1949.
- [29] F. H. Dickey, "Specific adsorption", J. Phys. Chem. vol.59, pp. 695-707, 1955.
- [30] L. Pauling, "A theory of the structure and process of formation of antibodies," J. Am. Chem. Soc., vol.62, pp. 2643-2657, 1940.
- [31] A. G. Mayes, M. J. Whitcombe, "Synthetic strategies for the generation of molecularly imprinted organic polymers," Adv. Drug. Del. Rev., vol. 57, pp. 1742-1778, 2005.
- [32] S. Piletsky, S. Piletsky, I. Chianella, "MIP-based sensors in molecularly imprinted sensors: Overview and applications," Elsevier, ISBN No. 978-0-444-56331-6, 2012.
- [33] D. A. Spivak, "Optimization, evaluation and characterization of molecularly imprinted polymers," Adv. Drug Del. Rev., vol. 57, pp. 1779-1794, 2005.
- [34] L. Chen, S. Xu, J. Li, "Recent advances in molecular imprinting technology: current status, challenges and highlighted applications," Chem. Soc. Rev., vol.40, pp. 2922-2942, 2011.
- [35] P. Wang, X. Sun, X. Su, T. Wang, "Advancement on molecularly imprinted polymers in food safety field," Analyst, pp. 141 3540-3553, 2016.
- [36] G. Wulff, S. Schauhoff, "Enzyme-analog-built-polymers: 27 Racemic-resolution of free sugars with macroporous polymers prepared by molecular imprinting-selectivity dependence on the arrangement of functional group versus requirements," J. Org. Chem. vol.56, pp. 395-400, 1991.
- [37] A. Kugimiya, J. Matsui, T. Takeuchi, K. Yano, H. Muguruma, A. V. Elgersma, I. Karube, "Recognition of sialic-acid using molecularly imprinted polymer," Anal. Lett., vol.28, 2317-2323, 1995.
- [38] A. Kugimiya, J. Matsui, H. Abe, M. Abrutani, T. Takeuchi, "Synthesis of castasterone selective polymers prepared by molecular imprinting," Anal. Chim. Acta., vol.365, pp. 75-79, 1998.
- [39] G. Wulff, J. Vietmeier, "Enzyme-analogue built polymers: 26. Enantioselective synthesis of amino acids using polymers possessing chiral cavities obtained by an imprinting procedure with template molecules," Makromol. Chem. vol.190, pp.1727-1735, 1989.

Chapter 1: Introduction and scope of the thesis

- [40] N. Sallacan, M. Zayats, T. Bourenko, A. B. Kharitonov, I. Wilner, "Imprinting of nucleotide and monosaccharide recognition sites in acrylamide phenylboronic acid-acrylamide copolymer membranes associated with electronic transducers," *Anal. Chem.*, vol. 74, pp.702-712, 2002.
- [41] S. H. Gao, W. Wang, B. H. Wang, "Building fluorescent sensors for carbohydrates using template-directed polymerizations," *Bioorg. Chem.* vol.29, pp. 308-320, 2001.
- [42] S. A. Piletsky, K. Piletskaya, E. V. Piletskaya, K. Yano, A. Kugimiya, A. V. Elgersma, R. Levi, U. Kahlow, T. Takeuchi, I. Karube, T. I. Panasyuk, A. V. Elskaya, "A biomimetic receptor system for sialic acid based on molecular imprinting," *Anal. Lett.*, vol.29, pp.157-170, 1996.
- [43] W. Wang, S. H. Gao, B. H. Wang, "Building fluorescent sensors by template polymerization: the preparation of a fluorescent sensors for D-fructose," *Org. Lett.*, vol.1, pp. 1209-1212, 1999.
- [44] Y. Kanekiyo, M. Sano, R. Iguchi, S. Shinkai, "Novel nucleotide-responsive hydrogels designed from copolymers of boronic acid and cationic units and their application as a QCM resonator system to nucleotide sensing," *J. Polym. Sci. A. Polym. Chem.* vol.38, pp.1302-1310, 2000.
- [45] A. Bossi, S. A. Piletsky, E. V. Piletska, P. G. Righetti, A. P. F. Turner, "Surface-grafted molecularly imprinted polymers for protein recognition," *Anal. Chem.*, vol. 73, pp. 5281-5286, 2001.
- [46] G. Wulff, R. Dederichs, R. Grotstollen, C. Jupe, "On the chemistry of binding sites: II. Specific binding of substances to polymers by fast and reversible covalent interactions in: T.C.J. Gribnau, J. Visser, R.J.F. Nivard (Eds.) , " *Affinity Chromatography and Related Tech.*, pp. 207-216, 1982.
- [47] G. Wulff, "Selective binding to polymers via covalent bonds-the construction of chiral cavities as specific receptor sites," *Pure Appl. Chem.* vol. 54, pp. 2093-2102, 1982.
- [48] C. Alexander, C. R. Smith, M. J. Whitecombe, E. N. Vulfsen, "Imprinted polymers as protecting groups for regioselective modification of polyfunctional substrates," *J. Am. Chem. Soc.*, vol.121, pp. 6640-6651, 1999.
- [49] G. Wulff, W. Best, A. Akelah, "Enzyme-analogue built polymers, 17 Investigations on the racemic resolution of amino acids," *React. Polym.* vol.2, pp. 167-174, 1984.
- [50] K. J. Shea, T. K. Dougherty, "Molecular recognition on synthetic amorphous surfaces-the influence of functional group positioning on the effectiveness of molecular recognition," *J. Am. Chem. Soc.* vol.108, pp. 1091-1093, 1986.
- [51] K. J. Shea, D. Y. Sasaki, "On the control of microenvironment shape of functionalized network polymers prepared by template polymerization," *J. Am. Chem. Soc.*, vol. 111, pp. 3442-3444, 1989.

- [52] K. J. Shea, D. Y. Sasaki, "An analysis of small-molecule binding to functionalized synthetic polymers by C-13 CP/MAS NMR and FT-IR spectroscopy," *J. Am. Chem. Soc.*, vol.113, pp. 4109-4120, 1991.
- [53] G. Wulff, G. Wolf, "On the chemistry of binding sites: Part 6. On the suitability of various aldehydes and ketones as binding sites of monoalcohols," *Chem. Ber.* vol.119, pp. 1876-1889, 1986.
- [54] R. Arshady, K. Mosbach, "Synthesis of substrate-selective polymers by host-guest polymerization," *Makromol. Chem.* vol.182, pp. 687-692, 1981.
- [55] M. Sibrian-Vazquez, D. A. Spivak, "Molecular imprinting made easy," *J. Am. Chem. Soc.*, vol. 126, pp. 7827-7833, 2004.
- [56] M. J. Whitcombe, M. E. Rodriguez, P. Villar, E. N. Vulfson, "A new method for the introduction of recognition site functionality into polymers prepared by molecular imprinting-synthesis and characterization of polymeric receptors for cholesterol," *J. Am. Chem. Soc.*, vol.117, pp. 7105-7111, 1995.
- [57] M. Lubke, M. J. Whitecombe, E. N. Vulfson, "A novel approach to the molecular imprinting of polychlorinated aromatic compounds," *J. A. Chem. Soc.*, vol.120, pp. 13342-13348, 1998.
- [58] A. Katz, M. E. Davis, "Molecular imprinting of bulk, microporous silica," *Nature*, vol.403, pp. 286-289, 2000.
- [59] A. L. Graham, C. A. Carlson, P. L. Edmiston, "Development and characterization of molecularly imprinted sol-gel materials for the selective detection of DDT," *Anal. Chem.*, vol.74, pp. 458-467, 2002.
- [60] C. J. Percival, S. Stanley, A. Braithwaite, M. I. Newton, G. McHale, "Molecular imprinted polymer coated QCM for the detection of nadrolone," *Analyst*, vol. 127, pp. 1024-1026, 2002.
- [61] M. Petcu, J. Cooney, C. Cook, D. Lauren, P. Schaare, P. Holland, "Molecular imprinting of a small substituted phenol of biological importance," *Anal. Chim. Acta*, vol.435, pp. 49-55, 2001.
- [62] J. U. Klein, M. J. Whitecombe, F. Mulholl, E. N. Vulfson, "Template-mediated synthesis of a polymeric receptor specific to amino acid sequences," *Angew. Chem. Int. Ed.* vol.38, pp. 2057-2060, 1999.
- [63] Q. Zhou, H. Y. Zhai, Y. F. Pan, K. Lia, "A simple and sensitive sensor based on a molecularly imprinted polymer-modified carbon paste electrode for the determination of curcumin in foods," *RSC Adv.* vol.7, pp. 22913-22918, 2017.
- [64] P. Gupta, R. N. Goyal, "Graphene and Co-polymer composite based molecularly imprinted sensor for ultra trace determination of melatonin in human biological fluids," *RSC Adv.* vol.5, pp. 40444-40454, 2015.
- [65] Z. Yu, J. Yang, J. Zhong, S. Wu, Z. Xu, Y. Tang, "Emodin voltammetric sensor based on molecularly imprinted polymer membrane-modified electrode using a multiple hydrogen bonds strategy," *J. Appl. Polym. Sci.*, vol.126, pp. 1344-1350, 2013.

- [66] S. Yang, X. Yang, R. Tang, L. Xiong, Y. Yang, Y. Hu, C. Zhan, Z. Zhao, "A novel rutin electrochemical sensor using reduced graphene oxide/magnetite/silver nanoparticle-molecularly imprinted polymer composite modified electrode," *Int. J. Electrochem. Sci.*, vol.13, pp. 2483 – 2497, 2018.
- [67] S. Rebocho, C. M. Cordas, R. Viveiros, T. Casimiro, "Development of a ferrocenyl-based MIP in supercritical carbon dioxide: Towards an electrochemical sensor for bisphenol A," *J Supercrit Fluids*, vol.135, pp.98–104, 2018.
- [68] Nihal Ermiş and Nihat Tınkılıç, "Preparation of molecularly imprinted polypyrrole modified gold electrode for determination of tyrosine in biological samples," *Int. J. Electrochem. Sci.*, vol.13, pp.2286 – 2298, 2018.
- [69] H. Baia, C. Wanga, J. Chena, Z. Lia, K. Fub, Q. Caoa, "Graphene@AuNPs modified molecularly imprinted electrochemical sensor for the determination of colchicine in pharmaceuticals and serum," *J. Electroanal. Chem.*, vol.816, pp.7–13, 2018.
- [70] X. Zhu, Y. Zeng, Z. Zhang, Y. Yang, Y. Zhai, H. Wang, L. Liua, J. Hua, L. Li, "A new composite of graphene and molecularly imprinted polymer based on ionic liquids as functional monomer and cross-linker for electrochemical sensing 6-benzylaminopurine," *Biosens. Bioelectron.* vol.108, pp.38–45, 2018.
- [71] S. Zeinali, H. Khoshafa, M. R. H. Bagher, "Fabrication of a selective and sensitive electrochemical sensor modified with magnetic molecularly imprinted polymer for amoxicillin," *Anal. Bioanal. Chem. Res.*, vol.5, pp.195-204, 2018.
- [72] I. Razavipanaha, E. Alipourb, B. Deiminiata, G. H. Rounaghia, "A novel electrochemical imprinted sensor for ultrasensitive detection of the new psychoactive substance mephedrone," *Biosens. Bioelectron.* vol.119, pp.163–169, 2018.
- [73] Y. Liu, M. Wei, Y. Hu, L. Zhu, J. Du, "An electrochemical sensor based on a molecularly imprinted polymer for determination of anticancer drug Mitoxantrone," *Sens. Actuators B Chem.* vol.255, pp.544–551, 2018.
- [74] B. Sun, X. Ni, Y. Cao, G. Cao, "Electrochemical sensor based on magnetic molecularly imprinted nanoparticles modified magnetic electrode for determination of Hb," *Biosens. Bioelectron.*, vol.91, pp.354–358, 2017.
- [75] M. Roushani, Z. Jalilianb, A. Nezhadalib, "A novel electrochemical sensor based on electrode modified with gold nanoparticles and molecularly imprinted polymer for rapid determination of terazosin," *Colloids Surf. B*, vol.172, pp.594–600, 2018.
- [76] L. Zheng, C. Zhang, J. Ma, S. Hong, Y. She, A.M. Abd El-Aty, He, Hailong Yu, H. Liu, J. Wang, "Fabrication of a highly sensitive electrochemical sensor based on electropolymerized molecularly imprinted polymer hybrid nano composites for the determination of 4-nonylphenol in packaged milk samples," *Anal. Biochem.* vol.559, pp.44–50, 2018.

- [77] M. Sebastian, B. Mathew, "Ion imprinting approaches for the fabrication an electrochemical sensor and sorbent for lead ions in real samples using modified multiwalled carbon nanotubes," *J. Mater. Sci.*, vol.53, pp. 3557–3572, 2018.
- [78] B. Huang, L. Xiao, H. Dong, X. Zhang, W. Gan, S. Mahboob, K. A. Al-Ghanim, Q. Yuan, Y. Li, "Electrochemical sensing platform based on molecularly imprinted polymer decorated N,S co-doped activated graphene for ultrasensitive and selective determination of cyclophosphamide," *Talanta*, vol.164, pp.601–607, 2017.
- [79] S. Alexander, P. Baranecddharan, S. Balasubrahmanyam and S. Ramaprabhu, "Highly sensitive and selective non enzymatic electrochemical glucose sensors based on Graphene oxide-molecular imprinted polymer," *Mater. Sci. Eng. C*, vol.78, pp.124–129, 2017.
- [80] P. E. Hande, A. B. Samui, P. S. Kulkarni, "An efficient method for determination of the diphenylamine (Stabilizer) in propellants by molecularly imprinted polymer based carbon paste electrochemical sensor," *Propellants Explos. Pyrotech.*, vol.42, pp.376–380, 2017.
- [81] X. Sun, C. Gao, L. Zhang, M. Yan, J. Yu, S. Ge, "Photoelectrochemical sensor based on molecularly imprinted film modified hierarchical branched titanium dioxide nanorods for chlorpyrifos detection," *Sens. Actuators B Chem.*, vol.251, pp.1–8, 2017.
- [82] M. Roushani, Z. Saedi, F. Hamdi, B. Z. Dizajdizi, "Preparation an electrochemical sensor for detection of manganese (II) ions using glassy carbon electrode modified with multi walled carbon nanotube chitosan-ionic liquid nanocomposite decorated with ion imprinted polymer," *J. Electroanal. Chem.*, vol.804, pp. 1–6, 2017.
- [83] T. Xie, M. Zhang, P. Chen, H. Zhao, X. Yang, L. Yao, H. Zhang, A. Dong, J. Wang, Z. Wang, "A facile molecularly imprinted electrochemical sensor based on graphene: application to the selective determination of thiamethoxam in grain," *RSC Adv.*, vol.7, 38884–38894, 2017.
- [84] W. Guo, F. Pi, H. Zhang, J. Sun, Y. Zhang, X. Sun, "A novel molecularly imprinted electrochemical sensor modified with carbon dots, chitosan, gold nanoparticles for the determination of patulin," *Biosens. Bioelectron.* vol.98, pp.299–304, 2017.
- [85] C. Qin, W. Guo, Y. Liu, Z. Liu, J. Qiu, J. Peng, "A novel electrochemical sensor based on graphene oxide decorated with silver nanoparticles–molecular imprinted polymers for determination of sunset yellow in soft drinks," *Food Anal. Methods*, vol.10, pp.2293–2301, 2017.
- [86] H. Song, Y. Wang, L. Zhang, L. Tian, J. Luo, N. Zhao, Y. Han, F. Zhao, X. Ying, Y. Li, "An ultrasensitive and selective electrochemical sensor for determination of estrone 3-sulfate sodium salt based on molecularly imprinted polymer modified carbon paste electrode," *Anal. Bioanal. Chem.*, vol.409, pp.6509–6519, 2017.

- [87] L. Yang, B. Xu, H. Ye, F. Zhao, B. Zeng, "A novel quercetin electrochemical sensor based on molecularly imprinted poly (para-aminobenzoic acid) on 3D Pd nanoparticles-porous graphene-carbon nanotubes composite," *Sens. Actuators B Chem.*, vol.251, pp.601–608, 2017.
- [88] F. Lopes, J. G. Pacheco, P. Rebelo, C. Delerue-Matos, "Molecularly imprinted electrochemical sensor prepared on a screen printed carbon electrode for naloxone detection," *Sens. Actuators B Chem.*, vol.243, pp.745–752, 2017.
- [89] M. Roushani, A. Nezhadali, Z. Jalilian, A. Azadbakht, "Development of novel electrochemical sensor on the base of molecular imprinted polymer decorated on SiC nanoparticles modified glassy carbon electrode for selective determination of loratadine," *Mater. Sci. Eng. C*, vol.71, pp.1106–1114, 2017.
- [90] A. A. Lahcen, A. A. Baleb, P. Baker, E. Iwuoha, A. Amine, "Synthesis and electrochemical characterization of nanostructured magnetic molecularly imprinted polymers for 17- β -Estradiol determination," *Sens. Actuators B Chem.*, vol.241, pp.698–705, 2017.
- [91] Y. Liang, L. Yu, R. Yang, X. Li, L. Qu, J. Li, "High sensitive and selective graphene oxide/molecularly imprinted polymer electrochemical sensor for 2,4-dichlorophenol in water," *Sens. Actuators B Chem.*, vol.240, pp.1330–1335, 2017.
- [92] A. L. Ahmad, N. F. C. Lah, S. C. Low, "Configuration of molecular imprinted polymer for electrochemical atrazine detection," *J. Polym. Res.*, vol.25, pp.243, 2018.
- [93] N. E. A. E. Hassani, E. Llobet, L. Popescu, M. Ghita, B. Bouchikhi, N. E. Bari, "Development of a highly sensitive and selective molecularly imprinted electrochemical sensor for sulfaguanidine detection in honey samples," *J. Electroanal. Chem.*, vol.823, pp.647–655, 2018.
- [94] Longhui Nie, Jianguo Yu, Mietek Jaroniec and Franklin Feng Tao, "Room-temperature catalytic oxidation of formaldehyde on catalysts," *Catal. Sci. Technol.*, vol 6, pp. 3649, 2016.
- [95] R. Karami-Osboo1, M. Khodaverdi, F. Ali-Akbari, "Antibacterial effect of effective compounds of *satureja hortensis* and *thymus vulgaris* essential oils against *erwinia amylovora*," *J. Agr. Sci. Tech.*, vol.12, pp.35–45, 2010.



Fabrication of electrochemical sensors towards the detection of food preservative: Formalin

This chapter discusses the learning process underway regarding the rapid electrochemical detection of noxious food additive formalin in the current study using three different approaches. The electrodes also illustrated highly accurate real sample analysis in mushroom and fish extracts.

Publication outcomes of this chapter

- Formalin Detection using Platinum Electrode-Based Electrochemical System, Journal of The Institution of Engineers (India): Series B, vol. 103, pp. 1159-1165, 2022.
- A simple nano cerium oxide modified graphite electrode for electrochemical detection of formaldehyde in mushroom, IEEE Sens. J., vol. 21, pp. 12019 – 12026, 2021.
- Fabrication of A Molecular Imprinted Polyacrylonitrile Engraved Graphite Electrode for Detection of Formalin in Food Extracts, IEEE Sens. J., vol. 22, pp. 42–49, 2022.

Chapter 2

Fabrication of electrochemical sensors towards the detection of food preservative: Formalin

2.1. Introduction

Formalin (37% aqueous solution of formaldehyde) (FAL) one of the toxic food additives, as discussed in the previous section is extensively used by the traders to preserve various items like fish, meat, mushroom, milk, fruits, and vegetables [1], [2]. Literature revealed several techniques for quantitative estimation of formalin contents. High-performance liquid chromatography (HPLC) is a suitable stand-alone method that can provide effective detection of formaldehyde concentrations in food samples like milk, fish, fruits, mushrooms, and also vegetables [2]. A multicommuted flow based spectrophotometric detection of formaldehyde in mushroom has also been reported to provide optimum results with decent linear response and detection limit [3]. Another effective research employing NIR spectroscopy to analyse many variables about milk adulteration with formalin has been established [4]. Electrical impedance spectroscopy has also been used for a number of other straightforward procedures for the identification of formalin contaminants in actual samples [5]–[7]. Yet to use these techniques, you need pricey, high-end equipment and skilled staff to run the machinery. Although certain rapid and on spot detection techniques based upon colorimetric changes are available, these methods may not provide effective calibrations [8]-[13]. On the other hand, instant qualitative formaldehyde detection and estimation in seafood using electronic nose with multivariate analysis techniques have been a potential choice [14]-[16]. Here, resistive thin film gas sensors were inadequately selective [17], [18]. To attain higher selectivity response profile, the polymer technology surpassed other techniques [19]-[22]. For instance, experimentation with an imprinted polymer of methacrylic acid infused with gold nanoparticles demonstrated higher interactions to the recognition sites with greater surface area [23]. Quartz Crystal Microbalance (QCM) coated with molecular imprinted polymers exhibited higher selectivity and sensitivity

profile of sensors [24], [25]. Unfortunately, these technologies were confined to the vapor state formaldehyde detection only. These processes may become time consuming and expensive for real time sample scanning. To overcome these challenges, electrochemical techniques can provide a rapid, simple, and effortless estimation of formaldehyde.

Studies on electrochemical analysis, reported so far using several conventional electrodes, encountered limitations like lack of selectivity, slow electron transfer rate, and low sensitivity. Electrochemical detection of formaldehyde in food sample using biosensors have been reported in [26]-[28]. Biosensors like 24-base adenine-thymine (AT), 15-base guanine, and 24-base guanine rich DNA sequences suffered a lack of reproducibility [26]. Similarly, Os(bpy)₂-poly(vinylpyridine) (POs-EA) modified screen printed electrode (SPE) and Formaldehyde dehydrogenase (FDH), gold nanoparticles (AuNPS), 1-ethyl-3 methylimidazolium trifluoro methane sulfonate ([EMIM][OTF]) and chitosan (CHIT) (FDH/AuNPS/([EMIM][OTF])/CHIT) modified electrode display reduced stability and low recovery rates respectively [27], [28]. But, the optimization of suitable biosensor materials is also difficult. In order to fabricate highly sensitive and selective sensors for FAL, it was necessary to develop highly robust and specific sensors. Thus, the electrochemical sensing approach has been explored and improvised with three different approaches to the purpose.

2.2. Formalin detection using platinum electrode-based electrochemical system

In this work, an electrochemical sensor system has been implemented as a novel and simple approach. Using chemometrics, this study investigated for the first time the electrochemical data obtained for formalin detection. Most of the reported works are based on vapor phase formalin detection and expensive spectroscopic methods. Hence, the significance of electrochemical measurement can be useful for quantitative, rapid and on spot food adulteration detection in liquid phase. The application of chemometrics over electrochemical data can thus establish a well-defined classification between different limits of formaldehyde adulteration in various food supplies from the traders. In the proposed work, a low cost, rapid electrochemical detection system of formalin (FAL) using a platinum (Pt) working electrode has been fabricated. The electrochemical performances were recorded using a three-electrode system and a potentiostat device. The responses obtained have been analyzed by means of cyclic voltammetry (CV) procedure in addition differential pulse voltammetry (DPV). Quantitative discrimination

among several formaldehyde contents has been established using principal component analysis (PCA). Quantitative estimation of formalin content was also analyzed with PLSR (partial least square regression) method along with PCR (principal component regression) process. Consequently, the Pt working electrode will be able to accomplish recognition of distinct formalin traces in a variety of food deliveries at the user end.

2.2.1. Experimental

2.2.1.1. Chemicals and reagents

Formalin (formaldehyde solution in aqueous medium, 37%) was acquired from the Merck, India. Potassium chloride (KCl) besides sodium hydroxide (NaOH) were obtained from the Sigma Aldrich, India. Analytical grade chemicals were used. Millipore water was used to prepare the experimental solutions. The experimentations were executed at ambient temperature.

2.2.1.2. Apparatus and Instruments

The analysis for electrochemistry was carried out using a three-electrode set up and a potentiostat PGSTAT101 (Metrohm Autolab, Netherlands). The three-electrode system comprised of a working electrode (Pt), a reference electrode (Ag/AgCl) with a counter electrode (steel). NOVA software provided by Metrohm Autolab demonstrated the graphical illustrations of CV and DPV responses. An ultrasonicator (Labman Scientific instrument) was used to blend the experimental solutions.

2.2.1.3. Experimental set-up

The electrochemical experiments were accomplished using a system comprising three different electrodes, a working electrode (Pt), a reference electrode (Ag/AgCl) and a counter electrode (steel) connected with potentiostat PGSTAT1010 which was then interfaced with a computer. The voltammetry responses were realized over NOVA interface for users. A graphic representation of the setup used during experimentation process is depicted in fig. 2.1.

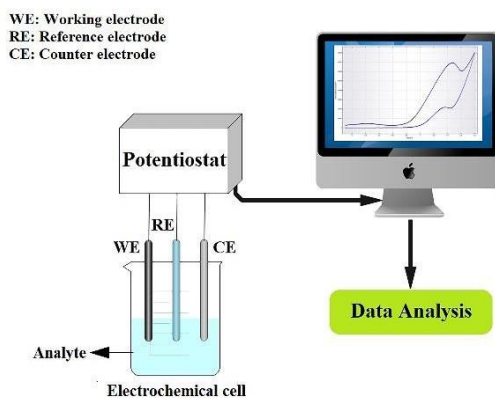


Fig.2.1 An illustration of the experimental setup.

2.2.1.4. Data analysis

The electrochemical data obtained was analysed using MATLAB 2017 version. Quantitative data investigation means principal component analysis (PCA) was exercised to investigate the Pt electrode performance. Four sets of repetitions were noted for each of the four concentrations 5 μ M, 10 μ M, 50 μ M and 100 μ M of FAL. Classification accuracy of the electrode was evaluated by support vector machine and linear discriminant classifiers. Quantitative estimation was also analyzed by PLSR and PCR tools.

2.2.2. Results and Discussions

2.2.2.1. Electrochemical behaviour of Pt working electrode

The electrochemical behaviour of the Pt working electrode was analysed using voltammetry technique. 2.5 mM of target analyte formalin was subjected to electrochemical analysis in the presence of the supporting electrolyte, 0.1 M NaOH. The CV response of the Pt electrode was observed over an applied potential of -0.1 to 1.6 V. Fig. 2.2 depicts a pair of redox peaks in the existence of target molecule FAL, whereas in the absence of target molecule the peak was absent. The electrochemical reaction was confirmed at the electrode surface due to the appearance a pair of redox peaks with an oxidation peak at potential 1.47 V; 694.86 μ A current and a reduction peak at potential 1.45V; 210.84 μ A current, in the presence of target analyte FAL.

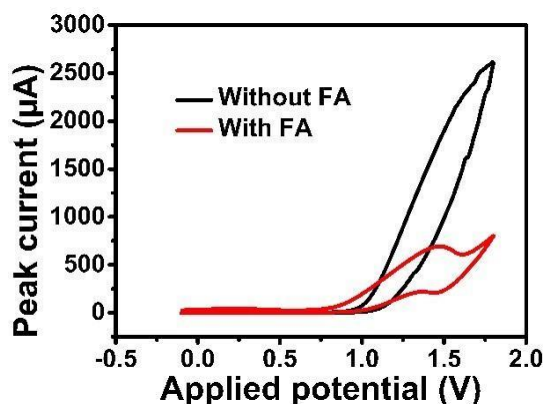


Fig. 2.2 CV outcome of working electrode (Pt) with and without FAL in 0.1 M NaOH.

2.2.2.2. Outcome for different scan rate variation

Consequence of varying scan rate and the effect on the peak current due to oxidation at the Pt electrode was inspected by CV technique. The responses were noted within a the applied range of potential 0.5 to 1.8 V. An increase of oxidation peak was detected as shown in fig. 2.3.a for increase in scan rate in the range 10 to 100 mV/s. A variation in scan rate causes changes in equilibrium at electrode surface and hence over voltage drifts may occur resulting a shift of peak potential. Fig. 2.3.b illustrates a regression plot which is linear for oxidation peak against scan rate then the regression equation obtained as, $y = 4.49x + 704.79$; $R^2 = 0.99$. The rise of maximum peak current through increase in scan rate confirmed an absorption-controlled process [29].

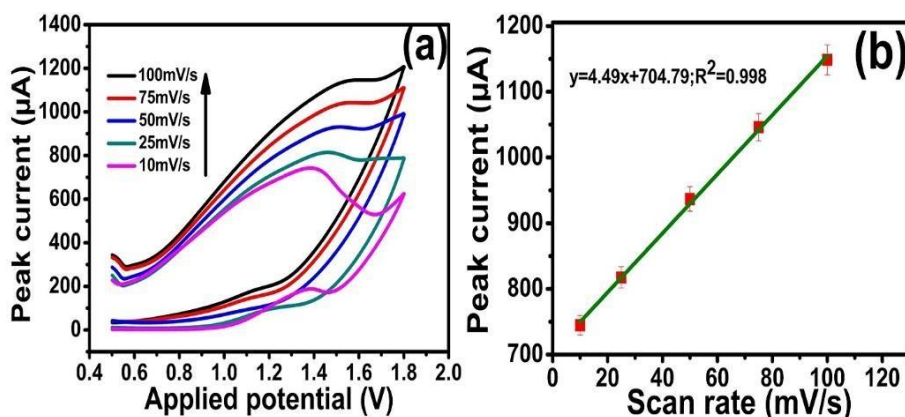


Fig.2.3 (a) CV outcome of varying peak current with different scan rate from 10 to 100 mV/s, (b) linear regression scheme of peak current vs. scan rate in 0.1M NaOH.

2.2.2.3. Effect of concentration variation

The DPV responses within a potential range from 0.8 to 1.6 V were noted with varying concentrations from 100 to 1000 μM FAL in 0.1M NaOH solution. Fig. 2.4.a shows the peak current increases with increase in concentration. fig. 2.4.b represents the linearity of peak current with concentration variation with the given equation $y = 0.32x + 99.27$; $R^2 = 0.975$. The lowest limit of detection was obtained as 5 μM using $\text{LOD} = 3 \sigma / m$ where σ is the standard deviation and m is the calibration curve slope respectively.

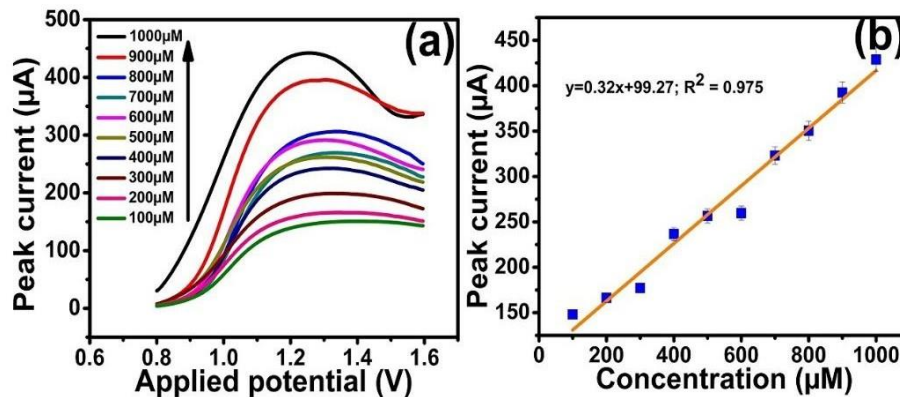


Fig. 2.4 DPV outcome for formaldehyde by means of Pt electrode within 0.1 M NaOH. (a) 100-1000 μM . (b) Linear regression plot for peak current vs. different concentration.

2.2.2.4. Principal component analysis

PCA does a transformation (orthogonal) of a set of data which is linear with good correlation into a set of variables without any correlation called principal components (PCs) [30]. The transformed data space directions for first two or three PCs provides a graphical representation of the multivariate data analysis. Separability index (SI) is a quantitative measurement of discrimination of diverse formalin concentrations. SI is demarcated by a fraction of trace between (S_b) to trace within (S_w) of class scatter matrix. The DPV responses obtained using Pt electrode for different FAL concentrations 5 μM , 10 μM , 50 μM and 100 μM were analysed using PCA. Four repetitions were taken for individual concentrations. Fig. 2.5 shows the PCA plot with successful data clustering. All the four different concentrations were

effectively discriminated using PCA. The PCA score plot depicts 97.5%, 2.02% and 0.39% of total variances respectively. A high value of class separability index was obtained as 25.68.

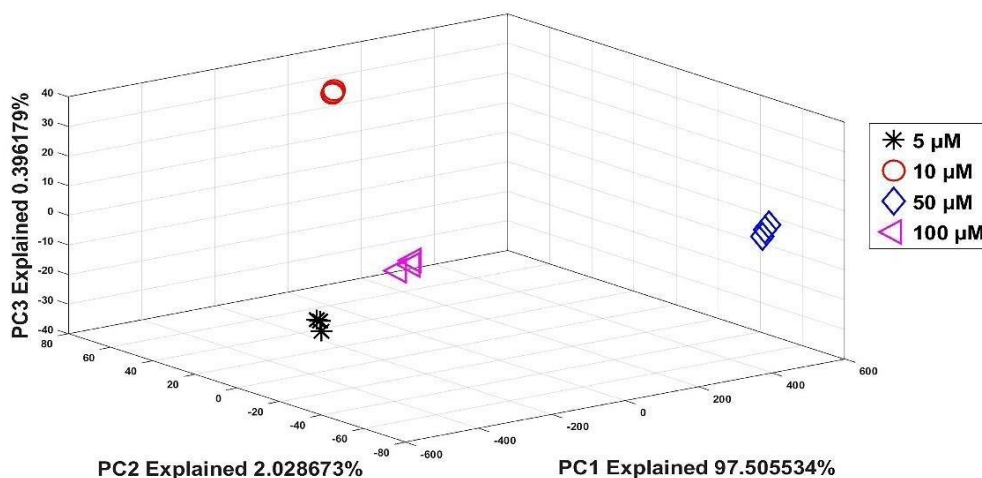


Fig. 2.5 Graphical illustration of DPV response analysis by PCA.

2.2.2.5. Partial least square regression (PLSR)

PLSR algorithm extracts the components through high correlation among predictors and response variable quantity thus reduces the predictors count [26]. In the present analysis cross validation (leave one out) has been used to estimate the investigative measurements for the sensor. Different parameter like correlation factor (CF), RMSEV (root mean square error of validation), and RMSEP (root mean square error of prediction) replicated the level of correlation among the predicted and actual values. Prediction capability of the Pt electrode has been estimated in this work using four diverse concentrations for formalin 5 μM , 10 μM , 50 μM , and 100 μM . For individual concentration, 75% data was considered as training set of data and 25% as the test set of data. A high prediction accuracy for the Pt electrode of 97.84% was obtained using PLSR. The prediction parameters have been summarized in the Table. 2.1 below.

Table 2.1 An evaluation for the actual, predicted levels of formalin based on PLSR

Sample No.	Actual Formalin Content	Predicted Formalin Content	Prediction Accuracy (%)
1	100	100.84	99.16
2	50	47.79	95.58
3	10	10.31	96.9
4	5	5.14	99.72
			Average prediction accuracy = 97.84 %

2.2.2.6. Principal component regression (PCR)

PCR algorithm is based on assessment of principal components [26]. In this technique, the predictors illustrated the extreme variance in the directions the same as the response variable quantities. A cross validation (leave one out) system has been utilized in the experiment.

Table 2.2 An evaluation of the actual and predicted levels of formalin based on PCR

Sample No.	Actual Formalin Level	Predicted Formalin Level	Prediction Accuracy (%)
1	100	100.52	99.48
2	50	47.70	95.54
3	10	10.40	96
4	5	5.19	99.62
			Average prediction accuracy = 97.66 %

Correlation measurement parameters like CF, RMSEV, and RMSEP have been used to estimate prediction capacity of the Pt electrode over four different concentrations 5 µM, 10 µM, 50 µM,

and 100 μM . The training data set was considered as 75% of the data and 25% as the testing data. The prediction accuracy of the electrode was as high as 97.66% Table. 2.2 comprises the prediction measures of the Pt electrode.

2.2.3. Summary

The current research encompasses a learning on rapid electrochemical detection of formalin using an optimized Pt electrode. The Pt electrode established an extensive linearity from 100 to 1000 μM with a good LOD of 5 μM . The DPV responses obtained at the Pt electrode for four various formalin concentrations were analysed using PCA tool and an effective discrimination of individual concentrations were observed. Successful data clustering with a high value of separability index 25.68 was achieved. Two regression models PLSR and PCR on the other hand provided 97.84% and 97.66% of prediction accuracies respectively. The results obtained were found comparable with the reported works. Hence, use of an electrochemical system and analysis using chemometrics may be highly efficient in the detection of formalin adulteration. To replace the expensive spectroscopy methods and vapor phase formalin detection for food adulteration, electrochemical measurements are useful for detecting liquid phase adulteration of food to decipher the food grade rapidly, quantitatively, and on the spot. The coupling of chemometrics with electrochemical data may provide a classification of different levels of formaldehyde adulteration in various food supplies, creating a new frontier of research going forward. This Pt electrode efficacy can serve for immediate on spot identification of varying formalin traces in a wide range of food stuffs.

2.3. Development of cerium oxide nanoparticles decorated graphite paste electrode for formaldehyde detection in mushroom

The noble metal modified electrodes provided satisfactory analytics but were quite expensive. Some of these noble metals modified electrodes like graphene oxide (GO) functionalized with p-xylylenediamine (Px) and supported by gold nanoparticles (Ag) (GOPx-Ag) [40] suffered poor reproducibility and slow speed of response while platinum nanoparticles (Pt) over polyaniline (PAN) coated multi wall carbon nanotubes MWCNTs (Pt/PAN/MWCNTs) [34] exhibited less stability. Likewise, electrochemically reduced graphene over glassy carbon (EG/GC) supported by platinum nanoparticles (Pt) (Pt/EG/GC) [35], Pt-based gold planar

electrodes [36], and palladium nanoparticles modified expanded graphite (EG) with carbon nanotubes (Pd-NP/EG-MWCNT) [37] were found to serve poor detection limits along with lack of molecule selectivity. Thus, the use of a fast formaldehyde selective low cost electrocatalyst with a sensitive detection limit has been a long-time challenge. The use of several modified carbon allotropes like glassy carbon electrode (GCE), carbon nanotubes (CNTs), graphene oxide (GO), and their drawbacks in terms of electroanalytical performances have already been reported in [33]-[37]. Initially, an experiment was performed using a bare graphite electrode. It was found reasonably effective after a long time of sonication possibly due to exfoliation. To further improve the electrode efficacy metal oxides were incorporated. In our previous reports, it was noted that metal oxide nanocomposites exhibit improved electrochemical activities [38]. Rare earth metal oxide nanocomposites like cerium oxide (CeO_2), neodymium oxide (Nd_2O_3) induced enhanced electrocatalytic activity due to high surface area with an increased number of active sites leading to supplementary molecular adsorption followed by amplified and fast electron transfer [39], [40]. These nano-crystallites of rare earth elements can exhibit high reproducibility and extreme sensitivity. This may be due to the higher surface area of the nano crystallites and proper matching of electronic levels of analyte and nano sized rare earth oxides. However, these rare earth metal oxides are not implemented for formalin detection to date. A typical rare earth metal oxide CeO_2 encased with graphite produces high electron transfer kinetics and versatile nature into electrochemical applications [39]. Owing to its exceptional characteristics, cerium oxide nanocomposites over graphite were considered to achieve formalin detection with excellent electroanalytical features.

In this work, a rare earth metal cerium oxide nanoparticle modified graphite electrode ($\text{CeO}_2\text{@GP}$) has been prepared for electrochemical detection of formalin (FAL) in mushrooms as shown in fig. 2.6. Mushroom, a crop rich in nutrients daily consumed by a large part of the world population sometime contains formaldehyde or is treated with formalin disinfectant during cultivation or preservation during transport [2], [4]. It is thus important to track the formalin content in mushrooms. Here in our work, CeO_2 nanoparticles have been synthesized by sol-gel technique, and an electrochemical sensor was fabricated based on CeO_2 nanocomposites. Electrochemical detection of formaldehyde in fresh mushroom extract using a budget electrode has been explored. The prepared electrode provided a wide linear range of $25\mu\text{M}$ - 1mM with a low detection limit of $1\mu\text{M}$. As already mentioned, the tolerable daily intake limit must be within

(0.15-0.2 mg per kg body weight per day) [31], [32] viz. approximately $6\mu\text{M}$; in such instance, the proposed electrode may be appropriate to control the quality of food.

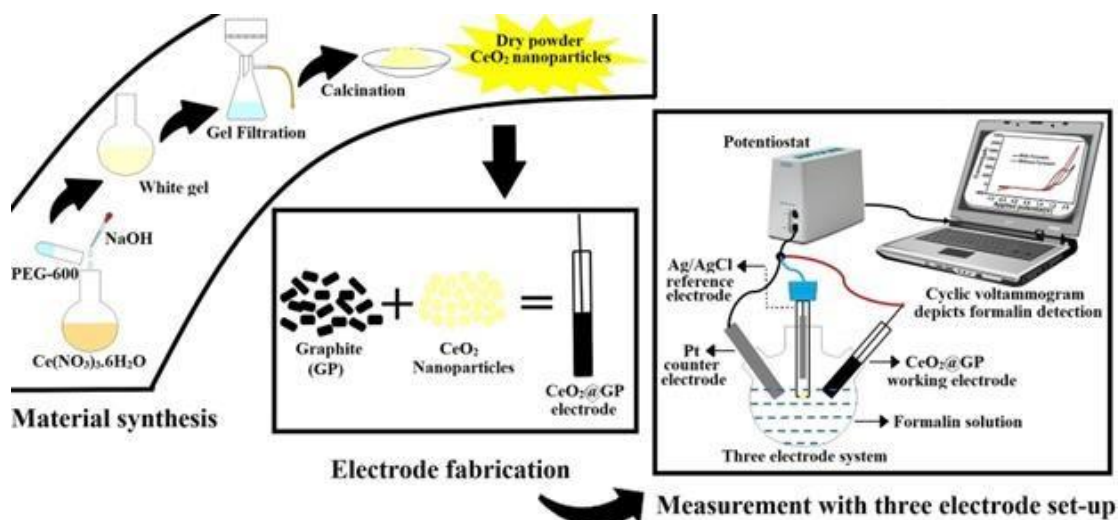


Fig. 2.6 Schematic of CeO_2 nanoparticles synthesis, electrode fabrication, and measurement using three electrode set-up.

2.3.1. Experimental process

2.3.1.1. Chemical and reagents

Graphite powder, cerium nitrate hexahydrate [$\text{Ce}(\text{NO}_3)_3 \cdot 6\text{H}_2\text{O}$], paraffin oil, and sodium hydroxide (NaOH) were procured from Sigma Aldrich, India. Formaldehyde 37% solution was attained from Merck, India. Altogether the chemicals were of pure analytical grade and utilized without any additional decontamination. The experimental solutions were prepared using Millipore water (resistance = $18\text{ M}\Omega$). The experiments were performed at room temperature.

2.3.1.2. Synthesis of Cerium Oxide Nanoparticles

Cerium oxide nanoparticles were synthesized using the sol-gel method [40]. In brief, 100 mL of 0.1 M, [$\text{Ce}(\text{NO}_3)_3 \cdot 6\text{H}_2\text{O}$] solution was engaged in a beaker and then 10 mL of 15% poly (ethylene glycol)-600 solution was poured into it. Next, 0.2 M NaOH solution was introduced dropwise into the above reaction mixture and thereafter white gel formation occurred. The resultant white gel was filtered immediately followed by repeated washing with

Millipore water. The obtained residue was dried in the hot air oven at 60° C. After drying in air, the white powder was further calcined at 600° C for 4 hours to get CeO₂ nanoparticles (nps). The resultant CeO₂ nps were then used for the characterization and preparation of the electrode.

2.3.1.3. Characterization Techniques

The morphology of the synthesized cerium oxide nanoparticles was studied using a JEM-2100 high-resolution transmission electron microscope (HRTEM). The sample preparation for transmission electron microscope (TEM) analysis was done by dispersing a small quantity of CeO₂ in acetone. A droplet of suspended CeO₂ was dried on a carbon coated copper TEM grid. The selected area electron diffraction pattern was also observed for the same sample. X-ray diffraction (XRD) pattern of the produced material was obtained using the Philips PW 1710 X-ray diffractometer (Eindhoven, Netherlands) functioned at 40 kV and 40 mA with CuK α radiation ($\lambda = 1.5406 \text{ \AA}$). The electrochemical study was carried out by three electrode system using a Potentiostat /Galvanostat PGSTAT101 (Metrohm Autolab, Netherlands). A Pt electrode was employed as a counter electrode, a silver-silver chloride (Ag/AgCl) as a reference electrode, and the CeO₂ modified graphite electrode (CeO₂@GP) acted as the working electrode. The voltammetry technique was exercised throughout the experiment. Cyclic voltammetry was carried out in the potential range of (-1.0 to 2.0 V) at 100 mV/s. All other experiments were performed using differential pulse voltammetry within (0.8 to 1.6 V) at 8 mV/s. The DPV responses as depicted in fig. 2.7 were obtained in the presence of various supporting electrolyte compositions like H₂SO₄, phthalate (PHT), acetate (ACT), phosphate (PHP), and NaOH with pH 1, 5, 6, 7, and 10 respectively. The optimum response was obtained in the presence of 0.1 M NaOH with pH 10. The presence of OH ions promote catalyst activity toward formalin oxidation as previously reported [8]. Hence, all the experiments were carried out in presence of 0.1 M NaOH supporting electrolyte.

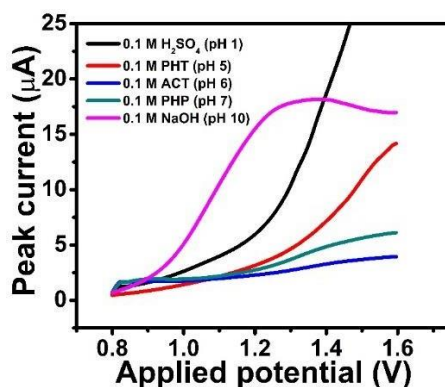


Fig. 2.7 Effect of various electrolyte compositions and pH over DPV measurements at the CeO₂@GP electrode.

2.3.1.4. Fabrication of CeO₂@GP Electrode

The prepared CeO₂ nps and graphite powder were taken in a weight ratio of 1:9 and then 300 mg of the material was blended thoroughly by a mortar-pestle. Paraffin oil (2-3 drops), as the binder, was added into the above mixture until a fine paste was obtained. Afterward, the resultant material was stuffed into a 2 mm inner diameter glass capillary tube. Electrical contact was established with the sensor material by inserting a platinum wire through the backside of the capillary tube. The bare graphite paste electrode (bare GP) was prepared similarly by using graphite powder only.

2.3.1.5. Real Sample Preparation

Fresh mushroom samples were procured from the local market. The mushrooms were processed and FAL extracts were collected according to the previous report [12]. 0.5 g of the mushroom sample was weighed, then cut into small pieces and transferred into a grinder. Thereafter, it was blended with 22 mL of water for 2 minutes and transferred into a flask containing 3 mL of 10% H₃PO₄ solution. Then the resultant solution was distilled for about 1 hour to get the real sample extract. The extract was stored in the refrigerator and used for further analysis.

2.3.2. Results and discussion

2.3.2.1. Study of X-ray Diffraction Characteristics of CeO₂

The X-ray diffraction pattern of synthesized CeO₂ material is depicted in fig. 2.8. The XRD pattern showed resemblance with the standard JCPDS card No. 34-0394 confirming the

successful formation of pure fluorite cubic phase of CeO₂ nps. The most intense peak was found at $2\theta = 28.7^\circ$ for (111) crystal plane along with other peaks at 33.0° (200), 47.6° (220), 56.4° (311), 59.2° (222), 69.6° (400), 76.8° (331), 79.2° (420) respectively. No crystalline contamination was observed to be present in the diffractogram indicating that the synthesized CeO₂ material was free from any other impurities. The crystallite size was estimated to be 4.84 nm by using the Debye-Scherrer formula [47].

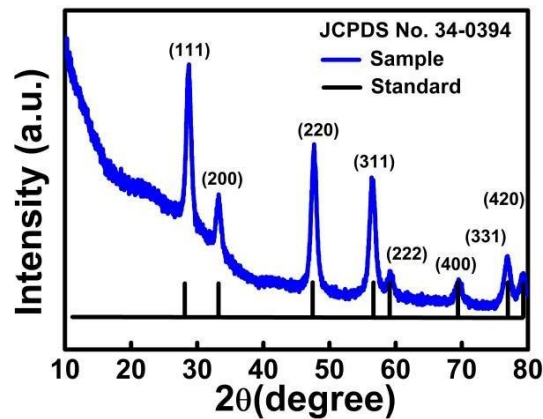


Fig. 2.8 X-ray diffraction pattern of synthesized CeO₂ nano crystallites.

2.3.2.2. Study of TEM Analysis of CeO₂

The morphology of prepared cerium oxide nanoparticle material was examined by TEM and presented in fig. 2.9 (a). The TEM image provided the information that prepared materials are composed of fine nano crystallites. The particle size of synthesized CeO₂ material was found to be 10.58 ± 1.33 nm respectively (inset of fig. 2.9 (a)). From Selected Area Electron Diffraction (SAED) pattern (Fig. 2.9. (b)), it is also observed that the prepared materials are crystalline in nature. From the SAED pattern, it was observed that the diffraction pattern well matched with the d value (interplanar spacing) of the XRD pattern.

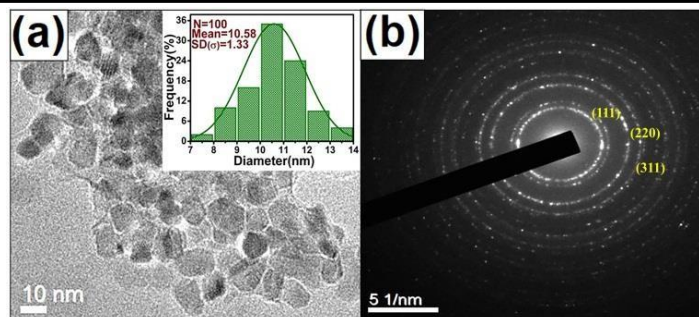


Fig. 2.9 (a)TEM image; the inset shows the particle size distribution graph and (b)SAED pattern of synthesized CeO_2 nanoparticle.

2.3.2.3. Electrocatalytic Behaviour of CeO_2 @GP Electrode

The electrochemical behavior of the CeO_2 @GP electrode was studied with the help of the voltammetry technique. Initially, the cyclic voltammetry (CV) response of the CeO_2 @GP was recorded in presence of 0.1 M NaOH as a supporting electrolyte in the range of (-1.0 to 2.0 V). In absence of the analyte molecule, no oxidation peaks were present in the response as shown in fig. 2.10 (a). Then, 1500 μM formalin was added to the above solution and the same experiment was repeated. Since anodic oxidation peak was obtained at a potential of 1.5 V; the detection of the analyte molecule was established. Next, a bare GP was replaced with the same solution. Fig.2.10 (b) illustrates the maximum peak current at the CeO_2 @GP. After incorporation of CeO_2 nanoparticles into bare graphite powder, the oxidation peak current of formalin increases by 1.4 times leading to higher electron kinetics in the presence of the target analyte molecule. This enhanced electrocatalytic activity of CeO_2 @GP may be due to the presence of CeO_2 nanoparticles which increases the electroactive surface area thereby leading to a faster flow of electrons transfer between the electrode surface and analyte molecule.

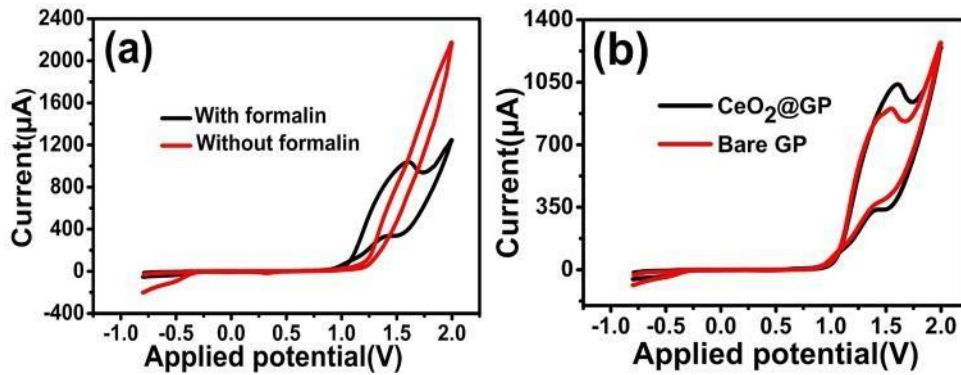


Fig. 2.10 CV response of CeO₂@GP electrode in 0.1 M NaOH (a) with and without FAL (b) comparative performance with bare GP.

2.3.2.4. Influence of Scan Rate Variation

The effect of various scan rate towards electrochemical determination of 1300 μM formalin (FAL) molecule at CeO₂@GP was investigated by means of CV technique within a range of -0.5 V to 2 V. From, fig. 2.11 (a) it was found that there is a linear increment of anodic peak current with increasing scan rate from 25 to 400 mV/s. This observation suggested the electrocatalytic oxidation of FAL molecule at CeO₂@GP as a surface-controlled phenomenon [45], [46]. The corresponding oxidation peak current vs. scan rate plot as represented in fig. 2.10 (b) upholds the linear regression equation $I_{FAL} = 2.37v + 388.73$; $R^2 = 0.97$. The number of electrons transferred during the oxidation process was calculated using equation (2.1) [49]

$$I_P = \frac{nFQv}{4RT} = \frac{n^2F^2A_0\Gamma_C}{4RT} \quad (2.1)$$

where I_P is the peak current, n is the number of electrons transferred, F is the Faraday's constant, R is the universal gas constant, T is the room temperature, A is the surface area of the electrode, Γ_C is the surface concentration of FAL, Q is the quantity of charge consumed during the oxidation and v is the scan rate [49]. After calculating the number of electrons transferred, n was obtained 1.09 ~1 which is comparable with the related work in [50], and the surface concentration of FAL, Γ_C was found to be 1.079×10^{-8} mole /cm². Further, the electron transfer coefficient was determined from the linear plot of peak potential (E_P) vs $\log v$ as shown in fig. 2.11 (c). The corresponding regression equation was obtained as $E_P = 0.33\log v + 0.8449$; $R^2 = 0.96$; the charge transfer coefficient $\alpha = 0.8$ as calculated from the slope of the

curve equal to $2.3RT/(1-\alpha)nF$ [51]. The rate of electron transfer k_s was calculated using Laviron's equation shown in equation (2.2)

$$\log k_s = \alpha \log(1-\alpha) + (1-\alpha) \log \alpha - \left(\frac{\log RT}{nFv} \right) - \left(\frac{nF\Delta E_p \alpha(1-\alpha)}{2.3RT} \right). \quad (2.2)$$

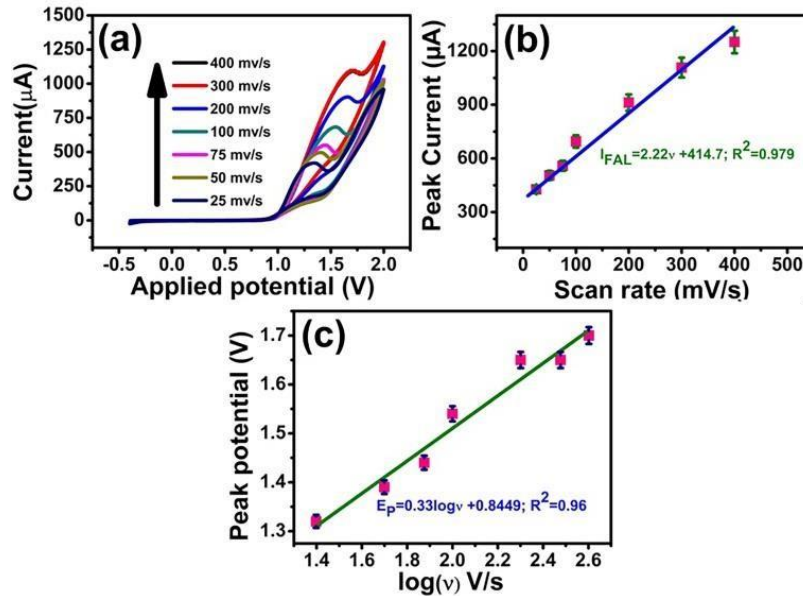


Fig. 2.11 CV response of $CeO_2@GP$ electrode in 0.1 M NaOH (a) variation of peak current with scan rate variation (b) linear plot of peak current vs scan rate (c) maximum peak potential vs log of scan rate.

The α (0.8) and k_s ($0.64s^{-1}$) derived from the above equations were found to be analogous and even improved than similar works [51]-[53] as summarized in Table 2.3. The degree of chemical reversibility of an electrochemical mechanism is controlled by the rate of the chemical reaction. A higher reaction rate constant may increase the extent of chemical irreversibility [49].

Table 2.3

Comparison of electron transfer kinetics at proposed CeO₂@GP with different electrodes

Electrode material	Charge transfer coefficient α	Rate of electron transfer k_s (s ⁻¹)	Ref.
Nano-NiPh	0.75	0.063	[51]
Ni-CoVSB-5/CPE	0.72	0.008	[52]
Ni-CHIT/CPE	0.73	0.174	[53]
CeO₂@GP	0.8	0.64	This work

2.3.2.5. Determination of Formalin

Differential pulse voltammetry (DPV) responses offer higher current sensitivity and higher resolution compared to CV and hence DPV measurements were recorded to examine the effect of different concentrations on the surface of CeO₂@GP in 0.1 M NaOH. Fig. 2.12 (a) depicts the relative increase of the oxidation peak current with the increase of concentration from 25 to 1000 μ M. Two linear relationships are obtained as revealed in fig. 2.12 (b). The first linear regression equation is obtained within the range of 25 to 120 μ M from the plot as followed $I_{\text{FAL}} = 0.043C_{\text{FAL}} + 5.80$; $R^2 = 0.99$ where I_{FAL} is the peak current and C_{FAL} is the corresponding concentrations of formalin. The second linear range of 120 to 1000 μ M yields the regression equation $I_{\text{FAL}} = 0.015C_{\text{FAL}} + 9.00$; $R^2 = 0.99$. The presence of two slopes in the calibration curve can be explained by Langmuir adsorption isotherm behavior [54] which states monolayered adsorption of analytes followed by multilayered adsorption. Due to the strong adsorption of CeO₂@GP, at a lower concentration range, the outermost accessible surface area of the electrode was covered by the first layer of molecules. Hence, in the higher concentration range, the second layer of molecules was screened by the first layer of molecules. So, the interaction strength of the second layer of molecules is different from the first layer of molecules thereby leading to excellent sensitivity and higher adsorption capacity at the low concentration

range. Similar observations have also been found earlier for the determination of other small biomolecules [55].

The lower limit of detection is calculated using the equation $LOD = \sigma/m$ and is found to be 1 μM , where σ is the standard deviation of maximum peak currents for the lowest detected concentration and m is the slope of the calibration curve respectively [56]. The main origin of the oxidation potential is due to the Schottky barrier which forms at the interface of $\text{CeO}_2@\text{GP}$ and formalin. Although this may vary with the acidity of electrolyte, scan rate, and adsorption of formalin at different concentrations. Here, the oxidation potential shifts after a particular concentration of formalin due to the dominant adsorption property of formalin into the $\text{CeO}_2@\text{GP}$ electrode surface. Similar phenomena have also been observed previously for the determination of dopamine and ascorbic acid also [56].

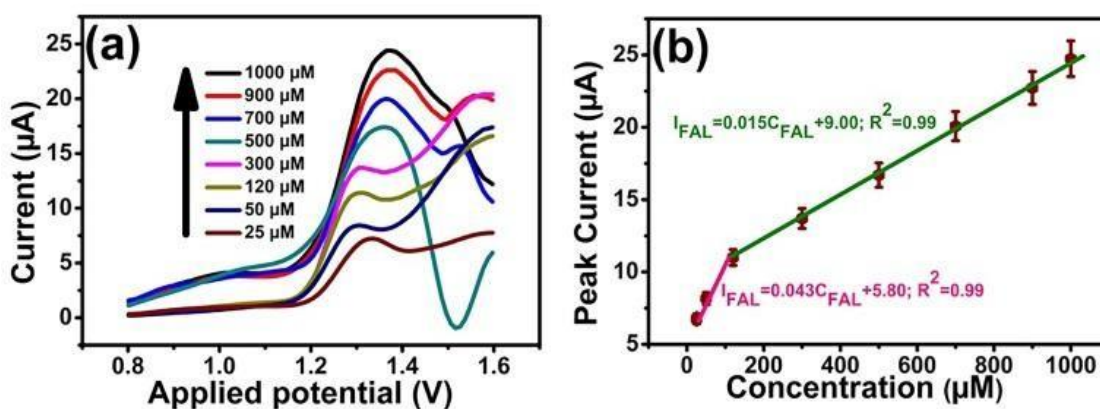


Fig. 2.12 DPV measurements for FAL using $\text{CeO}_2@\text{GP}$ electrode in 0.1 M NaOH (a) Concentration variation of 25, 50, 120, 300, 500, 700, 900, 1000 μM (b) linear plot of peak current vs concentration.

A comparative study of the present work with few previous related works is presented in Table 2.4 where the LOD is found to be much less compared to the previous reports.

Table 2.4

Comparison of proposed CeO₂@GP performance with the previous reports

Electrode material	Linear range (μM)	LOD (μM)	Ref.
Pt/EG/GC	125-2000	40	[35]
Cu/Cu ₂ O NPs	100-110000	10	[58]
Ni-Pd/GCE	10-1000	5.4	[59]
Pt-Pd/Nf/GCE	10-1000	3	[60]
Pd-Pt-graphene-Nafion-GCE	4.50-180	2.85	[61]
CeO₂@GP	25 – 120 – 1000	1	This work

2.3.2.6. Study of Repeatability, Reproducibility and Stability

To study the repeatability characteristics, the proposed sensor was subjected to five consecutive DPV measurements using 50 μM and 400 μM formalin content namely S1, S2, S3, S4, S5, and S1', S2', S3', S4', S5' respectively as represented in (Fig. 2.13 (a)) and (Fig. 2.13 (b)). No significant change in peak current was observed. Thereby, relative standard deviation (RSD) of 1.05% and 1.30% were obtained respectively. This result indicated a good measure of repeatability for the proposed sensor. Five similar CeO₂@GPs were developed to characterize the nature of reproducibility of the sensor. (Fig. 2.13 (c)) and (Fig. 2.13 (d)) demonstrate the DPV response of five electrodes namely T1, T2, T3, T4, T5, and T1', T2', T3', T4', T5' in 50 μM and 400 μM of formalin solution respectively. The oxidation peak currents are found to be nearly similar. RSD calculated for the above test was found to be 3.98% and 4.57 % respectively. Thus, a satisfactory degree of reproducibility was obtained for the fabricated sensor. During the study of the stability of the proposed sensor, a single CeO₂@GP electrode was examined over a period of one month and DPV responses were recorded in 50 μM and 400 μM formalin at an

interval of 15 days. The electrode was stored at room temperature during the entire period. DPV measurements were obtained as shown in (Fig. 2.14 (a)) and (Fig. 2.14 (b)). The RSD calculated for the study of stability was 4.93% and 3.40% respectively. (Fig. 2.14 (c)) and (Fig.2.14 (d)) describes negligible drop of oxidation peak current till 22 days of continuous use and little fall of peak current was found on the 30th day maybe due to the aging effect of the electrode after several uses during the long period.

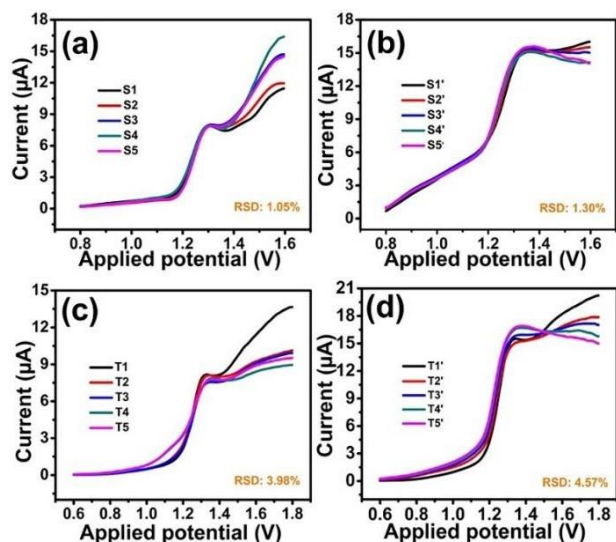


Fig. 2.13 DPV measurements of the $CeO_2@GP$ electrode in $0.1 M NaOH$ (a) five consecutive measurements in $50 \mu M FAL$ (b) in $400 \mu M FAL$ (c) five electrode response in $50 \mu M FAL$ (d) in $400 \mu M FAL$.

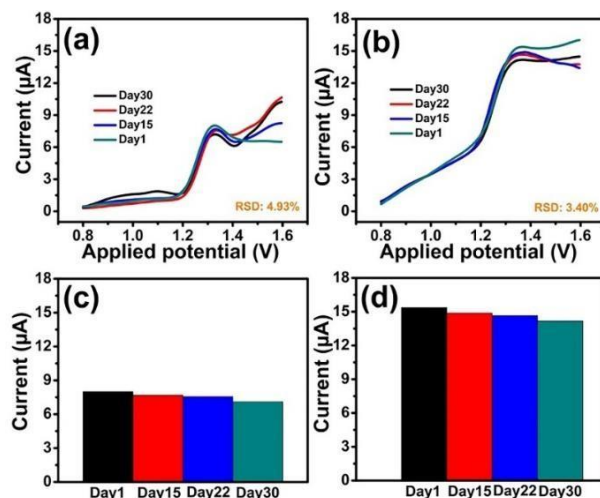


Fig. 2.14 DPV measurements of the $CeO_2@GP$ electrode in $0.1 M NaOH$ (a) Four measurements over a period of 1 month in $50 \mu M FAL$ (b) in $400 \mu M FAL$ (c) bar graph with peak current measure in $50 \mu M FAL$ (d) in $400 \mu M FAL$.

2.3.2.7. Interference Study

The CeO₂@GP was exposed to several possible interferences (ethanol, methanol, formic acid, benzaldehyde, and acetone) to analyze the selectivity of the sensor developed. The DPV responses were obtained, in the presence of 5-folds of each species interfering with 50 μM of the target analyte formalin. (Fig. 2.15.) depicts the selectivity profile of CeO₂@GP. The relative change of signal due to the presence of various interferences was plotted against the response obtained without interference or target analyte only. The presence of foreign materials over formalin manifested no significant change in peak current with a tolerance limit of ±5%. The ±5% tolerance outcomes suggest that the sensor offers good resistance to interference from the majority of interfering agents as reported in the literature [40]. Thus, indicating selective identification of target analyte on the fabricated sensor. This study confirmed the selective nature of the CeO₂@GP electrode.

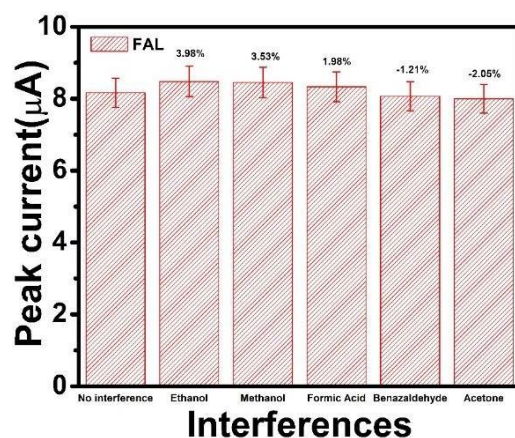


Fig. 2.15 Influence of interferences to voltammetry peak current responses of 50 μM FA in 0.1 M NaOH with the relative signal changes at the CeO₂@GP electrode.

2.3.2.8. Investigation of Real Sample

The extracts obtained from mushrooms were diluted with 0.1 M NaOH solution. The diluted FAL extracts were then subjected to measurements lacking any further treatment by the standard addition method. Different concentrations of FAL solutions were added into diluted mushroom extracts and were examined by the DPV technique. The outcomes obtained are concised in Table 2.5. The records from Table 2.5. were that the recovery rates of spiked samples are in the range of 98.5% to 101% with RSD value ranging from 1.37% to 1.46% respectively. Real food sample matrices contain various compounds

which may interfere with the measurements. These results indicate that the CeO₂@GP electrode is free from matrix effect during detection of FAL.

Table 2.5

Determination of FAL in fresh mushroom extract using CeO₂@GP electrode

Sample	Spiking (μM)	Detected (μM)	Recovery^a(%)	\pm R. S. D^b (%) (n=3)
Mushroom extract pure	0	175.33	-	1.45
Mushroom extract spiked	30	204.88	98.5	1.37
	35	239.78	99.7	1.46
	40	280.18	101	1.39

^a Recovery = [Detected (μ M)-Diluted sample (μ M)]/Spiking (μ M)

^b R.S.D (%) = [100x Standard deviation]/ Mean

2.3.3. Summary

In this work, the CeO₂ nano crystallites cast over graphite paste yielded improved electrochemical sensing for formaldehyde detection in fresh mushroom samples. A new electrochemical sensor with a rare earth metal oxide modifier has been successfully developed in this work for formalin detection. CeO₂@GP electrode manifested excellent electrochemical performance along with a wide linear range of operation. The limit of detection is much lower compared to the safety standards, which ensures healthy consumption of fresh mushrooms among the population. The observed results were found to be superior as compared to previous works in literature. The study of the electrocatalytic behavior of the CeO₂@GP electrode justified a surface-controlled process with a high electron transfer rate. Further, the proposed CeO₂@GP electrode was highly selective with excellent repeatability, reproducibility, and moderately stable over extended use for about a month. The application of the fabricated electrode over real mushroom sample extracts revealed excellent recovery rates. The use of CeO₂@GP can be thus validated for safety limit estimations of formaldehyde traces in agro-

industrial products. Thus, the proposed CeO₂@GP electrode, has demonstrated its potential to be a field-deployable cost-effective sensor for formalin trace detections in aqueous solutions in near future.

2.4. Fabrication of A Molecular Imprinted Polyacrylonitrile Engraved Graphite Electrode for Detection of Formalin in Food Extracts

The electrocatalytic effect of a rare earth metal cerium oxide for the determination of formalin was explored in our previous work [41]. The challenges from the previous work were such as limited linear range of operation, detection limit, and specific template molecule recognition capability. Thus, the solution to selective recognition was explored here using inexpensive polymer resources with longer stability. In recent times, polymers with recognition cavities, profound hydrogen bonding with multiple active sites play important roles in electrocatalytic activities [42]. In this context, molecular imprinted polymer (MIP) based electrochemical sensors have emerged as a constructive solution. MIP materials are built from natural or synthetic monomers with specific vacancies for the target molecules [43]. In the molecular imprinting technique, the target analyte acts as the template bonded covalently or non-covalently within a network of monomers and crosslinkers [43-45]. After the polymerization is complete the template is removed leaving behind a polymer matrix with a molecular memory. The fundamental adsorption process for each molecule relies on molecular recognition [45]. This technology has been developed for a variety of uses [46–51]. A few research groups have recently focused on the important role that polymers play in the identification of formaldehyde. In this regard, an electrospun polymethylmethacrylate (PMMA) biomimetic sensor has been synthesized to monitor formaldehyde traces through electrochemical impedance spectroscopy (EIS) [52]. However, a vigorous and time-consuming process of electrospinning for material fabrication has been established which may affect manufacturing demands. An approach of formaldehyde vapor detection based on Hantzsch reaction using a polyaniline sheet with ammonia memory reflected enhanced selectivity to water vapor and limited reproducibility [20]. Real time monitoring of biomolecule derivatives using quartz crystal microbalance (QCM) sensors demonstrated good estimation agreements [53]. Several works report QCM sensor fabrication using imprinted formaldehyde polymer materials like polymethacrylic acid and gold nanoparticles (PMAA/Au-NP), polymethacrylic

acid, and a copolymer of styrene and methacrylic acid [23-25]. However, it may be noted all these researches have limited applicability due to the sensing of formaldehyde in the vapor sense. But aqueous formalin detection is very much necessary to check food adulteration. This brings the idea to tailor a probe by means of MIP technology to sense formalin or aqueous formaldehyde. A large number of active imprinted sites is responsible for the boosted sensitivity of the sensor surface.

The aim of the present study was to engineer a polyacrylonitrile based molecular imprinted polymer infused in graphite (MiPAN@GP) electrode for detecting formalin (FAL) evidence in food products as shown in fig. 2.16. The novelty of the work lies in evolving a simple, cost effective, and easy technique of sensor fabrication. Analytical performances of the electrode have been exercised in detail and it produced a wide linear range of operation with good selectivity, high repeatability, high reproducibility, and long term stability characteristics. Moreover, the MiPAN@GP electrode was utilized to evaluate the electrode responses to FAL in mushroom and fish tissues with highly satisfactory results when compared to the HPLC analysis. Therefore, this technique can be recommended as a viable alternative for FAL determination in a wide variety of samples.

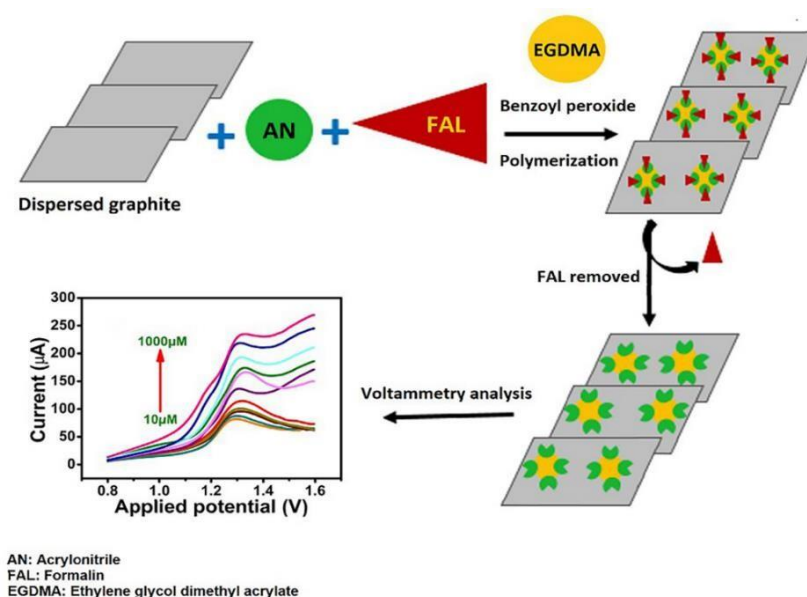


Fig. 2.16 Schematic representation of MiPAN@GP synthesis to evaluate the electrode responses to FAL in mushroom.

2.4.1. Experimental

2.4.1.1. Reagents and standards

Formaldehyde 37% solution was procured from Merck, India. Graphite powder (99%), acrylonitrile (AN), methacrylic acid (MAA), acrylamide (AA), ethylene glycol dimethylacrylate (EGDMA), benzoyl peroxide, H₂SO₄, phthalate (PHT), acetate (ACT), phosphate (PHP), and sodium hydroxide (NaOH) were procured from Sigma Aldrich, USA. Paraffin oil, ethanol, methanol, formic acid, benzaldehyde, and acetone were procured from Merck, India. All the chemicals were of pure analytical quality and thus no decontamination was required. Throughout the experiment, all the solutions were formulated with Millipore water (resistance = 18 MΩ). All the experimentations were performed at normal room temperature (25°C).

2.4.1.2. Methods and measurement

A Potentiostat/Galvanostat PGSTAT101 (Metrohm Autolab, Netherlands) with three electrode setup was used for electrochemical analysis. The three electrode system comprised of a Pt counter electrode, an Ag/AgCl reference electrode, and the MiPAN@GP working electrode. The synthesized polymer materials have been characterized using FTIR spectroscopy and Ultraviolet - Visible (UV-Vis) Spectroscopy. A Fourier transform infrared spectroscope (IR prestige 21, 200VCE, Shimadzu, Tokyo, Japan) was used for the measurements within the wavelength region of spectra 400–4000 cm⁻¹ using KBr pellets for calibration. The UV-1800 SHIMADZU, UV Spectrophotometer was used to obtain spectral data within the wavelength range of 200-400 nm. Surface morphology characterizations of the material synthesized were examined using ZEISS EVO 18 (United States) scanning electron microscope (SEM) operated at an acceleration voltage of 15 kV. The HPLC analysis was carried out using multidimensional liquid chromatography (MDLC-5698) with UV-Vis detector (Model no. 2487) from WATERS PVT. LTD.

2.4.1.3. Synthesis of molecular imprinted polymer

The polymer material was synthesized in the laboratory as previously reported in a similar work [54]. Initially, the powdered graphite (0.95 g) was disseminated in ethanol (15

mL) by ultrasonication for 40 mins. Thereafter, the monomer AN (0.05 g) and template FAL (0.05 g) were added followed by sonication for 60 mins. Next, the crosslinker EGDMA (400 μ L) along with benzoyl peroxide (1 mg) was added and sonicated for 60 mins. The prepared solution was next polymerized by heating in a water bath at 30°C for 40 mins. This prepared polymer was repeatedly rinsed with ethanol and distilled water (1:1). The template molecules were leached out during this process resulting in the MIP material. The sample was air dried and collected for further analysis. The non-imprinted polymer material (NIP) was synthesized in a similar process excluding the addition of the template molecule.

2.4.1.4. Fabrication of electrode

To devise the MiPAN@GP electrode; 300 mg of the synthesized MIP material was transferred into a mortar-pestle. The material was blended into a fine paste using 2-3 drops of paraffin oil during the process. The paste obtained was next packed inside a glass capillary of inner diameter 2.5 mm, using a thin metallic rod. Electrical contact was established by a platinum wire from the other side of the tube. The non imprinted graphite based polyacrylonitrile (NiPAN@GP) electrode was similarly fabricated using NIP material (excluding the template).

2.4.1.5. Real sample analysis

Two samples of shiitake mushroom and fresh carp were purchased from the local market. 0.5 g of each sample were blended in 25 mL of water and treated with 10% H_3PO_4 solution. The extracts were then obtained by distilling the resultant solution for about an hour as previously reported in [41], [32]. The resultant solutions were used for DPV and HPLC analysis. The samples were filtered using Whatman UNIFLO disposable sterile syringe filter of diameter 25 mm, pore size 0.22 μ m with polyvinylidene fluoride (PVDF) filter membrane in polypropylene housing before HPLC analysis. The aliquots were analyzed by HPLC system using UV-Vis detector. The column used was C18 reverse phase column (μ - Bondapack), dimension 3.9 \times 300 mm with silica particle size 10 μ m used at ambient temperature. The mobile phase used was a) 0.5% H_3PO_4 in H_2O b) 90% acetonitrile in H_2O with flow rate 1ml min⁻¹ for a total run time of 10 mins.

2.4.2. Results and discussion

2.4.2.1. Monomer optimization

Three different imprinted polymer materials were synthesized simultaneously for the selection of the optimized monomer. Three monomers namely methacrylic acid (MAA), acrylamide (AA), and acrylonitrile (AN) were used to prepare the MIP materials and corresponding electrodes. The method of synthesis and fabrication has been discussed in the previous section. Three electrodes were subjected to CV in the range of (0.5-2 V) and an irreversible redox peak was obtained at 1.5 V in the presence of 0.1M NaOH as a supporting electrolyte at 100 mV/s. As shown in fig.12.7, the maximum oxidation peak current was established by the AN imprinted polymer electrode, which is approximately 1.08 and 1.34 times higher compared to MAA and AA imprinted electrodes respectively. The interaction of template and monomer molecules during the prepolymerization stage can influence the behavior of recognition sites within the MIP and ultimately the electrochemical behaviour of the imprinted polymer material [54]. The strong dipole to dipole interactions between template and monomer in prepolymerization composite have incited the template recognition process and enhanced electrochemical performance at MiPAN@GP electrode surface [54]. Hence, AN was acknowledged as an ideal monomer for the proposed experimental work.

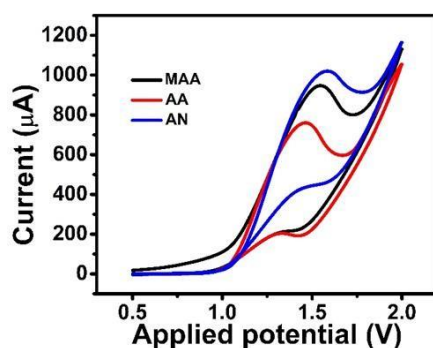


Fig. 2.17 CV response of different monomers in the presence of 0.1M NaOH.

2.4.2.2. Characterization of the synthesized material

1. FTIR analysis: The spectral analysis of the prepared polymer material before template removal (BTR) as depicted in fig. 2.18. (a) was obtained using FTIR spectroscopy. The band

at 2342 cm^{-1} and 2360 cm^{-1} represent the typical signature nitrile group $-\text{C}\equiv\text{N}$ stretching vibrations attributing to the formation of polyacrylonitrile [45]. The bending vibrations of the methylene group were observed at 1451 cm^{-1} . The sharp peak centered at 1720 cm^{-1} unveil the carbonyl stretching frequency ($\text{C}=\text{O}$) i.e. aldehyde [55], [56]. Thus, after template removal, this peak intensity was reduced to a large extent. However, fig. 2.18 (b) depicts the spectral response after template removal (ATR) that allows selection of the region for the presence of formaldehyde template in fig. 2.18 (a). The variance in spectrum distinguishes the template removal spectral regions before and after template extraction.

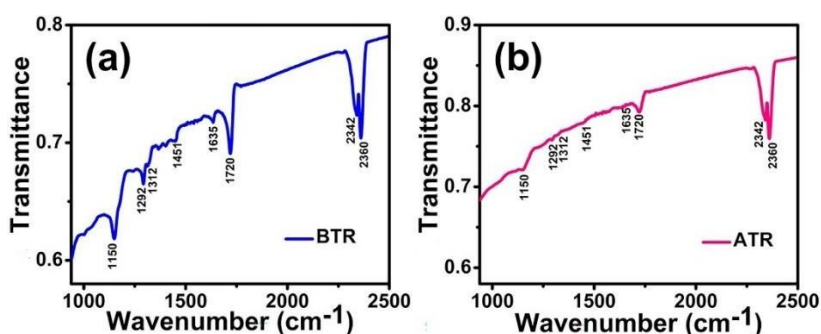


Fig. 2.18 FTIR spectra of MIP (a) before template extraction (b) after template extraction.

2. UV-Vis spectroscopy: The successful leaching out of the FAL molecule was again assured by UV-Vis spectroscopy and the responses obtained are portrayed in fig. 2.19. The spectral observation illustrated a sharp absorption peak at 230 nm for FAL which disappeared completely after template extraction [57]. This approved the complete template extraction and effective MIP preparation.

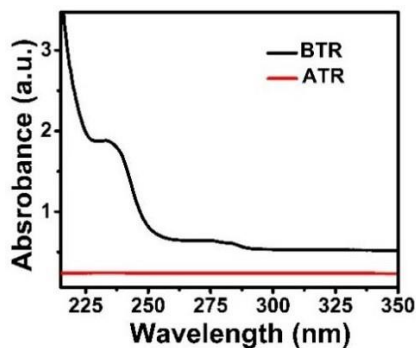


Fig. 2.19 UV-Vis spectra of MIP before and after template extraction.

2.4.2.3. SEM measurements

The SEM images as shown in fig. 2.20 reveal the surface morphology of the MIP and NIP synthesized materials respectively. The MIP surface appears to be wrinkled, rough, and rugged compared to the NIP surface after the template extraction process and this may be due to the formation of the imprinted cavities.

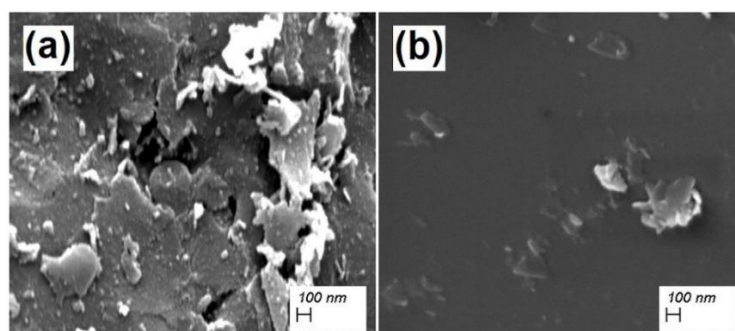


Fig. 2.20 SEM images of (a) MIP (b) NIP synthesized material.

2.4.2.4. Detection principle of FAL using MiPAN@GP

The MiPAN@GP synthesis schematic is presented in fig. 2.21. In both the AN and EGDMA, there are polar nitrile and oxygen groups. A molecular imprinted polymer embedded with graphite was produced following the addition of the initiator benzoyl peroxide. As a result of the cross linking, the polyacrylonitrile polymer became insoluble and rigid to accommodate the FAL molecules. Following the template removal, the FAL near the surface of the polymer matrix was removed, leaving rigid cavities for the FAL near the surface.

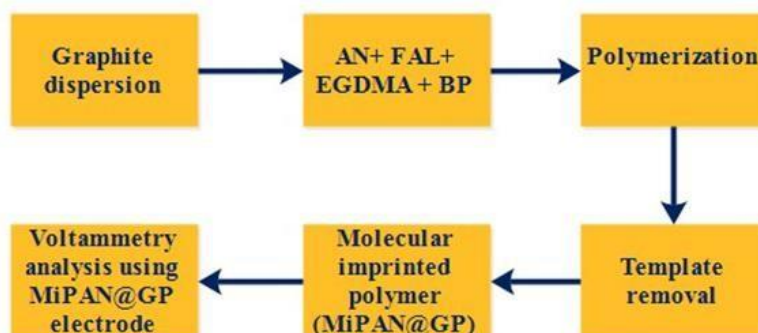


Fig. 2.21 The detection principle of FAL using MiPAN@GP electrode.

2.4.2.5. Electrochemical performance of MiPAN@GP electrode

The electrocatalytic performance of the MiPAN@GP electrode was investigated in two phases. In the first phase, a comparative analysis for the electrochemical oxidation of formalin at the surface of MiPAN@GP and NiPAN@GP electrodes was studied. The CV responses were recorded in the range of (0.5 to 2 V) in the presence of 0.1 M NaOH at 100 mV/s. Fig. 2.22 illustrates the enhanced oxidation peak at MiPAN@GP compared to the NiPAN@GP electrode. The MiPAN@GP electrode portrayed almost twice the maximum oxidation peak current compared to the NiPAN@GP electrode, which can be elucidated by the presence of molecule recognition sites within the imprinted sensor material. It led to effective analyte adsorption and hence high sensitive characteristic of formalin oxidation at the MiPAN@GP electrode surface was observed.

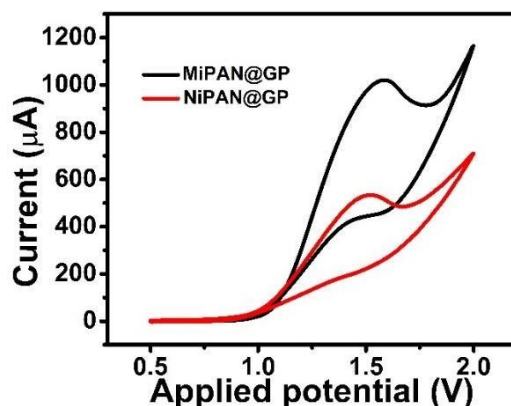


Fig. 2.22 CV response of MiPAN@GP electrode and NiPAN@GP electrode in 0.1M NaOH.

The MiPAN@GP electrode behavior was investigated with reference to a variety of supporting electrolyte compositions like H₂SO₄, phthalate (PHT), acetate (ACT), phosphate (PHP), and NaOH. The optimal DPV response was attained only in the presence of 0.1 M NaOH as depicted in fig. 2.23 (a), while no oxidation peak was illustrated by other supporting electrolytes. The presence of hydroxyl (OH) ions facilitates electrocatalytic activity to formalin oxidation as reported in our previous work [41]. All the experiments were thus carried out in the presence of 0.1 M NaOH. The MiPAN@GP electrode was also exposed for analysis in the absence of an analyte molecule. The response at the MiPAN@GP electrode was thus recorded without the FAL molecule. Fig. 2.23 (b) shows no defined oxidation peaks in the absence of

the target analyte.

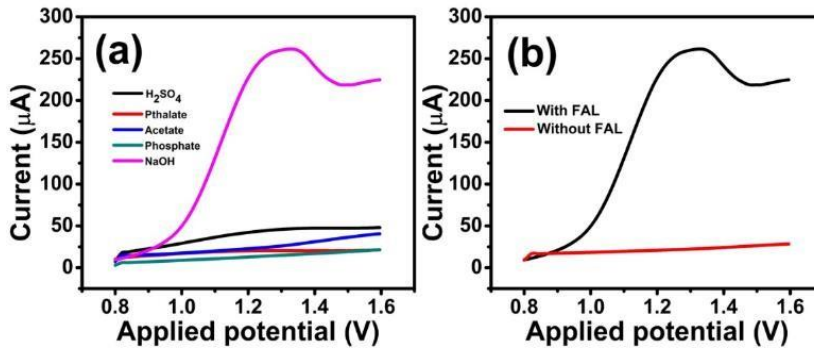


Fig. 2.23 (a) Effect of various electrolyte compositions (b) effect of FAL presence over DPV measurements at the MiPAN@GP electrode.

2.4.2.6. Effect of scan rate variation

The influence of various scan rates towards electrochemical detection of FAL molecule at MiPAN@GP electrode was investigated through the CV technique by varying the scan rates ranging from 8 mV/s to 100 mV/s (Fig. 2.24 (a)). From this figure, it is clearly observed that the oxidation peak current of FAL increases gradually with increasing the scan rate thereby indicating that the oxidation process of FAL is a surface controlled process at the MIP electrode surface [45]. Also, the anodic current versus scan rate plot (Fig. 2.24. (b)) maintains linearity which follows the linear regression equation (2.3)

$$I_{FAL} = 7.6v + 264.06; R^2 = 0.999. \quad (2.3)$$

The number of electrons transferred during electrochemical oxidation of FAL molecule is calculated by using the equation (2.4) [41] where n, F, Q, v, R and T represent no. of electrons transferred, Faraday's constant, the quantity of charge consumed, scan rate, the universal gas constant, room temperature respectively.

$$I_p = \frac{nFQv}{4RT} \quad (2.4)$$

The value of n was found to be 1.07 which almost equals unity and this result is in good accordance with the earlier reports related to electrochemical detection of formalin [41]. The linear relationship between oxidation peak potential vs logarithm of scan rate is represented in

Fig. 2.24 (c) and its slope is equal to $2.3RT/(1 - \alpha)nF$. The corresponding linear regression equation (2.5) can be expressed as

$$E_p = 0.386 \log u + 2.047; R^2 = 0.988. \quad (2.5)$$

The charge transfer coefficient (α) is calculated with the help of this slope and it is found to be 0.86.

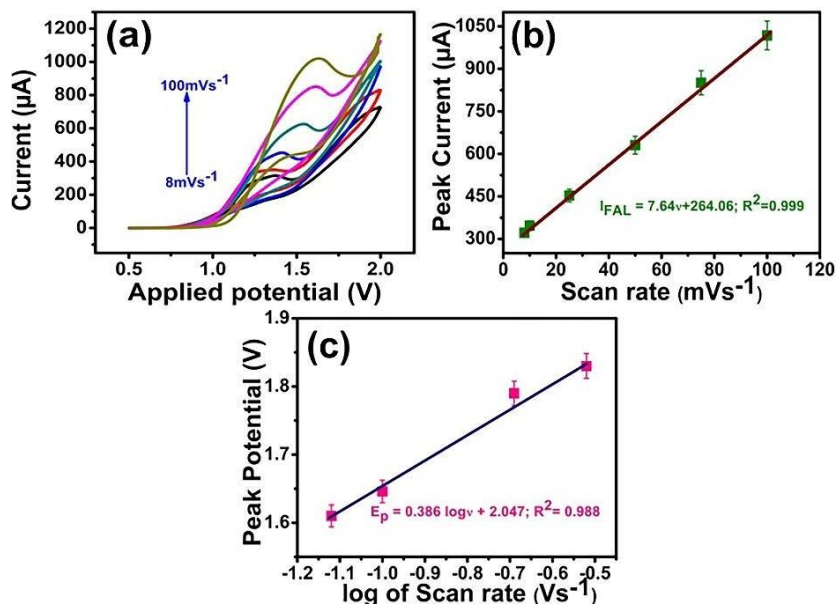


Fig. 2.24 CV response of MiPAN@GP electrode in 0.1M NaOH (a) variation of peak current with scan rate variation (b) linear plot of peak current vs scan rate (c) maximum peak potential vs log of scan rate.

2.4.2.7. Calibration curve and detection limit

The influence of several formalin concentrations at the MiPAN@GP electrode surface was surveyed using the DPV method. The highly sensitive DPV responses for different formalin contents were observed within the range of potential 0.8 to 1.6 V, in the presence of 0.1 M NaOH. Fig. 2.25 (a) portrays the gradual rise of peak current with the increase of formalin concentrations from 10 to 1000 μM at 50 mV/s. From fig. 2.25 (b), it was noticed that there are two linear regions in the calibration plot. The first linear range lies between 10 to 100 μM which follows the regression equation (2.6). The next linear range is attained from 100 to 1000 μM by following the regression equation (2.7). This electrochemical behavior can be

justified by multilayer adsorption following the monolayer adsorption phenomenon according to the Langmuir adsorption isotherm behavior [29]. Fig. 2.25 (b) represents the first linear relationship in the range of 10 to 100 μM and the regression equation (2.6) is obtained as

$$I_{FAL} = 0.59C_{FAL} + 74.67; R^2 = 0.98 \quad (2.6)$$

where I_{FAL} is the peak current and C_{FAL} is the corresponding formalin concentration. The next linear range was observed within 100 to 1000 μM and the regression equation (2.7) is obtained as

$$I_{FAL} = 0.106C_{FAL} + 131.38; R^2 = 0.99. \quad (2.7)$$

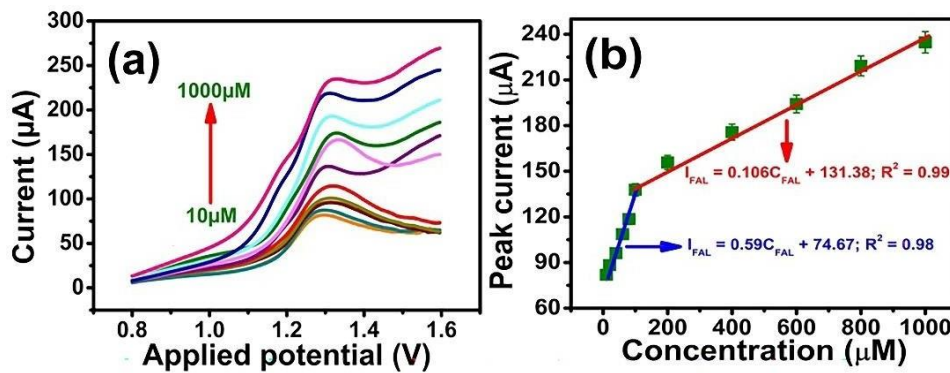


Fig. 2.25 DPV measurements for FAL using MiPAN@GP electrode in 0.1M NaOH (a) Concentration variation (b) linear plot of peak current vs concentration.

The lower limit of detection (LOD) for formalin was obtained as 0.63 μM using $\text{LOD} = 3 \sigma/m$ where σ is the standard deviation of peak currents at lowest detected concentration and m is the slope of the calibration curve. A comparative study of the electrochemical performances with the previously reported works represented in Table 2.6 shows that the proposed MiPAN@GP electrode exhibits a large linear range of operation with an excellent detection limit compared to our previous work [41] and other relevant studies.

Table 2.6

Comparison of proposed MiPAN@GP performance with the previous reports

Sensor material	Linear range (μM)	LOD (μM)	Ref.
Pt/EG/GC	125-2000	40	[35]
Cu/Cu ₂ O NPs	100-110000	10	[58]
Ni-Pd/GCE	10-1000	5.4	[59]
Pt-Pd/Nf/GCE	10-1000	3	[60]
Pd-Pt-graphene-Nafion-glassy carbon	4.50-180	2.85	[61]
CeO ₂ @GP	25-1000	1	[41]
MiPAN@GP	10-100-1000	0.63	This work

2.4.2.8. Study of Repeatability, Reproducibility and Stability

The MiPAN@GP sensor characteristics were evaluated in terms of their repeatability, reproducibility, and stability for 100 μM FAL in 0.1M NaOH. Initially, five consecutive DPV measurements were conducted using the MiPAN@GP electrode. Fig. 2.26 (a) depicts the repeatability of the sensor with relative standard deviation (RSD) as 1.23%. Simultaneously the analysis of reproducibility was also executed in this work. Three different sensors were fabricated in the same technique. Three DPV measurements were recorded as shown in fig.

2.26 (b) using the electrodes and a highly satisfactory reproducibility was achieved with RSD 3.11 %. Thereafter, the same electrode was stored at normal room temperature and the same test was performed at 15 days intervals for a period of one month. The electrode exhibited a decent stable behavior with RSD 4.35 % and negligible changes in peak current as presented in fig 2.26 (c). Also, there is no change in the peak position of the FAL molecule at the MiPAN@GP electrode. The sensor parameters have thus efficaciously established highly acceptable measures than our previous work [41].

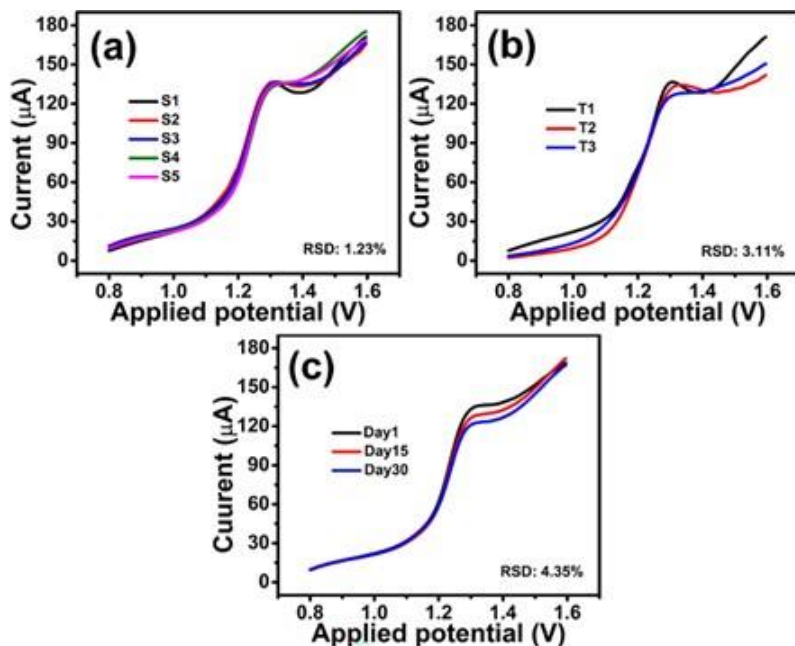


Fig. 2.26 Analytical characteristics of the MiPAN@GP electrode in 0.1M NaOH (a) repeatability (b) reproducibility (c) stability.

2.4.2.9. Interference and Selectivity Study

The MiPAN@GP electrode was exposed to various interferences namely ethanol, methanol, formic acid, benzaldehyde, and acetone to study the effect on electrochemical response. 200 µM of target analyte was subjected to 5 folds of each interfering species and DPV responses were obtained. Fig. 2.27 illustrates the effect of individual interferences on the maximum peak current. The relative signal change was negligible within a tolerance limit of $\pm 5\%$ [29]. This behavior signifies a highly selective performance of the MiPAN@GP electrode in the presence of other interfering agents compared to the non imprinted electrode or metal oxide electrode in previous work [41]. The effect of selectivity on each of the analytes FAL, ethanol, methanol, formic acid, benzaldehyde, and acetone was investigated. In fig. 2.28 the FAL analyte represented maximum peak current as compared to the other analytes. As a consequence, the MiPAN@GP electrode is established to be highly selective for the detection of FAL molecules.

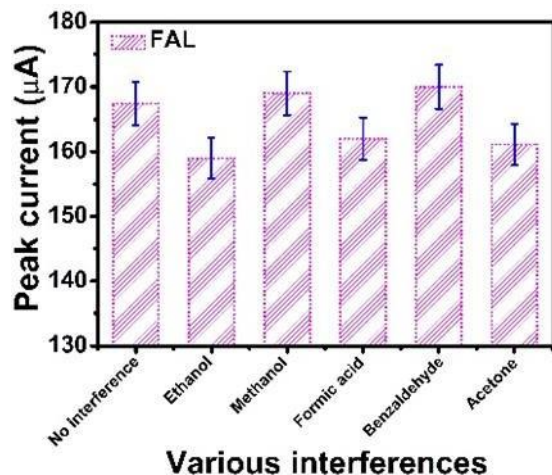


Fig. 2.27 Influence of interferences to voltammetry peak current responses of 200 μM FA in 0.1M NaOH at MiPAN@GP electrode.

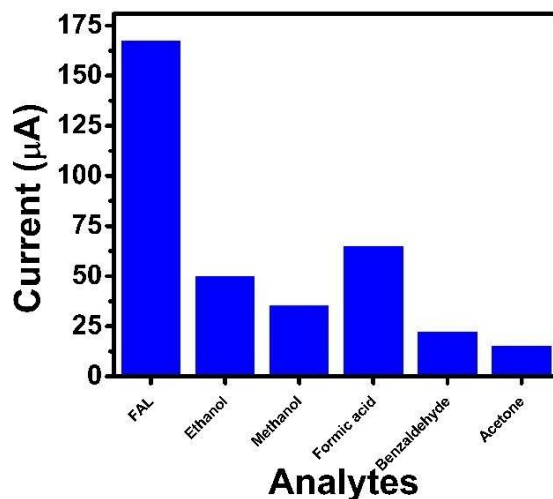


Fig. 2.28 Study of selectivity to different analytes in 0.1M NaOH at MiPAN@GP electrode.

2.4.2.10. Detection of FAL in real samples

The proposed technique was realized for the quantitative analysis of FAL in shiitake mushroom and fresh carp extracts and the results were compared with the HPLC analysis. The mean results are summarized in Table 2.7 for $m = 3$ where m is the no. of observations for each of the two real sample extracts. The MiPAN@GP electrode indicated effectively higher accuracy rates of 99.28 % and 96.72 % for the respective samples. The accuracy of the

proposed technique with reference to the HPLC method was also evaluated using a ‘t’ test analysis. The mean difference (\bar{X}_d) obtained is 0.18 and the standard deviation of the difference (S_d) is 0.049 for $n = 2$ where n is the number of samples. The absolute ‘t’ value was computed using $t = \frac{\bar{X}_d}{S_d/\sqrt{n}}$ [62]. The ‘t’ value was obtained as 5.57. The critical ‘t’ value was obtained from the ‘t’ distribution table for 95% confidence interval, significance level 0.05, and degree of freedom 1. The critical ‘t’ value is found to be 12.706.

The absolute ‘t’ value was less than the critical ‘t’ value which implied that no significant difference is observed between the proposed technique and the HPLC analysis for the mean FAL concentrations of the two different samples.

Table 2.7

Detection of FAL using MiPAN@GP electrode

Sample	FAL Detected (µg/g)		^a Error (%)	^b Accuracy (%)
	Proposed method	Ref. method		
	(Measured)	(True)		
Mushroom	31.71	31.94	0.72	99.28
Fish	3.95	4.11	3.89	96.72

% ^aError = $[(\text{Measured}-\text{True})/\text{True}]*100$; % ^bAccuracy = $(100- (\% \text{ } ^a\text{Error}))$

2.4.3. Summary

The MiPAN@GP electrode studied in this work exhibited a wide linearity range from 10 µM to 100 µM to 1000 µM with a limit of detection of 0.63 µM under optimized experimental conditions. The MiPAN@GP electrode demonstrated beneficial repeatability and reproducibility (RSD: 1.23% and 3.11% respectively) with reasonably good selectivity. The electrode also exhibited a stable electrochemical behavior over a month of extensive use. A novel MIP-based electrochemical sensor for FAL detection was thus developed, providing much improved performance in terms of linear range as well as LOD when compared to the

existing technologies. In addition, the electrode has been applied to study the FAL content in real food extracts like mushroom and fish with accuracy compared to the reference HPLC method. Overall, we can conclude the proposed sensor is a simple, cost effective key to efficient quantitative detection of FAL traces in our daily food intake items.

2.5. Conclusion

A learning process is underway regarding rapid electrochemical detection of noxious food additive formalin in the current study using three different approaches. Firstly, voltammetry responses performed in formalin with a noble metal Pt electrode reflected an extensive linearity. An index of high separability was achieved in successful data clustering using PCA. Furthermore, two regression models, the PLSR and the PCR, provided high prediction accuracies. In addition to their cost and lack of molecule selectivity, noble metal electrodes provided satisfactory analytical results. Hence, in the following work the metal oxide modification of the carbon paste was implemented to enhance electrode efficacy. Owing to its exceptional characteristics, CeO₂ nanocomposites over graphite were considered to achieve formalin detection with excellent electroanalytical features. Furthermore, the CeO₂@GP electrode moderately good electroanalytical characteristics over a period of time. The electrode also exhibited excellent performance over mushroom extracts. There were several challenges from the previous work, including limited linear range of operation, a limited detection limit, and a limited ability to recognize specific template molecules. Thus, inexpensive polymers with recognition cavities played a solution to selective electrocatalytic activities. Molecular imprinted acrylonitrile polymer (MIP) based electrochemical sensor was explored as a constructive solution. This MiPAN@GP electrode exhibited reasonably good selectivity and stable behaviour providing much improved performance in terms of linear range as well as LOD compared to the previous works. The electrode also illustrated highly accurate real sample analysis in mushroom and fish extracts as compared to HPLC technique.

References

- [1] S. Kongkaew, P. Kanatharana, P. Thavarungkul, and W. Limbut, "A preparation of homogeneous distribution of palladium nanoparticle on poly (acrylic acid)-functionalized graphene oxide modified electrode for formalin oxidation," *Electrochim. Acta*, vol. 247, pp. 229–240, Sep. 2017.
- [2] P. Wahed, M. A. Razzaq, S. Dharmapuri, and M. Corrales, "Determination of formaldehyde in food and feed by an in-house validated HPLC method," *Food Chem.*, vol. 202, pp. 476–483, Jul. 2016.
- [3] G. F. Pinto, D. L. Rocha, E. M. Richter, R. A. A. Muñoz, and S. G. Silva, "A multicommutated flow system for spectrophotometric determination of formaldehyde in mushroom," *J. Braz. Chem. Soc.*, vol. 29, pp. 1400-1405, 2018.
- [4] F. Mabood, J. Hussain, A. N. Moo, S. A. Gilani, S. Farooq, Z. Naureen, F. Jabeen, M. Ahmed, Z. Hussain, and A. A. Harrasi, "Detection and quantification of formalin adulteration in cow milk using near infrared spectroscopy combined with multivariate analysis," *J. Adv. Dairy Res.*, vol. 5, pp. 1-5, 2017.
- [5] P. K. Kannan, and R. Saraswathi, "An impedance sensor for the detection of formaldehyde vapor using ZnO nanoparticles," *J. Mater. Res.*, vol. 32, pp. 2800-2809, 2017.
- [6] G. Durante, W. Becari, F. A. S. Lima, and H. E. M. Peres, "Electrical impedance sensor for real-time detection of bovine milk adulteration," *IEEE Sens. J.*, vol. 16, pp. 861-865, 2016.
- [7] E. Zarei, M. R. Jamali, and F. Ahmadi, "Highly sensitive electrocatalytic determination of formaldehyde using a ni/ionic liquid modified carbon nanotube paste electrode," *Bull. Chem. React. Eng. Catal.*, vol. 13, pp. 529-542, 2018
- [8] Y. Cao, Z. Teng, J. Zhang, T. Cao, J. Qian, J. Wang, W. Qin, and H. Guo, "A fluorescent probe for distinguish detection of formaldehyde and acetaldehyde," *Sens Actuators B Chem.*, vol. 320, 2020.
- [9] S. Wang, X. Cui, and G. Fang, "Rapid determination of formaldehyde and sulfur dioxide in food products and Chinese herbals," *Food Chem.*, vol. 103, pp. 1487–1493, 2007.
- [10] X. Weng, C. H. Chon, H. Jiang, and D. Li, "Rapid detection of formaldehyde concentration in food on a polydimethylsiloxane (PDMS) microfluidic chip," *Food Chem.*, vol. 114, pp. 1079–1082, 2009.
- [11] W. Wongniramaikul, W. Limsakul, and A. Choodum, "A biodegradable colorimetric film for rapid low-cost field determination of formaldehyde contamination by digital image colorimetry," *Food Chem.*, vol. 249, pp. 154–161, 2018.
- [12] Y. Y. Maruo, J. Nakamura, M. Uchiyama, M. Higuchi, and K. Izumi, "Development of formaldehyde sensing element using porous glass impregnated with Schiff's reagent," *Sens. Actuators B Chem.*, vol. 129, pp.

544–550, 2008.

- [13] S. Zhang, N. Shapiro, G. Gehrke, J. Castner, Z. Liu, B. Guo, R. Prasad, J. Zhang, S. R. Haines, D. Kormos, P. Frey, R. Qin, and K. C. Dannemiller, “Smartphone app for residential testing of formaldehyde (smart-form),” *Build Environ.*, vol. 148, pp. 567–578, 2019.
- [14] S. Zhang, C. Xie, Z. Bai, M. Hub, H. Li, and D. Zeng, “Spoiling and formaldehyde-containing detections in octopus with an E-nose,” *Food Chem.*, vol. 113, pp. 1346–1350, 2009.
- [15] D. Gua, W. Liua, Y. Yana, W. Wei, J. Gana, Y. Lua, Z. Jiange, X. Wanga, and C. Xua, “A novel method for rapid quantitative evaluating formaldehyde in squid based on electronic nose,” *LWT - Food Sci Technol.*, vol. 101, pp. 382–388, 2019.
- [16] H. Tai, X. Bao, Y. He, X. Du, G. Xie, and Y. Jiang, “Enhanced formaldehyde-sensing performances of mixed polyethyleneimine-multiwalled carbon nanotubes composite films on quartz crystal microbalance,” *IEEE Sens. J.*, vol. 15, pp. 6904-6911, 2015.
- [17] J. A. Dirksen, K. Duval, and T. A. Ring, “NiO thin-film formaldehyde gas sensor,” *Sens Actuators B Chem.*, vol. 80, pp. 106-115, 2001.
- [18] D. Chen, and Y. Yuan, “Thin-film sensors for detection of formaldehyde: a review,” *IEEE Sens. J.*, vol. 15, pp. 6749-6760, 2015.
- [19] X. Tang, J. Raskin, D. Lahem, A. Krumpmann, A. Decroly, and M. Debliquy, “A formaldehyde sensor based on molecularly-imprinted polymer on a tio2 nanotube array,” *Sensors*, vol. 17, pp. 675-690, 2017.
- [20] S. A. Boampong, J. S. Peng, J. Carlan, and J. J. Belbruno, “A molecularly imprinted fluoral-p/polyaniline double layer sensor system for selective sensing of formaldehyde,” *IEEE Sens. J.*, vol. 14, pp. 1490-1498, 2014.
- [21] H. Dai, L. Gong, G. Xu, X. Li, S. Zhang, and Y. Lin, “An electrochemical impedimetric sensor based on biomimetic electrospun nanofibers for formaldehyde,” *Analyst*, vol. 140, pp. 582-589, 2015.
- [22] S. A. Boampong, and J. J. Belbruno, “Detection of formaldehyde vapor using conductive polymer films,” *Sens Actuators B Chem.*, vol. 182, pp. 300-306, 2013.
- [23] N. Iqbal, A. Afzal, and A. Mujahid, “Layer-by-layer assembly of low-temperature imprinted poly (methacrylic acid)/gold nanoparticle hybrids for gaseous formaldehyde mass sensing,” *RSC Adv.*, vol. 4, pp. 43121–43130, 2014.
- [24] M. Hussain, K. Kotova, and P. A. Lieberzeit, “Molecularly imprinted polymer nanoparticles for formaldehyde sensing with QCM,” *Sensors*, vol. 16, pp. 1011-1020, 2016.

Chapter 2: Fabrication of electrochemical sensors towards the detection of food preservative: Formalin

- [25] L. Feng, Y. Liu, X. Zhou, and J. Hu, "The fabrication and characterization of a formaldehyde odor sensor using molecularly imprinted polymers," *J. Colloid Interface Sci.*, vol.284, pp.378–382, 2005.
- [26] N. D. M. Sani, L. Y. Heng, R. S. P. M. Marugan, and N. F. Rajab, "Electrochemical DNA biosensor for potential carcinogen detection in food sample," *Food Chem.*, vol.269, pp.503–510, 2018.
- [27] Y. Herschkovitz, I. Eshkenazi, C.E. Campbell, and J. Rishpon, "An electrochemical biosensor for formaldehyde," *J. Electroanal. Chem.*, vol. 491, pp. 182–187, 2000.
- [28] B. N. Aini, S. Siddiquee, and K. Ampon, "Development of formaldehyde biosensor for determination of formalin in fish samples; malabar red snapper (*Lutjanus malabaricus*) and longtail tuna (*Thunnus tonggol*)," *Biosensors*, vol. 6, pp. 32-47, 2016.
- [29] S. Pradhan, S. Biswas, D.K. Das, R. Bhar, R. Bandyopadhyay, P. Pramanik, "An efficient electrode for simultaneous determination of guanine and adenine using nano-sized lead telluride with graphene." *New J. Chem.* 42, 564–573, 2018.
- [30] D. Das, T.N. Chatterjee, R.B. Roy, B. Tudu, S. Sabhapondit, A.K. Hazarika, P. Pramanik, R. Bandyopadhyay, "Discrimination of green tea using an Epigallocatechin-3-gallate (EGCG) sensitive molecular imprinted polymer (MIP) based electrode." *Carbon -Sci. Technol.* 10(4), 27–37, 2018.
- [31] M. S. Hoque, L. Jacxsens, and B. D. Meulenaer, A. K. M. N. Alam, "Quantitative risk assessment for formalin treatment in fish preservation: food safety concern in local market of Bangladesh," *Procedia Food Sci.*, vol. 6, pp. 151 – 158, 2016.
- [32] G. F. Pinto, D. P. Rocha, E. M. Richter, R. A.A. Munoz, and S. G. Silva, "Indirect determination of formaldehyde by square-wave voltammetry based on the electrochemical oxidation of 3,5-diacetyl-1,4-dihydrolutidine using an unmodified glassy-carbon electrode," *Talanta*, vol. 198, pp. 237–241, 2019.
- [33] A. Ejaza, Y. Jooa, J. C. Chob, J. M. Choib, J. Y. Kimb, S. Leeb, and S. Jeona, "Synthesis and catalytic activity of Ag nanoparticles dispersed on nitrogen doped GOPx toward direct electrooxidation of formaldehyde," *J. Electroanal. Chem.*, vol. 813, pp. 31–38, 2018.
- [34] G.P. Jin, J. Li, and X. Peng, "Preparation of platinum nanoparticles on polyaniline-coat multi-walled carbon nanotubes for adsorptive stripping voltammetric determination of formaldehyde in aqueous solution," *J. Appl. Electrochem.*, vol. 39, pp. 1889–1895, 2009.
- [35] Y. Chen, X. Liu, W. Zhang, Y. Zhang, L. Li, Z. Cao, H. Wang, G. Jia, Y. Gao, and J. Liu, "Electrocatalytic oxidation of formaldehyde on direct electrodeposited graphene-platinum nanoparticles composites electrode," *Anal. Methods.*, vol. 5, pp. 3915-3919, 2013.
- [36] O. Demkiv, O. Smutok, M. Gonchar, and M. Nisnevitch, "A Reagentless amperometric formaldehyde-

selective chemosensor based on platinized gold electrodes,” *Materials*, vol. 10, pp. 503-514, 2017.

[37] H. Li, Y. Zhang, Q. Wan, and Y. Li, N. Yang, “Expanded graphite and carbon nanotube supported palladium nanoparticles for electrocatalytic oxidation of liquid fuels,” *Carbon*, vol. 131, pp. 111-119, 2018.

[38] S. Biswas, S. Pradhan, H. Naskar, R. Bandyopadhyay, and P. Pramanik, “Sol gel synthesis of cubic titanium dioxide nanoparticle using poly (ethylene glycol) as a capping agent: voltammetric simultaneous determination of uric acid and guanine,” *Microchim. Acta.*, vol. 185, pp. 1-10, 2018.

[39] M.Enterría, A.G.Gonçalves, M.F.R.Pereira, J.I.Martins, and J.L.Figueiredo, “Electrochemical storage mechanisms in non-stoichiometric cerium oxide/multiwalled carbon, nanotube composites,” *Electrochim. Acta.*, vol. 209, pp. 25-35, 2016.

[40] S. Biswas, H. Naskar, S. Pradhan, Y. Wang, R. Bandyopadhyay, and P. Pramanik, “Simultaneous voltammetric determination of Adrenaline and Tyrosine in real samples by neodinium oxide nanoparticles grafted graphene,” *Talanta*, vol. 206, pp. 1-9, 2020.

[41] S. Nag, S. Pradhan, H. Naskar, R. B. Roy, B. Tudu, P. Pramanik, and Rajib Bandyopadhyay, “A simple nano cerium oxide modified graphite electrode for electrochemical detection of formaldehyde in mushroom,” *IEEE Sens. J.*, pp. 1–1, 2021.

[42] J.L. Lu, M. Y. Wu, X.L. Yang, Z.B. Dong, J.H. Ye, D. Borthakur, Q.L. Sun, and Y.R. Liang, “Decaffeination of tea extracts by using poly(acrylamide-co-ethylene glycol dimethylacrylate) as adsorbent,” *J. Food Eng.*, vol. 97, pp. 555–562, 2010.

[43] S. S. M. Hassan, H. I. Abdel Shafy, M. S. M. Mansour, and H. E. Sayour, “Quercetin Recovery from Onion Solid Waste via Solid-Phase Extraction Using Molecularly Imprinted Polymer Nanoparticles,” *International Journal of Food Engineering*, vol. 15, pp. 1–2, 2019.

[44] T. N. Chatterjee, R. B. Roy, B. Tudu, P. Pramanik, H. Deka, P. Tamuly, and R. Bandyopadhyay, “Detection of theaflavins in black tea using a molecular imprinted polyacrylamide-graphite nanocomposite,” *Sens Actuators B Chem.*, vol. 246, pp. 840-847, 2017.

[45] T. N. Chatterjee, D. Das, R. B. Roy, B. Tudu, A. K. Hazarika, S. Sabhapandit, P. Tamuly, and R. Bandyopadhyay, “Development of a nickel hydroxide nanopetal decorated molecular imprinted polymer based electrode for sensitive detection of epigallocatechin-3-gallate in green tea,” *Sens Actuators B Chem.*, vol. 283, pp. 69-78, 2019.

[46] W. de J. R. Santos, M. Santhiago, I. V. P. Yoshida, and L. T. Kubota, “Electrochemical sensor based on imprinted sol-gel and nanomaterial for determination of caffeine,” *Sensors and Actuators B: Chemical*, vol. 166–167, pp. 739–745, 2012.

Chapter 2: Fabrication of electrochemical sensors towards the detection of food preservative: Formalin

- [47] D. Das, T. N. Chatterjee, R. B. Roy, B. Tudu, A. K. Hazarika, S. Sabhapondit, and R. Bandyopadhyay, "Titanium Oxide Nanocubes Embedded Molecularly Imprinted Polymer-Based Electrode for Selective Detection of Caffeine in Green Tea," *IEEE Sens. J.*, vol. 20, pp. 6240–6247, 2020.
- [48] T. N. Chatterjee, D. Das, R. B. Roy, B. Tudu, S. Sabhapondit, P. Tamuly, P. Pramanik, and R. Bandyopadhyay, "Molecular Imprinted Polymer Based Electrode for Sensing Catechin (+C) in Green Tea," *IEEE Sens. J.*, vol. 18, pp. 2236-2244, 2018.
- [49] M. L. Quint, F. S. de Souza, A. Spinelli, and J. B. Domingos, "Low-Range Detection of the Phosphate Group by a Molecularly Imprinted Polymer-Modified Carbon Paste Electrode," *IEEE Sens. J.*, vol. 15, pp. 1012-1019, 2015.
- [50] H. Naskar, B. Ghatak, S. Biswas, P. P. Singh, B. Tudu and R. Bandyopadhyay, "Electrochemical Detection of Eugenol (EU) Using Polyacrylonitrile Molecular Imprinted Polymer Embedded Graphite (PAN-MIP/G) Electrode," in *IEEE Sensors Journal*, vol. 20, pp. 39-46, 2020.
- [51] D. Das, D. Biswas, A. K. Hazarika, S. Sabhapondit, R. B. Roy, B. Tudu, and R. Bandyopadhyay, "CuO Nanoparticles Decorated MIP-Based Electrode for Sensitive Determination of Gallic Acid in Green Tea," in *IEEE Sensors Journal*, vol. 21, pp. 5687-5694, 2021.
- [52] H. Dai, L. Gong, G. Xu, X. Li, S. Zhang, and Y. Lin, "An electrochemical impedimetric sensor based on biomimetic electrospun nanofibers for formaldehyde," *Analyst*, vol. 140, pp. 582-589, 2015.
- [53] P. Sharma, A. Ghosh, B. Tudu, S. Sabhapondit, B.D. Baruah, P. Tamuly, N. Bhattacharyya, and R. Bandyopadhyay, "Monitoring the fermentation process of black tea using QCM sensor based electronic nose," *Sens Actuators B Chem.*, vol. 219, pp. 146–157, 2015.
- [54] H. Naskar, S. Biswas, B. Tudu, R. Bandyopadhyay, and P. Pramanik, "Voltammetric Detection of Thymol (THY) Using Polyacrylamide Embedded Graphite Molecular Imprinted Polymer (PAM@G-MIP) Electrode," *IEEE Sens. J.*, vol. 19, no. 19, pp. 8583–8589, 2019.
- [55] B. Balan, A. S. Dhaulaniya, R. Jamwal, A., K. K. Sodhi, S. Kelly, A. Cannavan, and D. K. Singh, "Application of Attenuated Total Reflectance-Fourier Transform Infrared (ATR-FTIR) spectroscopy coupled with chemometrics for detection and quantification of formalin in cow milk," *Vib. Spectrosc.*, vol. 107, p. 103033, 2020.
- [56] A. B. D. Nandiyanto, R. Oktiani, and R. Ragadhita, "How to read and interpret FTIR spectroscopy of organic material," *IJOST*, vol. 4, p. 97, 2019.
- [57] M. R. Leonardo, L. A. B. d. Silva, M. T. Filho, R. S. d. Silva, and A., R. Preto, "Release of formaldehyde by 4 endodontic sealers," *Oral Surg Oral Med Oral Pathol Oral Radiol Endod.*, vol. 88, 221-225, 1999.

- [58] S. Momeni, and F. Sedaghati, "CuO/Cu₂O nanoparticles: A simple and green synthesis, characterization and their electrocatalytic performance toward formaldehyde oxidation," *Microchem. J.*, vol. 143, pp. 64–71, 2018.
- [59] E. O. Nachaki, P. M. Ndagili, N. M. Naumih, and E. Masika, "Nickel-palladium-based electrochemical sensor for quantitative detection of formaldehyde," *Chemistry Select*, vol. 3, pp. 384–392, 2018.
- [60] Z. L. Zhou, T. F. Kang, Y. Zhang, and S. Y. Cheng, "Electrochemical sensor for formaldehyde based on Pt–Pd nanoparticles and a Nafion-modified glassy carbon electrode," *Microchim. Acta.*, vol. 164, pp. 133–138, 2009.
- [61] J. Qiao, J. Chang, H. Wang, T. Sun, and C. Dong, "Determination of formaldehyde with a platinum–palladium–graphene nanocomposite glassy carbon electrode," *Anal. Lett.*, vol. 50, pp. 80-90, 2017.
- [62] S. Ngamchana, and W. Surareungchai, "Sub-millimolar determination of formalin by pulsed amperometric detection," *Anal. Chim. Acta.* vol.510 pp. 195–201, 2004.



Fabrication of electrochemical sensors towards the detection of food colourant: Metanil Yellow

This chapter presents the two different approaches being used in the present study to learn about the rapid electrochemical detection of food additive metanil yellow. The electrodes also demonstrated highly accurate analysis of turmeric powder and pigeon pea extracts.

Publication outcomes of this chapter

- Detection of Metanil Yellow Adulteration in Turmeric Powder Using Nano Nickel Cobalt Oxide Modified Graphite Electrode, IEEE Sens. J., vol.22, pp. 12515-12521, 2022.
- A Novel Molecular Imprinted Polymethacrylic Acid Decorated Graphite Electrochemical Sensor for Analyzing Metanil Yellow Adulteration in Food, IEEE Sens. J., vol.23, pp. 20951-20958, 2023.

Chapter 3

Fabrication of electrochemical sensors towards the detection of food colourant: Metanil Yellow

3.1. Introduction

Food products are illegally treated with artificial dyes in order to make them more appealing by imparting bright colors to the end users. In spite of the fact that food regulatory authorities have banned dyes such as metanil yellow, these dyes are used in many food products, including turmeric, sweets, pulses, soft drinks, and juices. It is a toxic and mutagenic monoazo dye (salt of m-[(p-anilinophenyl) azo] benzene sulphonic acid) [1]. The excessive use of these pigments in colored foods is extremely risky, as it can result in allergies, hyperactivity, liver damage, infertility, anemia, and cancer. It is still common for food products to be dyed with synthetic dyes despite their grave health risks [2]. Monitoring the presence of toxic substances in food samples is therefore imperative for public health and quality assurance. A number of analytical techniques are widely used in food safety laboratories, including high-performance liquid chromatography, gas chromatography, mass spectrometry, Raman spectroscopy [3-10]. However, complicated procedures, the requirement of specialist personnel, and high cost are causing the stakeholders to focus on the development of innovative sensors capable of offering a multitude of advantages such as precision, selectivity, robustness, low cost, good sensitivity, small size, reproducibility, and fast analysis. The advantages of electrochemical techniques are their sensitivity, accuracy, and precision, which make them ideal for determining biological and environmental parameters. Due to their improved selectivity, miniaturization, and high sensitivity, electrochemical sensors have emerged as excellent analytical tools in this context. Electroanalytical studies are more frequently employed in industrial settings and in environmental monitoring because of their superior and robust performance. The interpretation of electroanalytical data depends on constantly varying the applied potentials to the electrode and solution interface, which in turn impacts the current measured, therefore the modification of

electrode surfaces by any physical or chemical means will be vital in enhancing the sensitivity, selectivity, and reproducibility. A variety of methods have been used to develop the modified electrode for the quantification of different biological and environmental products. Generally, carbon-based electrodes like carbon paste, glassy carbon, carbon nanofibers, carbon nanotubes, etc. were used in addition to chemical compounds like nanomaterials, or ionic liquids as working electrodes [11] – [13]. The recognition layer of the electrochemical sensors is usually constituted of nanoparticles of different sizes and shapes. A great deal of their electrical properties makes gold nanoparticles valuable for use in electrochemical and colorimetric sensors. For sensing applications, gold nanoparticles have been used to prepare active surfaces using their binding potential. The electrochemical behaviour of carbon quantum dots modified glassy carbon electrodes (CQDs/GCE) and glassy carbon electrodes modified with calixarene and gold nanoparticles (calix8/Au NPs/GCE) was found to have poor detection limits and to be extremely costly [11], [13]. There has been a long standing challenge in developing a fast, effective, low-cost electrode for the selective oxidation of metanil yellow (MY). Hence, to improve the electrode efficacy two different approaches for MY detection has been explored as discussed below.

3.2. Detection of Metanil Yellow Adulteration in Turmeric Powder Using Nano Nickel Cobalt Oxide Modified Graphite Electrode

Nanocomposites based on metal oxides had previously been reported to exhibit enhanced electrochemical properties [14]. A high surface area with an increased number of active sites in metal oxide nanocomposites like neodymium oxide (Nd_2O_3) and cerium oxide (CeO_2) induce enhanced electron transfer [15], [17]. Due to their highly reproducible nature, nano crystallites have a high sensitivity. Nano crystallites may be responsible for this because of their higher surface area and because the electron levels of analyte and nano metallic oxides are perfectly matched. The mixed Ni and Co oxide has been found to be one of the most promising transition metal oxide materials, and is also a stable and cheap electrode material compared to the use of glassy carbon electrodes in [11]. There has been evidence to suggest that adding cobalt to nickel oxide/hydroxide enhances the electrochemical performance of the electrode [19]. Increased electrode conductivity is a major benefit of adding cobalt [19]. In this study, nickel cobalt oxide nanoparticles (NiCo_2O_4) were deposited onto graphite electrodes to detect MY in turmeric

powder using electrochemical methods. It is crucial to closely monitor the content of adulterants in turmeric powder to avoid contamination. NiCo₂O₄ nanoparticle has been synthesized in our work, and an electrochemical sensor has been developed by using its nanocomposites to detect MY in turmeric powder. With a linear range of 5 μM-1000 μM, the prepared electrode had a low detection limit of 100 nM. This electrode may prove to be useful for monitoring adulteration of turmeric and other foods.

3.2.1. Experimental

3.2.1.1. Chemicals and reagents

Graphite powder, nickel nitrate hexahydrate [Ni (NO₃)₂.6H₂O], cobalt acetate hexahydrate (C₄H₁₈CoO₁₀), nitric acid (HNO₃), ethanolamine (HOCH₂CH₂NH₂), and paraffin oil were acquired from Sigma Aldrich, India. Metanil yellow (MY) was procured from Merck, India. All the chemicals were of pure analytical grade and used without any further purification. The experimental solutions were prepared using Millipore water (resistance = 18 MΩ). The experiments were performed at room temperature.

3.2.1.2. Synthesis of Nickel-Cobalt oxide Nanoparticles

The following technique was used to synthesize NiCo₂O₄ nanoparticles. It consisted of adding drops of nitric acid to a cobalt solution. The solutions of nickel and cobalt were mixed with sugar and ethanolamine in a beaker. Then, the resultant solution was heated on a hot plate at about 150 °C inside a fume chamber for about 30 mins. The brownish fluffy mass obtained was next calcined in a muffle furnace at 800 °C for about 6 hours to get the NiCo₂O₄ nanoparticles (nps). The resultant nanoparticles were then used for electrode fabrication and material characterization.

3.2.1.3. Characterization Techniques

ZEISS EVO 18 (United States) was used to operate the scanning electron microscope (SEM) at an acceleration voltage of 15 kV to examine the morphology of the NiCo₂O₄ nanoparticles synthesized. This material was studied using the Philips PW1710 X-ray diffractometer (Eindhoven, Netherlands) at 40 kV and 40 mA with CuKα radiation (λ = 1.5406 Å) to obtain an XRD pattern. Three electrodes were utilized in the electrochemical analysis with

a Potentiostat/Galvanostat PGSTAT101 (Metrohm Autolab, Netherlands). The counter electrode was made up of a Pt electrode, the reference electrode was an Ag/AgCl electrode, and the working electrode was a NiCo₂O₄ modified graphite electrode (NiCo₂O₄@GP). Voltammetry was employed throughout the experiment. A similar approach was utilized to prepare a simple bare graphite electrode (Bare GP) with graphite powder only.

3.2.1.4. Fabrication of NiCo₂O₄@GP Electrode

The NiCo₂O₄ nanoparticles and graphite powder were taken in a different weight ratio of 1:9, 2:8, and 3:7, and then 300 mg by weight of each material were mixed together into fine paste by adding 2 to 3 drops of paraffin oil in a mortar-pestle. Next, the fine paste obtained was stuffed into the glass capillary tube with an inner diameter of 2 mm. Platinum wires were inserted into the sensor material to establish the electrical connections.

3.2.2. Results and discussion

3.2.2.1. Study of X-ray Diffraction Characteristics of NiCo₂O₄

An X-ray diffraction pattern of synthesized NiCo₂O₄ is depicted in fig. 3.1 (a). As confirmed by XRD patterns, the cubic phase of NiCo₂O₄ nps formed the standard JCPDS card No. 00-002-1074. The most intense peak was found at $2\theta = 28.7^\circ$ for (111) crystal plane along with other peaks at 31.18° (220), 36.86° (311), 44.6° (400), 55.29° (422), 58.97° (511), 64.67° (440), respectively. The diffractogram showed no crystalline contamination, indicating that the NiCo₂O₄ material synthesized was impurity-free. The Debye-Scherrer formula [18] estimated the crystallite size to be 18.75 nm. The XRD pattern of pure graphite is illustrated in fig.3.1 (b). The most intense peak was found at $2\theta = 26.5^\circ$ for (002) which closely matches the standard JCPDS card no. 00-012-0212. The diffraction pattern of NiCo₂O₄ modified graphite exhibited one sharp peak for graphite and corresponding peaks for NiCo₂O₄ nanoparticles. This indicates the successful formation of NiCo₂O₄ nanoparticle modified graphite material.

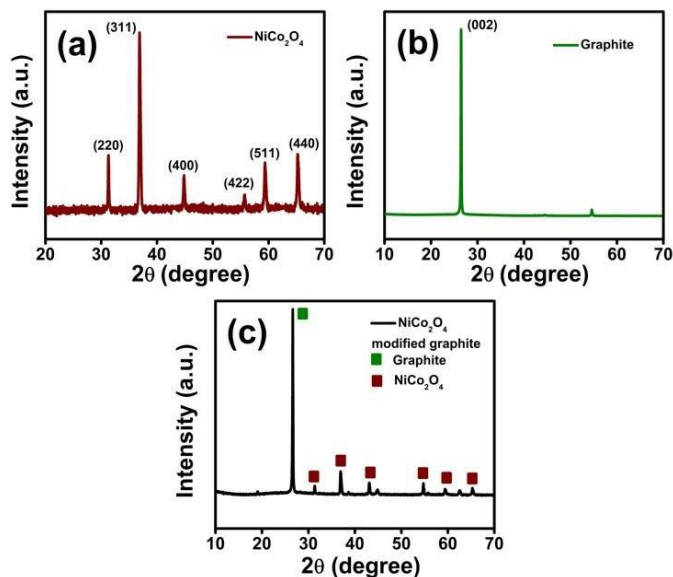


Fig. 3.1 X-ray diffraction pattern of (a) synthesized NiCo_2O_4 nano crystallites (b) Graphite (c) NiCo_2O_4 modified graphite.

3.2.2.2. Study of SEM Analysis of NiCo_2O_4

An examination of the morphology of prepared NiCo_2O_4 nanoparticles and pure graphite was performed by SEM. It was revealed by the SEM image that the prepared materials contain nano particles. The synthesized NiCo_2O_4 particles and pure graphite are depicted in fig. 3.2 (a) and fig. 3.2 (b) respectively.

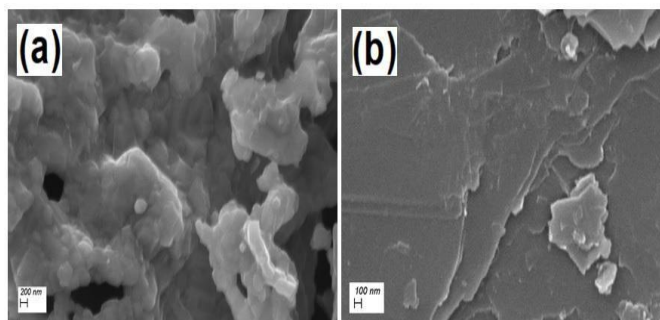


Fig.3.2 SEM image of (a) synthesized NiCo_2O_4 nanoparticles (b) pure graphite.

3.2.2.3. Study of FTIR Analysis of NiCo_2O_4

The FTIR analysis of synthesized NiCo_2O_4 nanoparticles is depicted in fig.3.3. It shows there are two high frequency noticeable bands at 558 cm^{-1} and 656 cm^{-1} regions. According to

the literature [26], [27], the two bands at 558 cm^{-1} and 656 cm^{-1} are distinctive features of the metal-oxygen bond which is related to the stretching vibrational mode of $(\text{Ni}^{2+})\leftrightarrow\text{O}$ or $(\text{Co}^{2+})\leftrightarrow\text{O}$. Additionally, the band at 558 cm^{-1} indicates the nickel-cobalt bond vibration. A new section has been included in the manuscript with the FTIR characterization of NiCo_2O_4 . The necessary modifications are included in the manuscript.

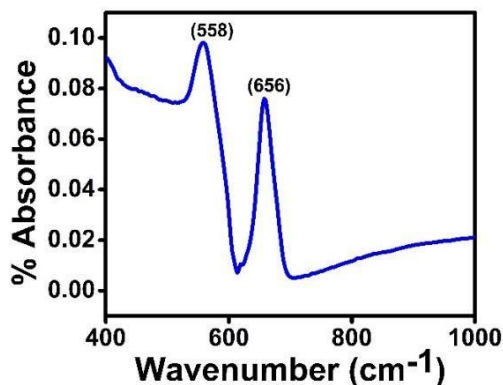


Fig. 3.3 FTIR pattern of synthesized NiCo_2O_4 nano crystallites

3.2.2.4. Electrocatalytic Behaviour of NiCo_2O_4 @GP Electrode

Using the cyclic voltammetry (CV) technique, the electrochemical behavior of the NiCo_2O_4 @GP electrode was investigated. The CV responses of the bare GP electrode and NiCo_2O_4 @GP electrode were recorded. As can be seen from fig.3.4 (a), the GP electrode modified with NiCo_2O_4 reveals a redox process with the oxidation and reduction peaks at 0.6 V and 0.4 V respectively. A notable rise in oxidation peak current ($12\text{ }\mu\text{A}$) and a reduction peak at the NiCo_2O_4 @GP electrode surface was observed when compared to the bare GP electrode. This rise in oxidation peak current, approximately three times the peak current of the GP electrode, may be due to faster electron kinetics owing to the modification of the GP electrode with NiCo_2O_4 . The electrochemical performance of graphite electrodes has been augmented by nickel and cobalt oxide addition. This may be due to nano crystallites, which have a higher surface area and whose electron levels can match analyte and nano metallic oxides perfectly. The ratio of the modifier i.e., NiCo_2O_4 to the graphite was experimentally optimized. Three electrodes were prepared using the modifier and graphite in the ratio of 1:9, 2:8, and 3:7. As in fig.3.4 (b), the maximum peak current of $12\text{ }\mu\text{A}$ was observed for the case when the modifier and the graphite

were mixed in a ratio of 1:9. The $\text{NiCo}_2\text{O}_4@\text{GP}$ electrode was imbibed in phosphate buffer saline (PBS) of varying pH, i.e., from pH 1 to pH 7.

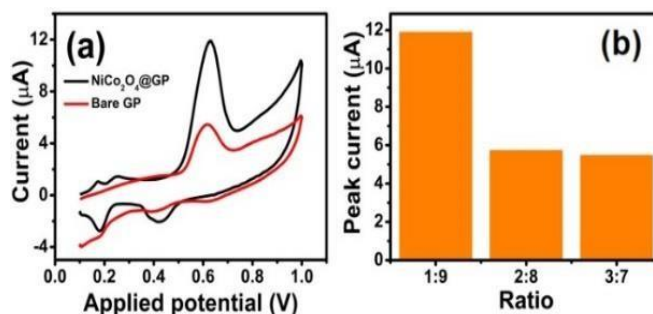


Fig. 3.4 (a) Comparative performance of $\text{NiCo}_2\text{O}_4@\text{GP}$ electrode with bare GP (b) Bar plot of modifier to graphite ratio vs peak current.

In fig.3.5 (a), the maximum peak current of $3.10 \mu\text{A}$ was observed due to oxidation of the target molecule in PBS 6. Therefore, PBS 6 was taken the optimized buffer throughout the experiment as it produced the maximum peak current.

As shown in fig.3.5.(b), in the absence of the target molecule (MY), no oxidation peaks were present. To the above solution, MY was added, and the experiment was repeated. The determination of the target molecule was confirmed because an anodic oxidation peak was observed at 0.6 V. This has been well-established in fig. 3.5 (b). The relationship of peak potential (E_p) vs pH was also studied. As the pH of the solution decreased (Fig.3.5 (c)), the oxidation peak potentials for MY shifted negatively, indicating that the phenolic group was dissociated during the oxidation process. Phenol dissociates into anion at higher pH, which is easily oxidized. There is a linear relationship between the oxidation peak potentials of MY and the pH of the solution, which is given in

$$E_p = -0.051\text{pH} + 0.90; R^2 = 0.93.$$

The slope from curve obtained as -0.051 was found to agree with the theoretical value of -0.059 reported by Nernst [17]. The results of this study indicate the electrode reactions involved the same number of protons and electrons.

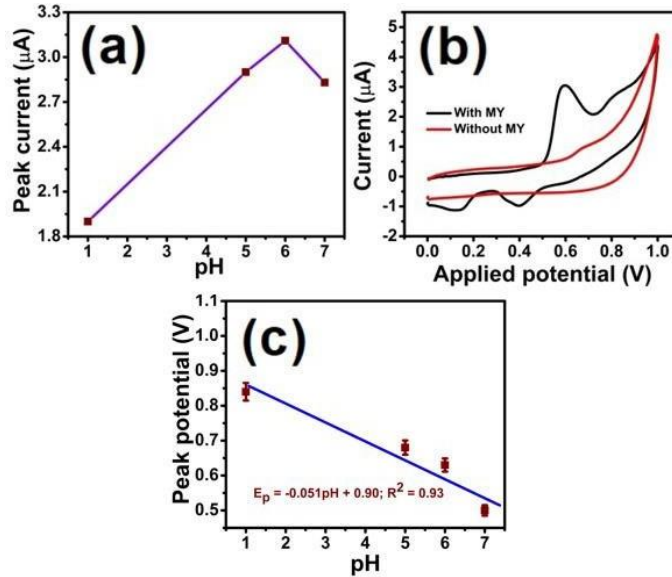


Fig. 3.5 (a) Plot of peak current vs pH value (b) CV response of NiCo₂O₄@GP electrode in PBS 6 with and without MY (c) peak potential vs pH value.

3.2.2.5. Influence of Scan Rate Variation

Using the CV approach, the influence of different scan rates on the electrochemical determination of MY molecule at NiCo₂O₄@GP was examined across a range of 0 V to 1 V. The variation of scan rate is depicted in fig.3.6 (a). It was established that on increasing the scan rate from 8 to 800 mV/s, a linear increase in anodic peak current was observed. This finding indicates that the electrocatalytic oxidation of the MY molecule at NiCo₂O₄@GP is a surface-controlled process [18], [20]. Fig.3.6 (b) displays the plot between oxidation peak current vs. scan rate. The linear regression equation $I_{MY} = 0.042 \nu + 2.412$; $R^2 = 0.98$ is supported by fig. 3.6(b).

$$I_p = \frac{nFQ\nu}{4RT} = \frac{n^2F^2A\nu\Gamma_C}{4RT} \quad (3.1)$$

Equation (3.1) [20] was used to compute the figure of electrons transported throughout the oxidation process where I_p is the peak current, n is the number of electrons transferred, F is the Faraday's constant, R is the universal gas constant, T is the room temperature, A is the surface area of the electrode, Γ_C is the surface concentration of MY, Q is the amount of charge used up during the oxidation and ν is the scan rate [20]. The number of electrons n exchanged was calculated to be 1. The electron transfer coefficient was also calculated using a linear plot of

peak potential (E_P) vs $\log v$ fig.3.6 (c). The charge transfer coefficient $\alpha = 0.4$ (indicates sluggish process) as calculated from the slope of the curve $2.3RT/(1-\alpha)nF$ [20], and the obtained regression equation was

$E_P = 0.095 \log v + 0.688$; $R^2 = 0.98$. Using Laviron's equation, the rate of electron transport k_s was estimated by using Eq. (3.2)

$$\log k_s = \alpha \log(1 - \alpha) + (1 - \alpha) \log \alpha - \left(\frac{\log RT}{nFv} \right) - \left(\frac{nF\Delta E_P \alpha(1-\alpha)}{2.3RT} \right). \quad (3.2)$$

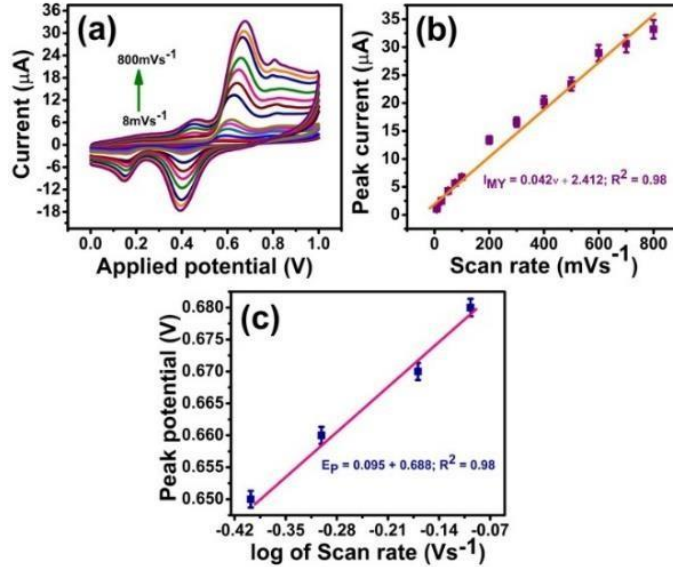


Fig. 3.6 CV response of NiCo₂O₄ electrode (a) variation of peak current with scan rate variation (b) linear plot of peak current vs scan rate (c) maximum peak potential vs log of scan rate.

The α value is 0.4 and k_s (0.0732 s^{-1}) generated from the preceding equations. The pace of the chemical reaction determines the degree of chemical reversibility of an electrochemical system.

3.2.2.6. Determination of Metanil Yellow

Owing to better current sensitivity and resolution than CV responses, DPV measurements were used to investigate the influence of varied concentrations on the surface of NiCo₂O₄@GP in PBS 6. The comparative rise in the oxidation peak current with increasing concentration from 5 to 1000 μM is depicted in fig.3.7 (a). A pair of oxidation peaks are seen at 0.6 and 0.8 V, with the first peak exhibiting a greater current than the second. Thus, the first oxidation peak current was used to study linearity and to compute the lower detection limit. As seen in fig. 3.7 (b), the linear range of the synthesized NiCo₂O₄@GP electrode was found to be from 5 to 1000 μM and the corresponding regression equation is $I_{MY} = 0.025C_{MY} + 2.77$; $R^2 = 0.98$ where I_{MY} is the peak current and C_{MY} is the corresponding concentrations of metanil yellow. LOD = $3 \sigma/m$ is

used to calculate the lower limit of detection. The standard deviation of maximum peak currents for the lowest detected concentration (LOD) is determined to be 0.1 μM , σ is the standard deviation of maximum peak currents for the lowest detected concentration and m is the slope of the calibration curve, respectively [21]-[25]. Table 3.1 shows a comparison of the present work with existing literature. The study shows that the electrode presented a wide linear range compared to CQDs/GCE in [11] and the LOD obtained in this work is satisfactorily comparable with previous publications.

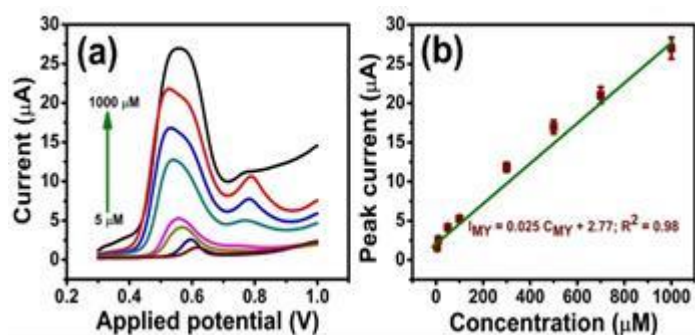


Fig. 3.7 DPV measurements for MY using NiCo₂O₄@GP electrode (a) Concentration variation of 5 to 1000 μM (b) linear plot of peak current vs concentration.

Table 3.1

Comparison of proposed NiCo₂O₄@GP performance with the previous reports

Sensor/Technique	Linear range (μM)	LOD (nM)	Ref.
CQDs/GCE	0.06 to 40	30	[11]
LC-UV	133-266.4	506	[4]
LC-DAD	13.32-799	-	[8]
NiCo₂O₄@GP	5 – 1000	100	This work

3.2.2.7. Study of Repeatability, Reproducibility, and Stability

The repeatability, reproducibility, and stability of the NiCo₂O₄@GP electrodes were investigated by DPV measurements. Relative standard deviation (RSD) of 1.51% is reported for

the sensor with four consecutive repetitions as shown in fig. 3.8 (a). Highly reproducible behavior was observed using three electrodes with RSD of 1.75 % in fig. 3.8. (b). Trials were carried out every 15 days for 45 days using the same electrode stored at room temperature. According to fig. 3.8. (c), this electrode displays stable behavior with a RSD of 3.87 %. In other words, this experiment illustrated successful sensor parameter assessment.

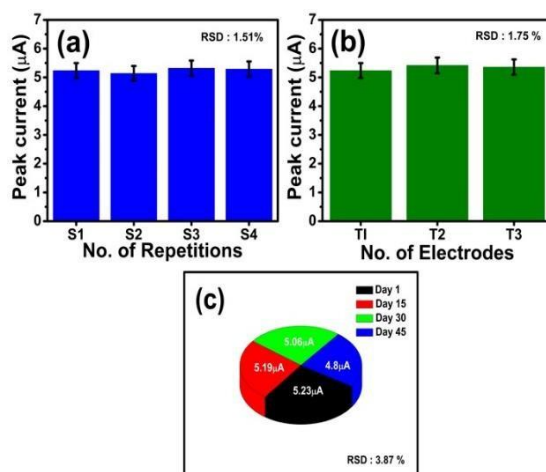


Fig. 3.8 Analytical characteristics of the NiCo₂O₄@GP electrode (a) repeatability(b) reproducibility(c) stability.

3.2.2.8. Study of Selectivity

NiCo₂O₄@GP sensor was subjected to different interferences Na⁺, K⁺, Zn²⁺, curcumin to determine how they affected its electrochemical characteristics. We obtained DPV responses after introducing each specific interfering species followed by the target analyte. fig. 3.9 shows the effect of each interfering agent on the peak current. The relative signal fluctuation did not exceed the tolerance of ±5% [20].

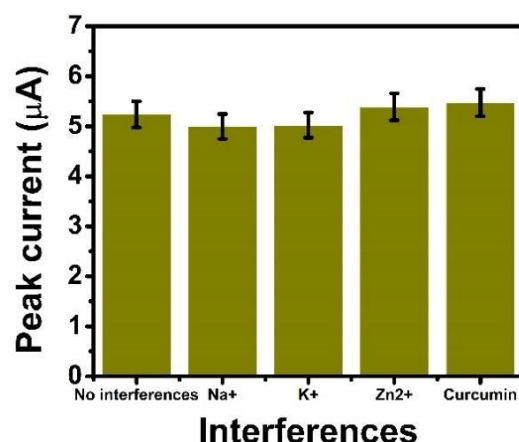


Fig.3.9 Influence of interferences to voltammetry peak current responses of MY at NiCo₂O₄@GP electrode.

3.2.2.9. Investigation of Real Sample

Turmeric powder sample was obtained from the market. 2 g of turmeric powder were dissolved in 100 milliliters of millipore water. The diluted extracts of turmeric were then measured by the standard addition method without any further pre-treatment. A DPV analysis was performed on diluted turmeric extracts spiked with various concentrations of MY solutions. The results of the analysis found in Table 3.2 explains that the recovery rates are in the range of 98% to 103.5% with RSD values between 1.17% and 1.90%. Using NiCo₂O₄@GP electrodes as MY sensors, the results indicate that there is no matrix effect.

Table 3.2
Determination of MY in turmeric using NiCo₂O₄@GP electrode

Sample	Spiking (µM)	Detected (µM)	Recovery ^a (%)	± R. S. D ^b (%) (n=3)
Turmeric powder pure	0	45	-	1.17
Turmeric powder spiked	10	54.8	98	1.90
	20	65.7	103.5	1.64

^a Recovery = [Detected (µM)-Diluted sample (µM)]/Spiking (µM); ^b R.S.D (%) = [100x Standard deviation]/ Mean

3.2.3. Summary

This study demonstrates improved electrochemical detection of MY in turmeric powder samples using NiCo₂O₄ nano crystallites cast over graphite paste. In this work, a new electrochemical sensor incorporating a metal oxide modifier was successfully developed for the detection of MY. An electrode made of NiCo₂O₄@GP demonstrated excellent electrochemical performance and a wide linear characterization range. Electrochemical studies of NiCo₂O₄@GP electrodes have justified a surface-controlled electrocatalytic process with a high electron transfer rate. The proposed NiCo₂O₄@GP electrode was highly selective, reproducible, repeatable, and stable over a period of about a month. The electrode was applied over turmeric powder samples with excellent recovery rates. Using NiCo₂O₄@GP, the safety limit estimation of MY traces in agro products can be validated. The NiCo₂O₄@GP electrodes proposed in this paper have thus proven that they can be deployed as cost-effective and field deployable sensors for MY trace detections.

3.3. A Novel Molecular Imprinted Polymethacrylic Acid Decorated Graphite Electrochemical Sensor for Analyzing Metanil Yellow Adulteration in Food

Although little has been explored by using electrochemical approaches to modify sensing materials such as glassy carbon electrodes and carbon quantum dots, chitosan tailored glassy carbon electrodes, glassy carbon electrodes decorated with calixarene, and gold nanocomposites [11-13]. The lack of a specific and highly selective sensing material prompted the synthesis and application of molecular imprinted polymer technology. Recent developments in polymers with cavities of recognition, profound hydrogen bonds, and multiple active sites contribute significantly to electrocatalytic activity [28]. Natural or synthetic monomers are incorporated into MIP materials to form vacancies that can capture targeted molecules [29]. Analytes that can act as templates usually are covalent or non-covalent bonded inside a complex of monomers with crosslinkers in molecular imprinting [24], [30]. The polymer matrix left behind by polymerization contains a molecular memory. The basic adsorption mechanism for any compound depends on molecular recognition [24]. The technology is appropriate for a series of applications [32-37]. A polymer substrate can be

Chapter 3: Fabrication of electrochemical sensors towards the detection of food colourant: *Metanil Yellow*

imprinted with active sites or cavities that have an affinity for specific metabolites, thereby creating receptors for them. This is considered polymer imprinting at a molecular level. Polymer synthesis occurs in the presence of an analyte or template molecule, and the template is removed after the polymerization is complete; the result is selective binding sites within the polymer. To achieve a higher degree of molecular recognition, these cavities are responsible for binding the template molecules based on shape, size, and functionality.

In the present work a sensitive, specific, low-cost, reusable electrochemical sensor for the detection of metanil yellow (MY) in food commodities has been developed based on a molecular imprinted polymer platform of methacrylic acid embedded on graphite and MY as a template. In terms of production of sensors, the accomplishment lies in developing a simple, cheap, easy and selective method. The electrode has been examined in detail analytically, demonstrating an extensive linear scale of operation with higher selectivity, repeatability, reproducibility, and stability over an extended time period. Furthermore, the MIP electrode was used to assess the electrochemical behavior in turmeric powder and pigeon pea samples from the market and achieved high-quality results in contrast to the HPLC investigation. The present system can therefore be endorsed for detection of MY in a widespread diversity of samples.

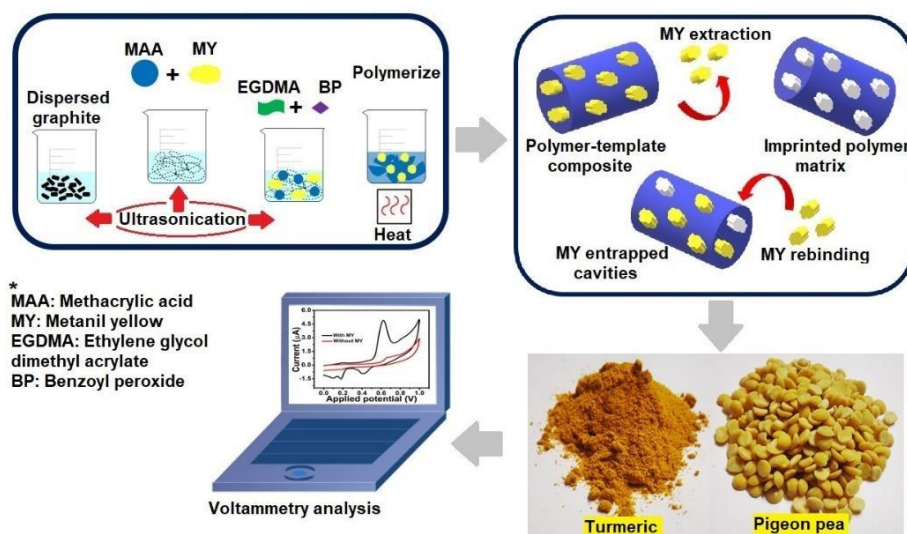


Fig. 3.10 Schematic representation of MIP synthesis to evaluate the electrode responses to MY in pigeon pea and turmeric powder.

3.3.1. Experimental

3.3.1.1. Reagents and standards

Metanil yellow (MY) was acquired from Merck, India. This study made use of graphite dust (99%), monomer methacrylic acid (MAA), cross linker ethylene glycol dimethyl acrylate (EGDMA), benzoyl peroxide, and paraffin oil procured from Sigma Aldrich, USA, and Merck, India respectively. The elements obtained were all analytical grade, and they did not require any refinement. The solutions were formulated using Millipore water (resistance = 18 M Ω). Entirely the experimentations were executed at an ambient temperature.

3.3.1.2. Methods and measurement

Electrochemical analysis was conducted using a Potentiostat/Galvanostat PGSTAT101 via three electrodes. Featuring three electrodes, the three electrode arrangement embraced a counter electrode made of Pt, an Ag/AgCl reference electrode, and a MIP working electrode. Spectroscopy techniques FTIR and UV-Vis have been used to characterize the synthesized polymer materials. A Fourier transform infrared spectroscope (Nicolet™ iS20, Thermo Fisher Scientific) was used in the 400–4000 cm⁻¹ wavelength section by means of KBr pellets designed for standardization. The UV-Vis UV-1800 SHIMADZU, UV Spectrophotometer has been utilized in the wavelength range from 200 to 400 nm. The morphology characterizations were surveyed by ZEISS EVO 18 scanning electron microscope (SEM) functioned at 15 kV acceleration potential. The HPLC evaluation was executed by means of WATERS PVT. LTD multidimensional liquid chromatography (MDLC-5698) by means of UV-Vis detector (Model no. 2487).

3.3.1.3. Synthesis of molecular imprinted polymer

In the laboratory, the polymer integration was done as reported previously in a similar study for the detection of caffeine [21]. Initially, ethanol (15 mL) was used to disperse the graphite powder (0.95 g) by ultrasonication for 40 minutes. Subsequently, the monomer MAA (0.05 g) and template MY (0.05 g) were added and sonicated for 60 minutes. Afterwards, crosslinker EGDMA was added (400 μ L) together with benzoyl peroxide (1 mg) to the solution and sonicated for about 60 minutes. In the next step, polymerization of the solution took place at 30 °C for 40 minutes in a water bath.

The polymer synthesized was next rinsed carefully with ethanol and distilled water repeatedly (1:1). All through this process, the MIP material was formed as the template molecules were leached out. The sample was collected and air dried before being analyzed. An alternative polymer material (NIP) that was not imprinted by template molecules was produced by a similar procedure.

3.3.1.4. Fabrication of electrode

During the fabrication of the MIP electrode, an amount of 300 mg MIP was taken in a mortar and pestle. Two to three drops of paraffin oil were used to blend the material into a fine paste. Subsequently, the paste was sealed into a glass capillary tube of inner diameter 2.5 mm, by using a thin metallic rod. Through the use of a platinum connecting wire at the opposite end of the capillary, an electrical connection was established. Using the NIP material (except for the template), a NIP electrode was prepared similarly.

3.3.2. Results and discussion

3.3.2.1. Monomer optimization

A selection of the optimized polymer was carried out during simultaneous synthesis of three different imprinted polymers. In order to prepare the molecular imprinted polymer materials, three monomers were used, viz. methacrylic acid, acrylamide, and acrylonitrile. After CV was applied to the three electrodes within the range 0-1 V, an oxidation peak at 0.6 V in 0.1M phosphate buffer with pH 6 (PBS6) was observed at 100 mVs^{-1} . As illustrated in fig. 3.11. In comparison to the imprinted polymer electrodes of acrylamide and acrylonitrile, the maximum oxidation peak current attained by methacrylic acid was 2.09 to 2.2 times higher respectively. MIP recognition sites can be affected by the interaction of monomer molecules and template molecules during prepolymerization, which influences the electrochemical behaviour of the MIP material [21]. By enhancing dipole-to-dipole exchanges amid the monomers and templates in the prepolymerization complex, the methacrylic acid (MAA) based MIP electrode have shown improved electrochemical performance [21]. Accordingly, MAA was deemed to the best monomer for achieving the objective of the proposed research.

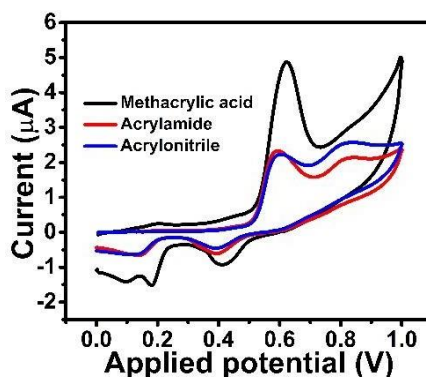


Fig. 3.11 CV response of different monomers in the presence of 100 μM MY in 0.1M PBS6.

3.3.2.2. Characterization of the synthesized material

1. FTIR analysis: FTIR spectroscopy was used to determine the spectral composition of the polymer before template removal (BTR) and after template removal (ATR) as shown in fig.3.12. In fig.3.12 a. the sharp bands at 1148 cm^{-1} , 1290 cm^{-1} and 1452 cm^{-1} represent (C-N) stretching (C-H) bending, (N-H) bending (C-C) stretching (C-N) stretching and (N=N) stretching (C-H) bending respectively. It is the sharp vibrational mode specific to the N=N site (1715 cm^{-1}) that most strongly identify the presence of the metanil yellow template in the BTR polymer sample. The peaks relevant to the MY were absent in the ATR sample that ensure complete removal of the MY template.

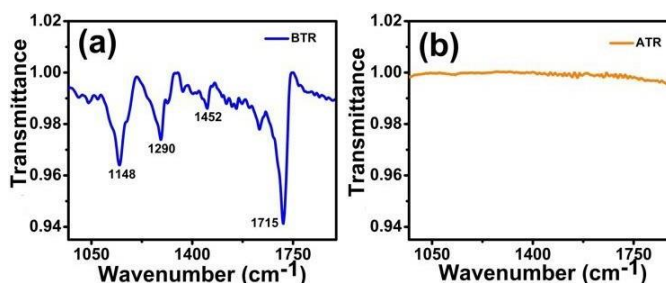


Fig. 3.12 FTIR spectra of the MIP (a) before (b) after template removal.

2. UV-Vis spectroscopy: UV-Vis technique of spectroscopy confirmed that the MY molecule was leached out successfully, and the results are shown in fig.3.13. After template extraction, a sharp peak at 436 nm was completely obscured from spectral observation. Thus, an effective MIP was prepared based on complete template extraction.

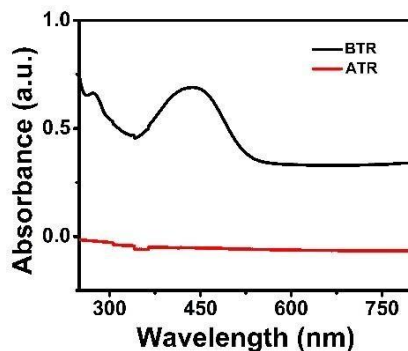


Fig. 3.13 UV-Vis spectra of MIP before and after template extraction.

3.3.2.3. SEM measurements

The SEM images of synthesized materials, MIP and NIP, as represented in fig.3.14 illustrate their surface morphology. MIP surfaces after the extraction process of the template appear crumpled, coarse, and craggy in comparison to the NIP surfaces. These characteristics are likely owed to the presence of the cavities imprinted.

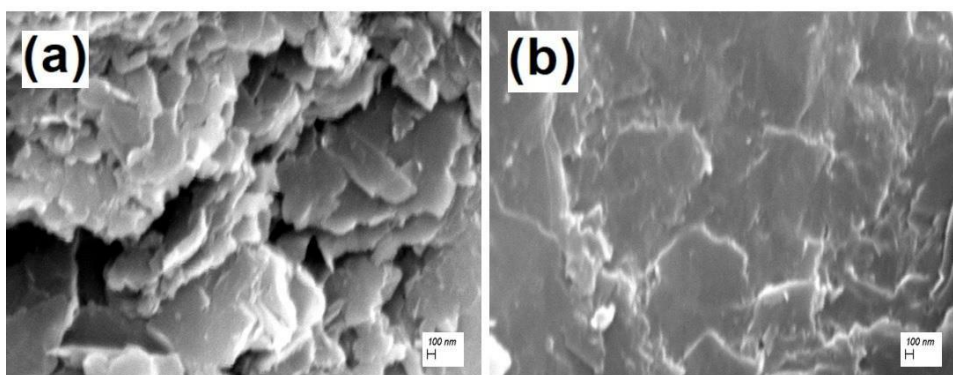


Fig. 3.14 SEM images of synthesized (a) MIP and (b) NIP material.

3.3.2.4. Electrochemical performance of MIP electrode

A two-phase study of the electrocatalytic performance of the MIP electrode was conducted. The first phase of this research entailed a comparison of the electrochemical MY oxidation on the surface of MIP and NIP electrodes. CV results were measured within 0 to 1 V at 100 mV/s with 0.1M PBS6. fig.3.15 a. exemplifies the intensified oxidation peak at the MIP electrode in contrast to the NIP electrode. The electrode surface of the MIP had specific recognition sites for MY, thus exhibiting a greater rate of adsorption, which is reflected in the

larger MIP electrochemical performance of 2.4 times greater than the NIP. In order to establish MY detection, the MIP electrode response was evaluated in the presence and absence of 100 μM target analyte as depicted in fig.3.15 b. No MY oxidation peak was observed in the absence of target molecule.

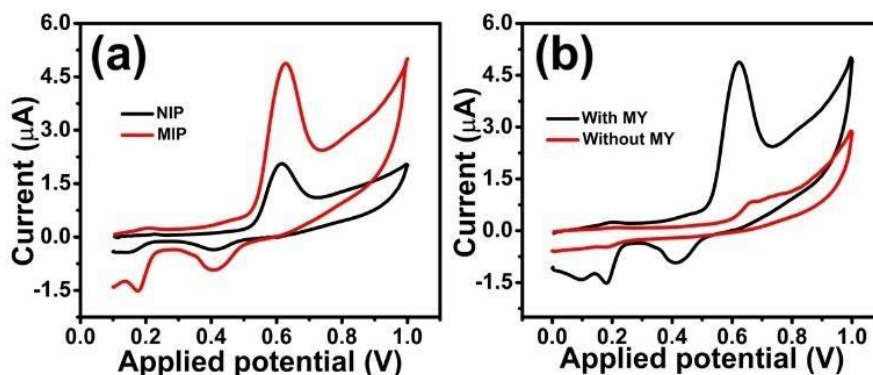


Fig. 3.15 CV response of (a) MIP and NIP electrodes (b) MIP electrode with and without the presence of 100 μM MY in 0.1 M PBS6.

An investigation of the MIP electrode behavior was conducted with different supporting electrolyte compositions, including phosphate, phthalate, acetate, H_2SO_4 , and NaH_2PO_4 . The maximum response was only obtained in the presence of phosphate supporting electrolyte, as displayed in fig. 3.16 a, compared to the other supporting electrolytes. Simultaneously, the effect of pH variation in the phosphate supporting electrolyte was observed and the optimum peak current was obtained at a pH 6 as shown in fig. 3.16 b. Therefore, all the experiments were conducted with 0.1M phosphate supporting electrolyte of pH 6 (PBS6).

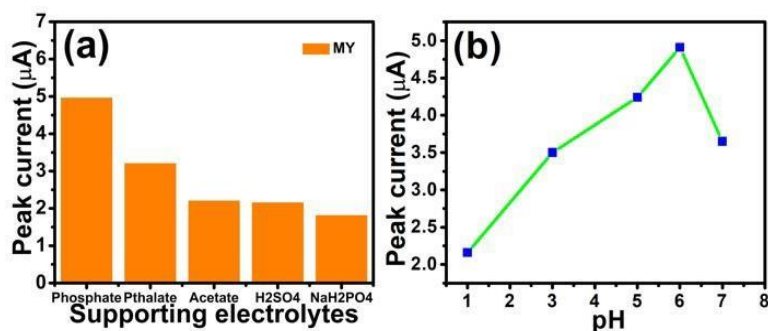


Fig. 3.16 (a) Influence of different supporting electrolyte compositions (b) influence of phosphate supporting electrolyte with different pH on the peak current in the presence of 100 μM MY.

3.3.2.5. Effect of scan rate variation

The impact of varying scan rate on the electron transfer kinetics within the three-electrode system has been observed by CV. The response of MIP electrode has been obtained by subjecting it to MY solution of 100 μM at scan rates varying from 1 to 1000 mVs^{-1} (Fig.3.17 a). The oxidation peak current for MY can be seen by looking at this figure, increases proportionately for each the scan rate thus signifying that the oxidation phenomena of MY are surface regulated progression at the MIP electrode interface [22]. Likewise, the anodic current (I_{MY}) vs scan rate (v) plot (Fig. 3.17 b) upholds linearity 1 to 900 mVs^{-1} which trails the linear regression equation (3.3)

$$I_{MY} = 0.05v + 2.04; R^2 = 0.99. \quad (3.3)$$

A shift in positive peak potential (E_p) was obvious through the analysis of the MIP-MY electrode adsorption kinematics by a linear upsurge with $\log v$ (Fig. 3.17 (c)). Calculations of the number of electrons (n) transferred was performed using the following Eq. (4)

$$I_p = \frac{nFQv}{4RT} \quad (3.4)$$

where n , F , Q , v , R and T represent no. of electrons transferred, Faraday's constant, the quantity of charge consumed, scan rate, the universal gas constant, room temperature respectively.

The n computed from Eq. (3.4) is 1.1 approximately equals to 1. The n so attained entitles that the MIP-MY electrode holds acceptable adsorption capability to the MY molecules. The linear regression (3.3) is obtained from fig.3.17 c and the slope is $2.3RT/(1 - \alpha)nF$. The consequent linear regression equation (3.5) can be articulated as

$$E_p = 0.11 \log v + 0.69; R^2 = 0.99. \quad (3.5)$$

The value of the heterogeneous rate constant (k_s) is obtained as 0.06 s^{-1} during the oxidation process using Laviron's equation (3.6) [23], [31]

$$\log k_s = \alpha \log(1 - \alpha) + (1 - \alpha) \log \alpha - \left(\frac{\log RT}{nFv} \right) - \left(\frac{nF\Delta E_p \alpha(1-\alpha)}{2.3RT} \right). \quad (3.6)$$

The value of the electron transfer coefficient (α) was determined as 0.5 from the calibration curve slope of Eq. (3.5).

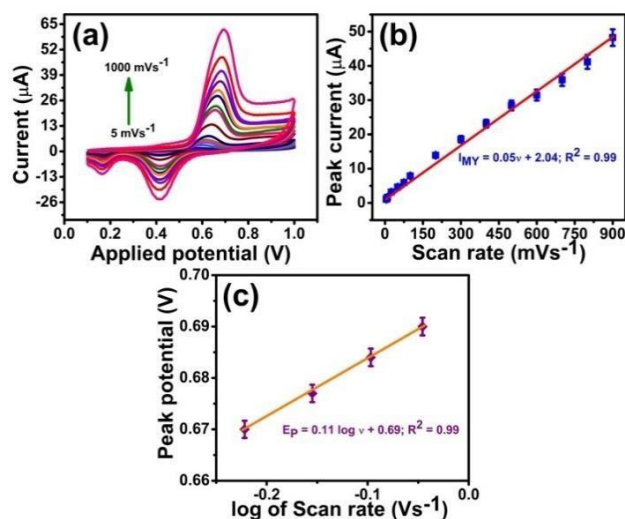


Fig. 3.17 CV measurements of MIP electrode in 0.1M PBS6 (a) peak current variation with scan rate (b) linear plot for the peak current vs scan rate (c) maximum peak potential vs log of scan rate.

3.3.2.6. Calibration curve and detection limit

The effect of various MY contents over the MIP electrode interface was investigated by the DPV technique. DPV observations with the MIP electrode were exercised to record the current response as the concentration of the MY analyte (C_{MY}) raised. The voltage window of the DPV experiment was set to 0.3 V–1.0 V at scan rate 50 mVs⁻¹ in 0.1 M PBS6. Fig.3.18 a illustrates two of the oxidation peaks at 0.6 and 0.78 V, the first revealing increased current than the later. For this reason, the study of linearity and the lower detection limit computation was carried out based on the first oxidation peak current. The calibration for MY (Fig. 3.18 b) designates two linear sections: 1 nM to 5 µM, with the regression equation (3.7) obtained as,

$$I_{MY} = 0.21C_{MY} + 0.45; R^2 = 0.98 \quad (3.7)$$

where I_{MY} is the peak current and C_{MY} is the corresponding MY concentration; and the second linear region 5 to 1000 µM with the regression equation (3.8) as,

$$I_{MY} = 0.02C_{MY} + 2.08; R^2 = 0.99. \quad (3.8)$$

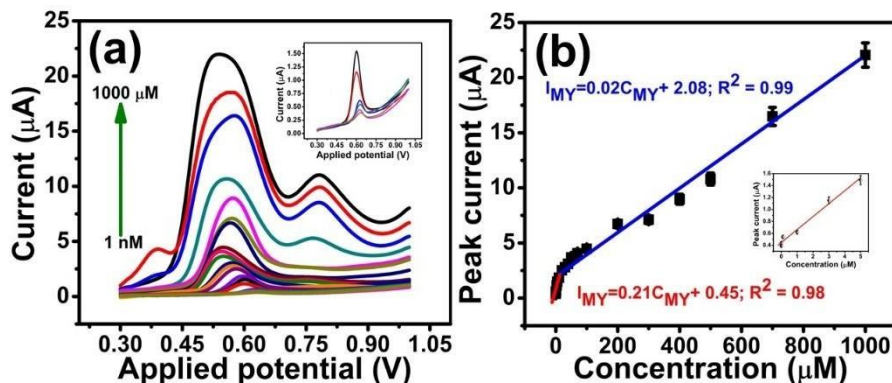


Fig. 3.18 DPV response of MY using MIP electrode in 0.1M PBS6 (a) Variation of concentration (b) linearplot of the peak current vs concentration.

This type of electrochemical behaviour of the MIP electrode can be vindicated via multiple layer adsorption succeeding monolayer adsorption mechanism [18]. As a result, the MIP electrode is highly sensitive in the lower linear range, which is desirable. Based on $LOD = 3\sigma/m$, here σ is the standard deviation of lowest concentration peak currents and m , the calibration slope [18]; the LOD was resolute as 0.67 nM. Analysing the electrochemical performance of the MIP electrode in comparison to previous works demonstrated an excellent detection limit and wide linear range of operation as depicted in Table 3.3.

Table 3.3

Comparison of proposed MIP performance with the previous reports

Sensor material	Linear range (μM)	LOD (nM)	Ref.
CQDs/GCE	0.06 to 40	30	[11]
Calix8/Au NPs/GCE	0.05 to 45	9.8	[13]
NiCo ₂ O ₄ @GP	5 to 1000	100	[39]
MIP	0.001 to 1000	0.67	This work

3.3.2.7. Study of Repeatability, Reproducibility and Stability

The repeatability and reproducibility of the MIP sensor was explored with 100 μM MY and the stability in 200 μM MY in 0.1 M PBS6 [20]. In the initial experiment, the MIP electrode was used to conduct four consecutive DPV measurements. The sensor repeatability is high with a relative standard deviation (RSD) of 1.08% in fig.3.19 a. In this work, reproducibility was also analyzed simultaneously. With the same fabrication technique, three sensors were made. Based on the electrode measurements in fig.3.19 b, there was a high degree of reproducibility with an RSD of 1.29 %. Following that, the same electrode was stored at room temperature for 15 days followed by the same tests conducted every 15 days in a row for 45 days. This electrode displayed a stable performance through a RSD of 2.77 % and barely changed peak current values as revealed in fig.3.19 c. There is also no variation of the peak location of MY analyte at the MIP electrode. Therefore, the sensor parameter evaluation has effectively established an alternative measure.

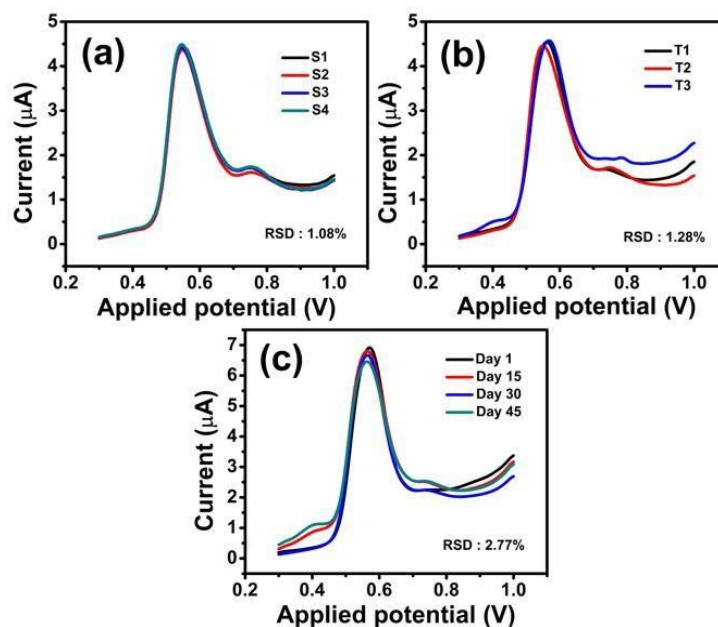


Fig. 3.19 Analytical characteristics of the MIP electrode (a) repeatability (b) reproducibility (c) stability.

3.3.2.8. Interference Study

Various interferences were applied to the MIP electrode in order to study how they affected its electrochemical characteristics. The interferences included Na^+ , K^+ , Ca^{2+} , Cd^{2+} , Zn^{2+} , Cu^{2+} , Mg^{2+} , curcumin, citric acid, tartaric acid. DPV responses were obtained utilizing $100\ \mu\text{M}$ of the target analyte after additions of each interfering species. An illustration of the outcome of specific interferences on the highest peak current is given in fig.3.20. There was no relative signal variation within a tolerance level of $\pm 5\%$ [20]. Compared to previous studies, this indicates that MIP electrode exhibit high selectivity in the incidence of other interfering analytes.

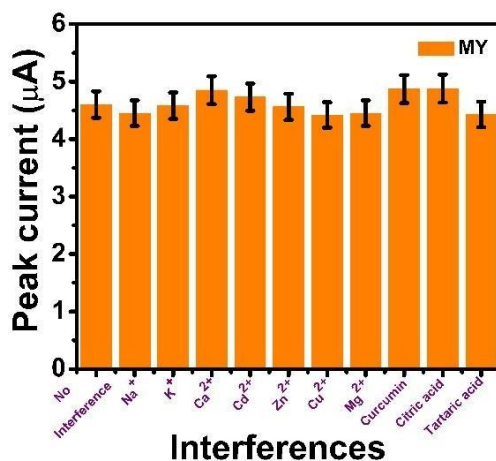


Fig. 3.20 Impact of various interferences on the voltammetry response of $100\ \mu\text{M}$ MY in 0.1M PBS6 at MIP electrode.

3.3.2.9. Detection of MY in real samples

In this study, MY adulteration in turmeric powder and pigeon pea samples were examined by the projected technology and the outcomes were compared to those attained by high performance liquid chromatography (HPLC). The turmeric powder and pigeon pea samples were procured from the local market. 2 g of turmeric powder was dissolved in 100 mL of millipore water and 5 gm of pigeon pea was boiled in 500 mL of millipore water. Both the samples were sieved by means of Whatman UNIFLO not reusable sterilized syringe filter with 25 mm diameter, $0.22\ \mu\text{m}$ pore size through PVDF filter film in polypropylene case prior to investigation. The aliquots obtained were analysed using DPV and HPLC techniques.

For $m = 3$ observations, the mean outcomes are abridged in Table 3.4. The MIP electrode consistently showed higher accuracy rates of 99.84 % and 98.89 % respectively. An analysis of the 't' test was carried out as well to assess the accuracy of the proposed method compared to the HPLC method. A mean difference ($\overline{X_d}$) = 0.045 is obtained and the standard deviation of the difference (S_d) = 0.06 for $n = 2$. The absolute 't' value was calculated by means of $t = \frac{\overline{X_d}}{S_d/\sqrt{n}}$ [38]. The 't' value calculated is 0.55. The critical 't' value at 95% confidence intervals, significance level 0.05 for degree of freedom 1 was calculated from the 't' distribution table. In this case, the critical 't' value is 12.706. The absolute 't' value for both samples, was below the critical value, indicating that the proposed procedure and HPLC analysis did not show any significant differences in their mean MY concentrations.

Table 3.4

Detection of MY using MIP electrode (m=3)

Sample	MY Detected (μM)		^a Error (%)	^b Accuracy (%)
	Proposed	Ref.		
	method (Measured)	method (True)		
Turmeric powder	12.5	12.48	0.16	99.84
Pigeon Pea	6.19	6.26	1.11	98.89

% ^aError = $[(\text{Measured}-\text{True})/\text{True}]*100$; % ^bAccuracy = $(100- (\% \text{ } ^a\text{Error}))$

3.3.3. Summary

Food adulteration is a major concern now and in order to detect a commonly used adulterant metanil yellow in food products like turmeric and pigeon pea, a low cost electrode was targeted to be fabricated. Towards this end, a sensitive, specific, and accurate molecular imprinted polymer based electrode with an electrochemically induced approach for detecting MY, was developed and is presented here. As a result of the active recognition sites, the dye

oxidation signals on the molecular imprinted electrode surface were significantly improved over traditional electrode surfaces. To generate intense current signals for the target MY at MIP surface, conditions like pH of the medium and supporting electrolytes were optimized. The sensor also excelled in terms of lower detection limit 0.67 nM for MY with a wide linear range 1 nM to 1000 μ M. Additionally, the MIP sensor demonstrated reproducibility (1.28%), repeatability (1.08%), broad linear range and significant longevity (2.77%). In addition, MIP analysis efficiently detected the different quantities of MY in real turmeric powder and pigeon pea samples and the responses were validated with the results from HPLC analysis. The electrode material is not expensive and can be used extensively for rapid measurements for the detection of MY adulteration.

3.4. Conclusion

There are two different approaches being used in the present study to learn about the rapid electrochemical detection of food additive metanil yellow. As a first step, we analyzed voltammetry responses in metanil yellow while modifying the carbon paste with metal oxides to increase electrode efficacy. The electroanalytical features of NiCo₂O₄ nanocomposites over graphite are considered excellent due to their exceptional characteristics. Moreover, the NiCo₂O₄@GP electrode over time demonstrated moderate electroanalytical properties. Furthermore, the electrode performed well against turmeric powder. From the previous work, the linear range of operation, the detection limit, and the ability to recognize specific template molecules were limited. A solution to selective electrocatalytic activity was therefore found in inexpensive polymers with recognition cavities. Electrochemical sensors based on molecule imprinted methacrylic acid polymer (MIP) were investigated as a possible solution. Compared to the previous work, this MIP electrode demonstrated reasonable selectivity and stable behavior, significantly improving linear range and LOD. Compared to HPLC technique, the electrode also demonstrated highly accurate analysis of turmeric powder and pigeon pea extracts.

References

- [1] P. Nath, P. Sarkar, K. Tarafder, P. Mondal, M. Das, K., and G. Paul, "Practice of using metanil yellow as food colour to process food in unorganized sector of West Bengal - A case study," *Int. Food Res. J.*, vol. 22, pp. 1424-1428, 2015.
- [2] C. Das, S. Chakraborty, N.K. Bera, K. Acharya, D. Chattopadhyay, A. Karmakar, and S. Chattopadhyay, "Impedimetric Approach for Estimating the Presence of Metanil Yellow in Turmeric Powder from Tunable Capacitance Measurement," *Food Anal. Methods.*, vol. 12, pp. 1017-1027, 2019.
- [3] S. Dixit, S.K. Khanna, and M. Das, "A simple 2-directional high-performance thin-layer chromatographic method for the simultaneous determination of curcumin, metanil yellow, and sudan dyes in turmeric, chili, and curry powders," *J. AOAC Int.*, vol. 91, pp. 1387-1396, 2008.
- [4] H.S. Lim, E. Choi, J.-H. Lee, G. Lee, and M. Kim, "Analysis of illegal colourants (citrus red II, diethyl yellow, dimethyl yellow, metanil yellow and rhodamine B) in foods by LC-UV and LC-MS/MS," *Food Addit. Contam. Part A Chem. Anal. Control Expo. Risk Assess.*, vol. 37, pp. 895-904, 2020.
- [5] K. Kourani, N. Kapoor, A. Badiye, and R.K. Shukla, "Detection of synthetic food color "Metanil Yellow" in sweets: a systematic approach," *JPC-J Planar Chromat.*, vol. 33, pp. 413-418, 2020.
- [6] M. Nurdin, "Photocurrent Responses of Metanil Yellow and Remazol Red B Organic Dyes by Using TiO₂/Ti Electrode," *IOP Conf. Ser.: Mater. Sci. Eng.*, vol. 367, pp. 012048, 2018.
- [7] V. Ashok, N. Agrawal, A. Durgbanshi, J. Esteve-Romero, and D. Bose, "A novel micellar chromatographic procedure for the determination of metanil yellow in foodstuffs," *Anal. Methods.*, vol. 7, pp. 9324-9330, 2015.
- [8] S. Bonan, G. Fedrizzi, S. Menotta, and C. Elisabetta, "Simultaneous determination of synthetic dyes in foodstuffs and beverages by high-performance liquid chromatography coupled with diode-array detector," *Dyes and Pigments.*, vol. 99, pp. 36-40, 2013.
- [9] S. Dhakal, K. Chao, W. Schmidt, J. Qin, M. Kim, and D. Chan, "Evaluation of Turmeric Powder Adulterated with Metanil Yellow Using FT-Raman and FT-IR Spectroscopy," *Foods.*, vol. 5, 2016.
- [10] S. Kar, B. Tudu, A.K. Bag, and R. Bandyopadhyay, "Application of Near-Infrared Spectroscopy for the Detection of Metanil Yellow in Turmeric Powder," *Food Anal. Methods.*, vol. 11, pp. 1-12, 2017.
- [11] R.M. Shereema, T.P. Rao, V.B. Sameer Kumar, T.V. Sruthi, R. Vishnu, G.R.D. Prabhu, and S. Sharath Shankar, "Individual and simultaneous electrochemical determination of metanil yellow and curcumin on carbon quantum dots based glassy carbon electrode," *Mater. Sci. Eng. C Mater. Biol. Appl.*, vol. 93, pp. 21-27, 2018.

Chapter 3: Fabrication of electrochemical sensors towards the detection of food colourant: Metanil Yellow

- [12] M. Roushani, Z. Rahmati, and B.Z. Dizajdizi, "Fabrication of novel metanil yellow/multi wall carbon nanotubes-chitosan/modified glassy carbon electrode and its application for sensitive determination of persulfate," *Journal of Electroanalytical Chemistry.*, vol. 847, pp. 113192, 2019.
- [13] A. Shah, "A novel electrochemical nanosensor for the simultaneous sensing of two toxic food dyes," *ACS Omega.*, vol. 5, pp. 6187–6193, 2020.
- [14] S. Biswas, S. Pradhan, H. Naskar, R. Bandyopadhyay, and P. Pramanik, "Sol gel synthesis of cubic titanium dioxide nanoparticle using poly (ethylene glycol) as a capping agent: voltammetric simultaneous determination of uric acid and guanine," *Microchim. Acta.*, vol. 185, pp. 1-10, 2018.
- [15] M.Enterría, A.G.Gonçalves, M.F.R.Pereira, J.I.Martins, and J.L.Figueiredo, "Electrochemical storage mechanisms in non-stoichiometric cerium oxide/multiwalled carbon, nanotube composites," *Electrochim. Acta.*, vol. 209, pp. 25-35, 2016.
- [16] S. Biswas, H. Naskar, S. Pradhan, Y. Wang, R. Bandyopadhyay, and P. Pramanik, "Simultaneous voltammetric determination of Adrenaline and Tyrosine in real samples by neodinium oxide nanoparticles grafted graphene," *Talanta*, vol. 206, pp. 1-9, 2020.
- [17] S. Pradhan, S. Biswas, D. K. Das, R. Bhar, R. Bandyopadhyay, and P. Pramanik, "An efficient electrode for simultaneous determination of guanine and adenine using nano-sized lead telluride with graphene," *New J. Chem.*, vol. 42, pp. 564-573, 2018.
- [18] S. Nag, S. Pradhan, H. Naskar, R. B. Roy, B. Tudu, P. Pramanik, and R. Bandyopadhyay, "A simple nano cerium oxide modified graphite electrode for electrochemical detection of formaldehyde in mushroom," *IEEE Sens. J.*, vol. 21, pp. 12019 – 12026, 2021.
- [19] R. D. Armstrong, G. W. D. Briggs, and E. A. Charles, "Some effects of the addition of cobalt to the nickel hydroxide electrode," *J. Appl. Electrochem.*, vol. 18, no. 2, pp. 215–219, Mar. 1988, doi: 10.1007/BF01009266.
- [20] S. Nag, S. Pradhan, D. Das, B. Tudu, R. Bandyopadhyay and R. B. Roy, "Fabrication of A Molecular Imprinted Polyacrylonitrile Engraved Graphite Electrode for Detection of Formalin in Food Extracts," *IEEE Sens. J.*, vol. 22, pp. 42–49, 2022.
- [21] D. Das, T. N. Chatterjee, R. B. Roy, B. Tudu, A. K. Hazarika, S. Sabhapondit, and R. Bandyopadhyay, "Titanium Oxide Nanocubes Embedded Molecularly Imprinted Polymer-Based Electrode for Selective Detection of Caffeine in Green Tea," *IEEE Sens. J.*, vol. 20, pp. 6240–6247, 2020.
- [22] D. Das, D. Biswas, A. K. Hazarika, S. Sabhapondit, R. B. Roy, B. Tudu, and R. Bandyopadhyay, "CuO Nanoparticles Decorated MIP-Based Electrode for Sensitive Determination of Gallic Acid in Green Tea," in *IEEE Sensors Journal*, vol. 21, pp. 5687-5694, 2021.

- [23] D. Das, S. Nag, S. De, A. K. Hazarika, S. Sabhapondit, B. Tudu, R. Bandyopadhyay, P. Pramanik and R. B. Roy, " Electrochemical Detection of Epicatechin in Green Tea Using Quercetin-Imprinted Polymer Graphite Electrode," in *IEEE Sensors Journal*, vol. 21, pp. 26526-26533, 2021.
- [24] T. N. Chatterjee, D. Das, R. B. Roy, B. Tudu, A. K. Hazarika, S. Sabhapandit, P. Tamuly, and R. Bandyopadhyay, "Development of a nickel hydroxide nanopetal decorated molecular imprinted polymer based electrode for sensitive detection of epigallocatechin-3-gallate in green tea," *Sens Actuators B Chem.*, vol. 283, pp. 69-78, 2019.
- [25] T. N. Chatterjee, D. Das, R. B. Roy, B. Tudu, S. Sabhapondit, P. Tamuly, P. Pramanik, and R. Bandyopadhyay, "Molecular Imprinted Polymer Based Electrode for Sensing Catechin (+C) in Green Tea," *IEEE Sens. J.*, vol. 18, pp. 2236-2244, 2018.
- [26] M. Naseri, A. Dehzangi, H.M. Kamari, A. See, M. Abedi, R. Salasi, A.N. Golikand, P.Dianat, F. Larki, A. Abedini, J. Hassan, A.K. Far, and B.Y. Majlis, Structure and physical properties of NiO/Co3O4 nanoparticles, *Metals*, vol. 181, 2016.
- [27] Synthesis and characterization of antibacterial activities nickel doped cobalt oxide nanoparticles M. Mayakannan, S. Gopinath, and S. Vetrivel, *Materials Chemistry and Physics*. vol. 242, pp. 122282, 2020.
- [28] A. Shaabani, R. Afshari, S. E. Hooshmand, and M. K. Nejad, "Molecularly imprinted polymer as an eco compatible nanoreactor in multicomponent reactions: a remarkable synergy for expedient access to highly substituted imidazoles," *ACS Sustainable Chem. Eng.*, vol. 5, 9506–9516, 2017.
- [29] G. Sharma, and B. Kandasubramanian, "Molecularly imprinted polymers for selective recognition and extraction of heavy metal ions and toxic dyes," *J. Chem. Eng. Data.*, vol. 65, 396-418, 2020.
- [30] M. V. Pereira, A. C. Marques, D. Oliveira, R. Martins, F. T. C. Moreira, M. Goreti F. Sales, and E. Fortunato, "Paper-based platform with an in situ molecularly imprinted polymer for β -amyloid," *ACS Omega.*, vol. 5, 12057-12066, 2020.
- [31] T. N. Chatterjee, R. B. Roy, B. Tudu, P. Pramanik, H. Deka, P. Tamuly, and R. Bandyopadhyay, "Detection of theaflavins in black tea using a molecular imprinted polyacrylamide-graphite nanocomposite," *Sens Actuators B Chem.*, vol. 246, 840-847, 2017.
- [32] W. J. R. Santosa, M. Santhiago, I. V. P. Yoshida, and L. T. Kubota, "Electrochemical sensor based on imprinted sol-gel and nanomaterial for determination of caffeine," *Sens Actuators B Chem.*, vol. 166-167 739–745, 2012.
- [33] N. Bhattacharyya, R. Bandyopadhyay, M. Bhuyan, B. Tudu, D. Ghosh, and A. Jana, "Electronic nose for black tea classification and correlation of measurements with 'Tea Taster' marks," *IEEE Trans. Instrum. Meas.*, vol. 57, no. 7, pp. 1313–1321, Jul. 2008.

**Chapter 3: Fabrication of electrochemical sensors towards the detection of food colourant:
Metanil Yellow**

- [34] M. B. Banerjee *et al.*, “Development of a Low-Cost Portable Gas Sensing Based on Molecularly Imprinted Quartz Crystal Microbalance Sensor for Detection of Eugenol in Clove Oil,” *IEEE Trans. Instrum. Meas.*, vol. 70, 1–10, 2021.
- [35] X. Tan, Q. Hu, J. Wu, X. Li, P. Li, H. Yu, X. Li, and F. Lei, “Electrochemical sensor based on molecularly imprinted polymer reduced graphene oxide and gold nanoparticles modified electrode for detection of carbofuran,” *Sens. Actuators B Chem.*, vol. 220, 216–221, 2015.
- [36] L. Wang, L. Miao, H. Yang, J. Yu, Y. Xie, L. Xu, and Y. Song, “A novel nanoenzyme based on Fe₃O₄ nanoparticles@thionine-imprinted polydopamine for electrochemical biosensing,” *Sens. Actuators B Chem.*, vol. 253, 108–114, 2017.
- [37] J. Huang, X. Zhang, S. Liu, Q. Lin, X. He, X. Xing, W. Lian, and D. Tang, “Development of molecularly imprinted electrochemical sensor with titanium oxide and gold nanomaterials enhanced technique for determination of 4-nonylphenol,” *Sens. Actuators B Chem.*, vol. 152, 292–298, 2011.
- [38] S. Ngamchana, and W. Surareungchai, “Sub-millimolar determination of formalin by pulsed amperometric detection,” *Anal. Chim. Acta.*, vol. 510, 195–201, 2004.
- [39] S. Nag, D. Das, H. Naskar, B. Tudu, R. Bandyopadhyay, and R. B. Roy, “Detection of Metanil Yellow Adulteration in Turmeric Powder Using Nano Nickel Cobalt Oxide Modified Graphite Electrode,” *IEEE Sens. J.*, 2022.



Fabrication of electrochemical sensors towards the detection of food flavourant: Vanillin

This chapter presents a MIP based sensor for estimation of vanillin in desserts. The comparative study with other research reports of vanillin determination has been presented. The electrodes also demonstrated highly accurate analysis of desserts.

Publication outcome of this chapter

- Voltammetry application of molecularly imprinted polyacrylamide as vanillin receptor in desserts, IEEE Sens. J., vol.23, pp. 3446-3452, 2023.

Chapter 4

Fabrication of electrochemical sensors towards the detection of food flavourant: Vanillin

4.1. Introduction

Vanilla occupies a prominent place in modern food culture among a variety of natural flavours used in diverse foods, such as confectionery, beverages, pharmaceuticals, food, and perfumery [1]. Vanillin (4-hydroxy-3-methoxybenzaldehyde) in vanilla is the main aromatic component (1.0–2.0 weight %) among more than 200 compounds in natural vanilla, which are responsible for the desirable flavour and aroma [1]. The natural vanillin in vanilla has antimicrobial, anticarcinogenic, and antimutagenic properties which attributes to the benefits for human health [1]. As well as suppressing UV and X-ray-induced chromosomal aberrations, it functions as a DNA-PK inhibitor that assists in DNA strand repair and prevents mutations at the CD59 locus on human chromosomes [1]. A mere 0.2% of the market demand is covered by natural vanillin made from vanilla, while the remaining 98% is synthetic vanillin obtained via chemical or biochemical means. While synthetic vanillin is widely used due to its lower price and availability, extensive research shows that excessive consumption can trigger headaches, nausea, and vomiting, as well as cause kidney and liver damage [1-3]. In food science, medicine, and pharmacology, it is increasingly important to develop simple, accurate, and economical techniques for the measurement and quality control of vanillin. The determination of natural vanillin from various food samples or vanilla extracts has been determined using a wide diversity of chemical practices, like thin layer chromatography, gas chromatography, UV spectrophotometry, high-performance liquid chromatography, capillary electrophoresis, and micellar electrokinetic chromatography, among others [4-11]. As a result, these methods are hardly suitable for the detection of vanillin outside of a laboratory environment due to their high cost and complicated and time-consuming procedures aimed at the pretreatment of samples. Electroanalytical methods have been studied recently and have been shown to offer an efficient and rapid alternative to these

problems. Electrochemical sensors for detecting and quantifying vanillin may be enhanced by combining noble metals with carbon-based sensors [11-16]. The excellent physical and chemical properties of graphene allow it to be used in a wide range of applications. It is also known that graphene-based nanocomposites Au NPs incorporate because of their high surface area, high electrical conductivity, and excellent electrocatalytic properties [17]. Several such techniques of electrode surface modification have been proposed in recent times as a means of combating the high overpotential for vanillin oxidation at bare electrodes, as well as poor reproducibility, which affects selectivity and/or sensitivity. A nanocomposite with a core-shell composition of Fe@Fe₃C-C for the ultrasensitive assessment of VNL [18]. Additionally, VNL sensors were made using AuPd NPs-graphene [19] and MnO₂-graphene [20]. These VNL sensors' selectivity, meanwhile, was insufficient. Molecularly imprinted polymers (MIPs) have garnered more interest recently as a specialized recognition material [21]. Molecular imprinting involves bonding the target analyte to a network of monomers and crosslinkers in a covalent or noncovalent manner [22]. The template is removed after polymerization to leave behind a molecularly stacked polymer matrix. In general, molecular recognition is fundamental to the adsorption process for any compound [22]. A wide range of applications can be achieved with this technology [23-25].

4.2. Voltammetry Application of Molecularly Imprinted Polyacrylamide as Vanillin Receptor in Desserts

The synthesis approach, which has been developed in a number of methods, is often tied to the MIPs' properties. In several situations, for the implanting of recognition sites in the polymer, the surface imprinting method is used. Carbon nanotubes act as good substrates for imprinting in addition to being a support material. They must be modified to attach the monomers prior to synthesis, for example, by reacting with thionyl chloride or conjugating with silicone coupling agents. The coupled assembly of multi-walled carbon nanotubes (MWNTs) and the distinctive assembly of polydopamine (PDA) were recently used in a new approach [26]. On a modified electrode made of CCNTs/IL/AuNPs/MIP, vanillin's electrochemical activities were investigated [27]. The electrochemical activities are increased due to the higher electrical conductivity and specific identification of changed materials. However, these procedures are difficult and time-consuming. A low cost, simpler MIP technology can be used to design a sensor that detects vanillin using this technology. Sensitivity of the sensor surface is boosted by a large number of active

imprinted sites. To detect vanillin (VNL) evidence in food products, a molecular imprinted polymer (MIPAM/GP) based on polyacrylamide was engineered. This work is novel in that it involves the creation of a simple, cost-effective, and simple technique for fabricating sensors. Long-term stability, repeatability, and reproducibility were all produced by this device as a result of intensive analyses of its analytical performances. Furthermore, the MIPAM/GP electrode demonstrates highly satisfactory results when compared with HPLC analysis when assessing VNL in icecream, yogurt, custard, and milkshake. VNL determination in a wide variety of samples can therefore be accomplished using this technique.

4.2.1. Experimental

4.2.1.1. Chemicals and reagents

Vanillin was purchased from Merck, India. Powdered graphite (99%), acrylonitrile, acrylamide (AM), acrylic acid, ethylene glycol dimethylacrylate (EGDMA), benzoyl peroxide was procured from Sigma Aldrich, USA. The paraffin oil and ethanol were procured from Merck, India. As all chemicals were analytical grade, purification was not necessary. For the experiment, Millipore water was used with the resistance of 18 M Ω . The researches were all performed at 25 °C.

4.2.1.2. Apparatus and techniques

To conduct the electrochemical analysis, Metrohm Autolab's PGSTAT101 Potentiostat/Galvanostat with three electrodes was used. An Ag/AgCl reference electrode, a Pt counter electrode, and a MiPAM/GP working electrode made up the three electrode system. FTIR spectroscopy and UV-Vis spectroscopy were used to characterize the synthesized polymer materials. Measurements were conducted using KBr pellets for calibration using an infrared spectroscope based on Fourier transform (IR prestige 21, 200VCE, Shimadzu, Tokyo, Japan). Spectral data were obtained between 200-400 nm using the UV-Vis UV-1800 SHIMADZU Spectrophotometer. SEM (scanning electron microscope) operated at a 15 kV acceleration voltage was used for characterization of surface morphology of the material synthesized. The Agilent's infinity preparative HPLC system-DEABG0597, G1161B was used for the HPLC analysis. The HPLC system was equipped with an Agilent 1260 Infinity II DAD detector.

4.2.1.3. Synthesis of molecular imprinted polymer

An earlier study reported synthesis of the polymer material in the laboratory [21]. After ultrasonication 0.95 grams of graphite powder in 15 mL of ethanol for 40 minutes, the powder was dispersed. Following the addition of AM (0.05 g) and VNL (0.05 g), sonication was performed for 60 minutes. After that, benzoyl peroxide (1mg) and the crosslinker EGDMA (400 L) were added and sonicated for 60 minutes before being added to the mixture. Polymerization followed by heat at 30 °C for 40 mins was performed on the prepared solution. A repeat distilled water rinse was performed with the prepared polymer. MIP material was created by leaching the template molecules out of the process. Further analysis was performed on the sample after it was air dried. An identical process was followed for synthesizing the non-imprinted polymer material (NIP), except that the template molecule was not added.

4.2.1.4. Fabrication of electrode

A mortar-pestle was used to fabricate the MIPAM/GP electrode. In the process of grinding, 2-3 drops of paraffin oil were added to 300 mg of synthesized MIP material. An inner diameter of 2.5 mm glass capillary was packed with the paste obtained next, using a thin metallic rod. From the other side of the tube, a platinum wire created electrical contact. Similar fabrications were performed with NIPAM/GP electrode with the NIP material.

4.2.1.5. Real sample analysis

Evaluation of electrode performance was conducted using four samples of ice cream, yogurt, custard, and milkshake. Each sample of 2 g was blended with 100 mL of water. DPV and HPLC analyses were conducted on the resultant solutions. Before HPLC analysis, Whatman (UNIFLO) one-use sterilized syringe filters of 25 mm (diameter) in polypropylene housing with 0.22µm pore size were used to filter the samples. HPLC systems with DAD detectors were used to analyze the aliquots. A Biosuite-C18 column, dimensioned 4.6 × 150 mm and using silica particles of 3 µm was used at ambient temperature in this experiment. For a total run time of 10 minutes, the mobile phase was made up of a) 0.1% TFA in H₂O and b) 100% acetonitrile at 1 ml min⁻¹.

4.2.2. Results and discussion

4.2.2.1. Monomer optimization

Towards the aim of optimizing the best monomer, three distinct imprinted polymer materials were simultaneously synthesized. The MIP materials and associated electrodes were made using three monomers: acrylamide, acrylonitrile, and acrylic acid. In 0.1M PBS 5 as a supporting electrolyte at 50 mV/s, CV was applied to the three electrodes from the 0.2-1 V range, and an oxidation peak was found at 0.7 V. According to fig.4.1, the acrylamide imprinted polymer electrode, which is roughly 2 times higher than acrylonitrile and acrylic acid imprinted electrodes, respectively, established the highest oxidation peak current. The behaviour of the MIP recognition sites and the polymer that has been imprinted will ultimately perform electrochemically might be affected by the interactions between template and monomer molecules during the pre-polymerization stage. The pre-polymerization composite's high dipole-to-dipole interactions between the template and monomer sparked the template detection course and improved electrochemical performance at the surface of MIPAM/GP electrode. Acrylamide was, therefore, recognized as the ideal monomer for the suggested experimental work.

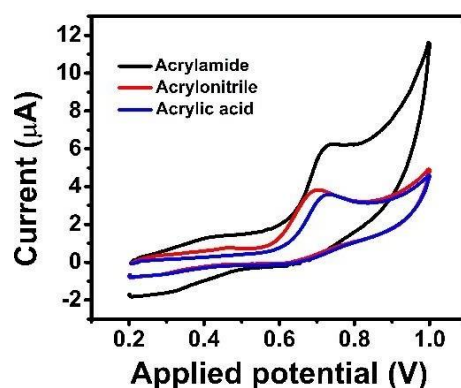


Fig. 4.1 CV response for monomer optimization in 100 µM VNL at 0.1 M PBS 5.

4.2.2.2. Material characterization

FTIR study: An FTIR spectrum of the prepared polymer prior to and post template exclusion is shown in fig.4.2. A long chain aliphatic compound has an absorption band of 2982 cm^{-1} . In addition to the bond, a peak of 951 cm^{-1} is followed. The band at 2982 cm^{-1} represents the $-\text{CH}_2$

group asymmetric stretching vibration ascribing to the foundation of polyacrylamide [28]. The sharp peak centered at 1715 cm^{-1} and 1160 cm^{-1} C=O stretching of carbonyl groups and C-O-C stretching [29] is responsible for VNL presence in the before template wash sample (BW). It follows, then, that the peak intensity was greatly reduced after the template was removed (AW). After template removal, there is a critical difference in spectrum between the spectral regions that were removed from templates.

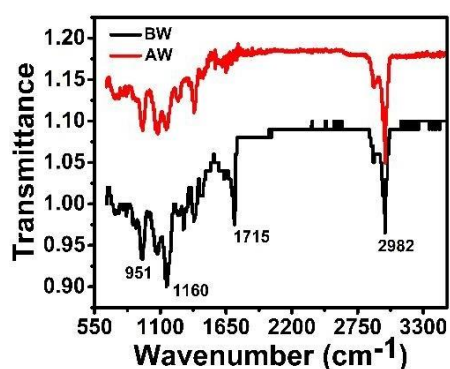


Fig. 4.2 FTIR spectra of MIP before and after template removal.

UV-Vis spectroscopy: UV-Vis spectroscopy was used to confirm that the VNL molecule was successfully removed, and fig.4.3 shows the results. After template extraction, a prominent absorption peak for VNL at 277 nm [30] that was seen in the spectral observation totally vanished. This gave approval for efficient MIP preparation and full template extraction.

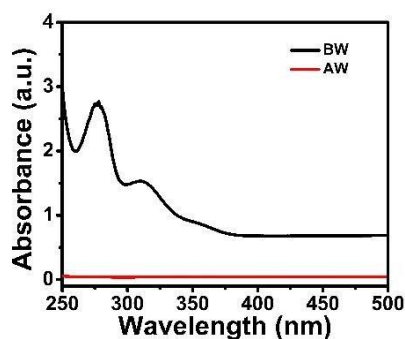


Fig. 4.3 UV-Vis spectra of MIP before and after template removal.

4.2.2.3. SEM measurements

Fig. 4.4 illustrates the SEM images that depict the surface patterns of the MIP and NIP prepared polymers respectively. The formation of imprinted cavities on the MIP surface may be responsible for this, which appears rugged, rough, and wrinkled after the template extraction process compared to the NIP surface.

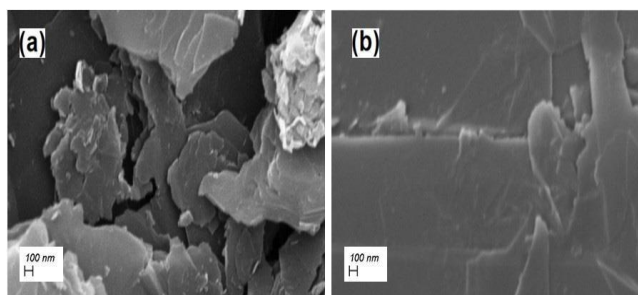


Fig. 4.4 SEM pictures of (a) MIP (b) NIP.

4.2.2.4. Electrochemical performance of MIPAM/GP electrode

The electrochemical behaviour of the MIPAM/GP electrode was examined using the cyclic voltammetry (CV) method. CV responses were recorded using the MIPAM/GP electrode and the NIP electrode. As seen in the fig.4.5 (a), the MIP electrode exhibited approximately six times higher current than the NIP electrode. This increase in oxidation peak current may be caused by quicker electron kinetics and the presence of recognition sites. The MIPAM/GP electrode was subjected to 100 μ M VNL stock solution and pure buffer which does not contain the vanillin molecule. From the fig.4.5 (b), it can be observed that when the MIPAM/GP electrode was exposed to the stock solution a notable peak current of 6 μ A can be observed, unlike the case when it was subjected to the pure buffer solution.

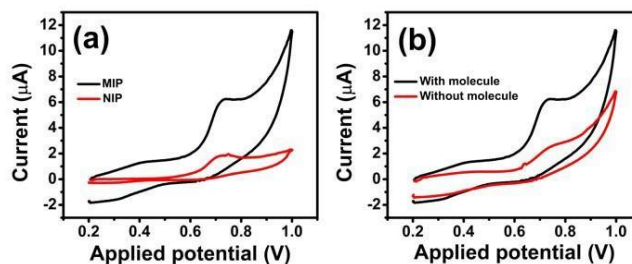


Fig. 4.5 CV response of (a) MIP and NIP electrode (b) with and without VNL molecule in 0.1M PBS 5.

In order to better understand the behaviour of the MIPAM/GP electrode, a number of supportive electrolyte compositions, including phosphate buffer saline (PBS), acetate buffer saline (ABS) and citrate buffer saline (CBS), were examined. Only in the presence of PBS, as shown in fig.4.6 (a), the optimal DPV response achieved; no such oxidation peak was revealed by other supporting electrolytes. Thus, the MIP vanillin electrode response was investigated in PBS buffer of variable pH from 2 to 7 in order to discover a suitable electrochemical environment for better performance of the synthesized vanillin electrode. Due to the target molecule's oxidation in PBS 5, fig. 4.6 (b) shows the highest peak current of 6.2 μA . Due to its ability to generate the highest peak current, PBS 5 was therefore regarded as the ideal buffer during the entire trial. As can be seen in fig.4.5 (b), there were no oxidation peaks in the absence of the target molecule (vanillin). The experiment was repeated after vanillin was added to the aforementioned solution. An anodic oxidation peak was seen at 0.7 V, which supported the identification of the target chemical. This is clearly demonstrated in fig.4.5 (b).

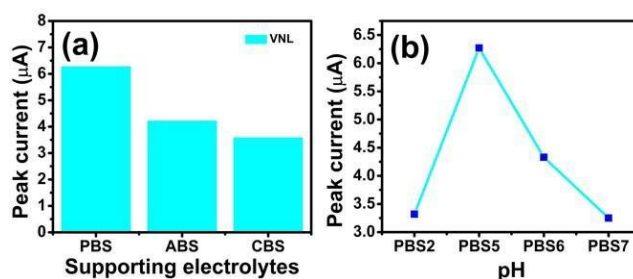


Fig. 4.6 Plot of (a) peak current vs supporting electrolytes (b) peak current vs pH in 100 μM VNL.

4.2.2.5. Effect of scan rate variation

The consequence of several scan rates on the electrochemical measurement of the VNL at MIP vanillin was inspected using the CV procedure from the 0.2 V - 1 V range. Fig.4.7 (a) shows the variations in current with scan rate. It was discovered that the anodic peak current increased linearly with the scan rate from 5 to 500 mV/s. This result suggests that the VNL molecule's electrocatalytic oxidation at MIP vanillin is a surface-controlled process [31], [32]. The plot between oxidation peak current and scan rate is shown in Fig. 4.7. (b). Fig. 4.7.(b) provides evidence in favour of the linear regression equation; $I_{VNL} = 0.025 \nu + 1.84$; $R^2 = 0.97$.

$$I_p = \frac{nFQv}{4RT} \quad (4.1)$$

Equation (4.1) [32], where I_p is the peak current, n is the figure of electrons transported, F is the Faraday's constant, R is the universal gas constant, T is the room temperature, Q is the amount of charge consumed during oxidation, and v is the scan rate, was used to calculate the oxidation process electrons. The n , transferred was computed to be 1.142, which is approximately equal to 1. A linear plot of peak potential (E_p) vs. $\log v$ was also used to compute the electron transfer coefficient in fig. 4.7 (c). The slope of the curve $2.3RT / (1 - \alpha)nF$ [32] yielded a charge transfer coefficient (α) of =0.9406, and the resulting regression equation was

$$E_p = 0.039 \log v + 0.78; R^2 = 0.98 \quad (4.2)$$

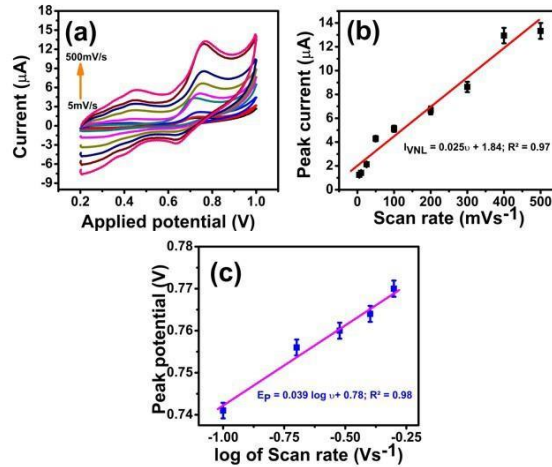


Fig. 4.7 MIPAM/GP electrode CV response to 100 μM VNL in 0.1M PBS 5 (a) current varying with scan rate (b) Peak current plot against scan rate (c) Peak potential plot against the log of scan rate

4.2.2.6. Calibration curve and detection limit

Using DPV measurements, the effect of various concentrations was studied in detail using MIPAM/GP electrode in PBS 5. DPV responses have been recorded since they are more sensitive to current and have greater resolution than CV responses. Fig.4.8 shows the comparable current increase in the peak oxidation from 0.1 to 1000 μM concentration. As can be seen from the fig.4.8 (a), at 0.65 V, a sharp oxidation peak is visible.

It is observable from fig.4.8 (b) that the MIPAM/GP electrode exhibits two linear ranges, viz. 0.1 μM to 50 μM and from 50 μM to 1000 μM . The corresponding linear regression for the first linear range is; $I_{VNL} = 0.074C_{VNL} + 1.56; R^2 = 0.99$. The related regression equation is $I_{VNL} = 0.021C_{VNL} + 4.49; R^2 = 0.97$. where I_{VNL} is the peak current and C_{VNL} represents the

appropriate vanillin concentrations. To determine the lower limit of detection, $LOD = 3 \sigma/m$ was employed [32]. σ is the standard deviation of maximum peak currents for the lowest detected concentration, and m is the slope of the calibration curve, respectively. The limit of detection (LOD) is calculated to be $LOD=1.43$ nM. A comparison of the current work with prior literature is shown in Table 4.1.

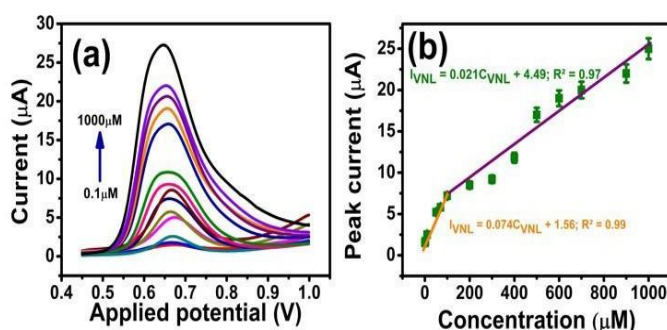


Fig. 4.8 VNL DPV response (a) Concentration variance (b) Peak current plot against concentration by MIPAM/GP electrode in 0.1M PBS 5.

Table 4.1

Comparison of MIPAM/GP behaviour with the preceding reports

Sensor/Technique	Linear range (μM)	LOD (nM)	Ref.
CNT-SPE	2.5-750	1.03	[1]
Ag NPs/GN/GCE	2-100	0.33	[15]
MoS ₂ -CNF	0.3-135	0.15	[13]
AuPd/GCE	0.1-7	0.02	[19]
	10-40		
Fe@Fe ₃ C-C/GCE	0.01-50	2.36	[18]
MWNTs-PDA	0.2-10	0.1	[27]
MIPAM/GP	0.1-50-1000	0.00143	Present work

4.2.2.7. Repeatability, Reproducibility, and Stability Analysis

The reproducibility, repeatability, and stability of the MIPAM/GP electrode were studied in 100 μM vanillin in PBS 5. Initially, the MIPAM/GP electrode was used to record five consecutive DPV measurements. The repeatability of the electrode is shown in fig.4.9 (a), where the relative standard deviation (RSD) is shown as 1.17%. In this paper, the analysis of reproducibility was done concurrently. The same process was used to create three distinct sensors. The results of three DPV measurements, displayed in fig.4.9 (b) revealed a good repeatability with an RSD of 1.39%. Following that, the identical electrode was kept at room temperature and a similar trial was run every fifteen days over a month. The electrode performed reasonably steadily. According to fig.4.9 (c). the electrode revealed acceptable stability with an RSD of 1.86% and barely noticeable fluctuations in peak current.

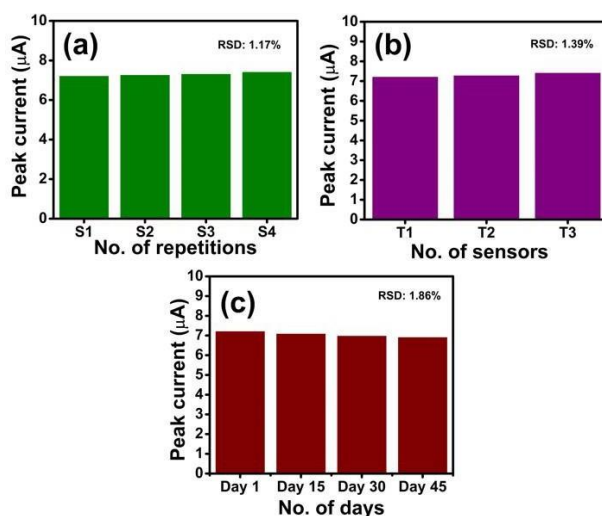


Fig. 4.9 Sensory characteristics of the MIPAM/GP electrode showing (a) repeatability (b) repeatability and (c) stability.

4.2.2.8. Interference and Selectivity Study

To study the selectivity and interference of the MIPAM/GP electrode, the electrode was exposed to several interferences, including caffeine, hydroquinone, resorcinol, Na^+ , Cu^+ and K^+ . DPV responses were obtained after five folds of each interfering species were applied to 100 μM of the analyte. The impact of individual interferences on the maximum peak current is shown in fig.4.10 within a tolerance limit of 5%, the relative signal change was insignificant. A very selective performance of the MIPAM/GP electrode when other agents are interfering was

observed. The vanillin analyte (no interference) showed the highest peak current in fig.4.10 when compared to the other analytes. As a result, it is demonstrated that the MIPAM/GP electrode has higher affinity for the vanillin molecules.

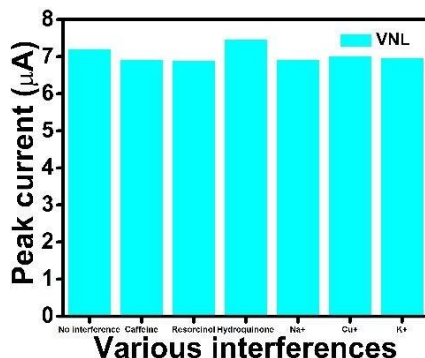


Fig. 4.10 Sensory characteristics of the MIPAM/GP electrode showing interference study.

4.2.2.9. Detection of VNL in real samples

A quantitative analysis of VNL was conducted in ice cream, yogurt, custard, and milkshake using the proposed technique and compared with HPLC results. In Table 4.2, the mean results for $m = 3$ are summarized, where m is the number of trials per real sample extract. MIPAM/GP electrodes showed 98.94 %, 99.79%, 99.48%, and 98.85 % accuracy rates, respectively. A 't' test analysis was also conducted to assess the accuracy of the proposed method when compared to the HPLC method. For $n = 4$, where n is the sample quantity, the mean difference ($\overline{X_d}$) is 0.102, while the standard deviation (S_d) is 0.062. In order to obtain the absolute value of 't', $t = \frac{\overline{X_d}}{S_d/\sqrt{n}}$ was used [33]. In this study, the 't' value is 0.825. According to the t distribution table, 3.182 is the critical 't' value with 95% confidence intervals, a significance level of 0.05, and three degrees of freedom. According to the HPLC analysis, there is no substantial variance as compared the proposed technique for the mean VNL concentrations of the four samples since the t (absolute) value is smaller than the t (critical) value.

Table 4.2
Detection of VNL using MIPAM/GP electrode

Sample	VNL Detected ($\mu\text{g/g}$)		^a Error (%)	^b Accuracy (%)
	Proposed method	Ref. method		
	(Measured)	(True)		
Ice cream	17.72	17.91	1.06	98.94
Yogurt	13.79	13.82	0.21	99.79
Custard	11.29	11.35	0.52	99.48
Milkshake	11.45	11.32	1.14	98.85

$$\% \text{ }^a\text{Error} = [|(Measured-True)/True|*100]; \% \text{ }^b\text{Accuracy} = (100- (\% \text{ }^a\text{Error}))$$

4.3. Conclusion

An application of polyacrylamide based MIP electrode for detecting synthetic food flavourant, vanillin is discussed in this paper. Molecular cavities were observed in the experimental studies to provide the basis for selective adsorption of VNL. This work explored the linearity of the MIPAM/GP electrode from 0.1 μM to 1000 μM and a detection limit of 1.43 nM. In terms of repeatability and reproducibility, the MIPAM/GP electrode demonstrated a good performance (RSD: 1.17% and 1.39% respectively) as well as selectivity. After extensive use over a month, the electrode exhibited a stable electrochemical behavior (RSD: 1.86%). In comparison with existing technologies, the proposed MIP-based electrochemical sensor for VNL detection has significantly improved linear range and limit of detection. A comparison between the electrode and a reference HPLC method has also been conducted for analyzing VNL content in desserts like ice cream, yogurt, custard and milkshake. In summary, we may conclude that the proposed sensor is an effective, simple, and economical method for quantitative VNL detection in commercial food and beverage samples.

References

- [1] L. Chen, K. Chaisiwamongkhon, Y. Chen, and R. G. Compton, "Rapid electrochemical detection of vanillin in natural vanilla," *Electroanalysis*, vol. 31, no. 6, pp. 1067–1074, Jun. 2019.
- [2] A. Sharma, S. C. Verma, N. Saxena, N. Chadda, N. P. Singh, A. K. Sinha, "Microwave- and ultrasound-assisted extraction of vanillin and its quantification by high-performance liquid chromatography in *Vanilla planifolia*," *J. Sep. Sci.*, vol. 29, pp. 613–619, 2006.
- [3] E. Anklam, S. Gaglione, A. Müller, "Oxidation behaviour of vanillin in dairy products," *Food Chem.*, vol. 60, pp. 43–51, 1997.
- [4] G. Lamprecht, F. Pichlmayer, and E.R. Schmidt, "Determination of the authenticity of vanilla extracts by stable isotope ratio analysis and component analysis by HPLC," *J. Agric. Food Chem.*, vol. 42, pp. 1722–1727, 1994.
- [5] K.N. Waliszewski, V.T. Pardio, and S.L. Ovando, "A simple and rapid HPLC technique for vanillin determination in alcohol extract," *Food Chem.*, vol. 101, pp. 1059–1062, 2006.
- [6] Y. Shen, C. Han, B. Liu, Z.F. Lin, X.J. Zhou, C.J. Wang, and Z.O. Zhu Z, "Determination of vanillin, ethyl vanillin, and coumarin in infant formula by liquid chromatography-quadrupole linear ion trap mass spectrometry," *J. Dairy Sci.*, vol. 97, pp. 679–686, 2014.
- [7] T. Sostaric, M.C. Boyce, and E.E.J. Spickett, "Analysis of the volatile components in vanilla extracts and flavorings by solid-phase microextraction and gas chromatography," *J. Agric. Food Chem.*, vol. 48, pp. 5802–5807, 2000.
- [8] D.L. Jager, G.A. Perfetti, and G.W. Diachenko, "Comparison of headspace-SPME-GC-MS and LC-MS for the detection and quantification of coumarin, vanillin, and ethyl vanillin in vanilla extract products," *Food Chem.*, vol. 107, pp. 1701–1709, 2008.
- [9] M.C. Boyce, P.R. Haddad, and T. Sostaric, "Determination of flavour components in natural vanilla extracts and synthetic flavourings by mixed micellar electrokinetic capillary chromatography," *Anal. Chim. Acta.*, vol. 485, pp. 179–186, 2003.
- [10] M. Ohashi, H. Omae, M. Hashida, Y. Sowa, and S. Imai, "Determination of vanillin and related flavor compounds in cocoa drink by capillary electrophoresis," *J. Chromatogr.*, vol. A 1138, pp. 262–267, 2007.
- [11] A. Longares-Patron, and M.P. Canizares-Macias, "Focused microwave-assisted extraction and simultaneous spectrophotometric determination of vanillin and p-hydroxybenzaldehyde from vanilla fragans," *Talanta*, vol. 69, pp. 882–887, 2006.

- [12] N. Hareesha, J. G. Manjunatha, B. M. Amrutha, N. Sreeharsha, S. M. Basheeruddin Asdaq, and Md. K. Anwer, "A fast and selective electrochemical detection of vanillin in food samples on the surface of poly(glutamic acid) functionalized multiwalled carbon nanotubes and graphite composite paste sensor," *Colloids and Surfaces A: Physicochemical and Engineering Aspects*, vol. 626, p. 127042, Oct. 2021.
- [13] M. Qianwen, D. Yaping, L. Li, W. Anqing, D. Dingding, and Z. Yijun, "Electrospun MoS₂ composite carbon nanofibers for determination of vanillin," *Journal of Electroanalytical Chemistry*, vol. 833, pp. 297–303, Jan. 2019.
- [14] A. B. Monnappa, J. G. G. Manjunatha, A. S. Bhatt, and H. Nagarajappa, "Sensitive and selective electrochemical detection of vanillin at graphene based poly (methyl orange) modified electrode," *Journal of Science: Advanced Materials and Devices*, vol. 6, no. 3, pp. 415–424.
- [15] L. Huang, K. Hou, X. Jia, H. Pan, and M. Du, "Preparation of novel silver nanoplates/graphene composite and their application in vanillin electrochemical detection.," *Mater. Sci. Eng. C Mater. Biol. Appl.*, vol. 38, pp. 39–45, May 2014.
- [16] T. Zabihpour, S.-A. Shahidi, H. Karimi-Maleh, and A. Ghorbani-HasanSarai, "Voltammetric food analytical sensor for determining vanillin based on amplified NiFe₂O₄ nanoparticle/ionic liquid sensor," *Food Measure.*, vol. 14, no. 2, pp. 1039–1045, Apr. 2020.
- [17] X. Wang, C. Luo, L. Li, and H. Duan, "An ultrasensitive molecularly imprinted electrochemical sensor based on graphene oxide/carboxylated multiwalled carbon nanotube/ionic liquid/gold nanoparticle composites for vanillin analysis," *RSC Adv.*, vol. 5, no. 113, pp. 92932–92939, 2015.
- [18] J. Sun, T. Gan, K. Wang, Z. Shi, J. Li, and L. Wang, "A novel sensing platform based on a core–shell Fe@Fe₃C–C nanocomposite for ultrasensitive determination of vanillin," *Anal. Methods*, vol. 6, no. 15, p. 5639, Jun. 2014.
- [19] L. Shang, F. Zhao, and B. Zeng, "Sensitive voltammetric determination of vanillin with an AuPd nanoparticles-graphene composite modified electrode.," *Food Chem.*, vol. 151, pp. 53–57, May 2014.
- [20] T. Gan, Z. Shi, Y. Deng, J. Sun, and H. Wang, "Morphology–dependent electrochemical sensing properties of manganese dioxide–graphene oxide hybrid for guaiacol and vanillin," *Electrochim. Acta*, vol. 147, pp. 157–166, Nov. 2014.
- [21] S. Nag, S. Pradhan, D. Das, B. Tudu, R. Bandyopadhyay, and R. B. Roy, "Fabrication of A Molecular Imprinted Polyacrylonitrile Engraved Graphite Electrode for Detection of Formalin in Food Extracts," *IEEE Sens. J.*, vol. 22, pp. 42–49, 2022.
- [22] D. Das, T. N. Chatterjee, R. B. Roy, B. Tudu, A. K. Hazarika, S. Sabhapondit, and R. Bandyopadhyay, "Titanium Oxide Nanocubes Embedded Molecularly Imprinted Polymer-Based Electrode for Selective Detection

of Caffeine in Green Tea,” *IEEE Sens. J.*, vol. 20, pp. 6240–6247, 2020.

[23] D. Das, S. Nag, S. De, A. K. Hazarika, S. Sabhapondit, B. Tudu, R. Bandyopadhyay, P. Pramanik, and R. B. Roy, “Electrochemical Detection of Epicatechin in Green Tea Using Quercetin-Imprinted Polymer Graphite Electrode,” *IEEE Sens. J.*, vol.21, 26526-26533, 2021.

[24] D. Das, D. Biswas, A. K. Hazarika, S. Sabhapondit, R. B. Roy, B. Tudu, and R. Bandyopadhyay, “CuO Nanoparticles Decorated MIP-Based Electrode for Sensitive Determination of Gallic Acid in Green Tea,” in *IEEE Sensors Journal*, vol. 21, pp. 5687-5694, 2021.

[25] D. Das et al., “Amine Functionalized MWCNTs Modified MIP-Based Electrode for Detection of Epicatechin in Tea,” *IEEE Sens. J.*, vol. 22, no. 11, pp. 10323–10330, Jun. 2022.

[26] W. Wu et al., “Sensitively Voltammetric Determination of Vanillin with a Molecularly Imprinted Ionic Liquid Polymer-Carboxyl Single-Walled Carbon Nanotubes Composite Electrode,” *Int. J. Electrochem. Sci.*, pp. 6009–6022, Jul. 2016.

[27] W. Wu, L. Yang, F. Zhao, and B. Zeng, “A vanillin electrochemical sensor based on molecularly imprinted poly(1-vinyl-3-octylimidazole hexafluoride phosphorus) –multi-walled carbon nanotubes@polydopamine–carboxyl single-walled carbon nanotubes composite,” *Sensors and Actuators B: Chemical*, vol. 239, pp. 481–487, Feb. 2017.

[28] B. Balan, A. S. Dhaulaniya, R. Jamwal, A., K. K. Sodhi, S. Kelly, A. Cannavan, and D. K. Singh, “Application of Attenuated Total Reflectance-Fourier Transform Infrared (ATR-FTIR) spectroscopy coupled with chemometrics for detection and quantification of formalin in cow milk,” *Vib. Spectrosc.*, vol. 107, p. 103033, 2020.

[29] A. B. D. Nandiyanto, R. Oktiani, and R. Ragadhita, “How to read and interpret FTIR spectroscopy of organic material,” *IJOST*, vol. 4, p. 97, 2019.

[30] M. Nouri, S. Shahriari, and G. Pazuki, “Increase of vanillin partitioning using aqueous two phase system with promising nanoparticles,” *Sci. Rep.*, vol. 9, no. 1, p. 19665, Dec. 2019.

[31] S. Nag, S. Pradhan, H. Naskar, R. B. Roy, B. Tudu, P. Pramanik, and R. Bandyopadhyay, “A simple nano cerium oxide modified graphite electrode for electrochemical detection of formaldehyde in mushroom,” *IEEE Sens. J.*, vol. 21, 12019 – 12026, 2021.

[32] S. Nag, D. Das, H. Naskar, B. Tudu, R. Bandyopadhyay, and R. B. Roy, “Detection of Metanil Yellow Adulteration in Turmeric Powder Using Nano Nickel Cobalt Oxide Modified Graphite Electrode,” *IEEE Sens. J.*, 2022.

[33] S. Ngamchana, and W. Surareungchai, “Sub-millimolar determination of formalin by pulsed amperometric detection,” *Anal. Chim. Acta.* vol.510 pp. 195–201, 2004.



**Towards the development of an
App based low cost, portable
food quality assessment device**

This chapter proposes a concept towards fabrication of a low-cost, portable food quality assessment device that has been developed based on App-based display.

Chapter 5

Towards the development of an App based low cost, portable food quality assessment device

5.1. Background of the work

In [1], “DStat” is designed as a general-purpose open-source potentiostat that can be used alone or in conjunction with additional instruments. DStat features picoampere range of current measurement, a small USB-powered architecture, and cross-platform software that is easy to use. DStat is simple and affordable to create, can be freely customised, and performs reasonably well at low current levels that other lab-fabricated devices cannot. The “EcoStat” designed in [2] is a low-cost, digitally controlled potentiostat with various advantages over other low-cost instruments, including lower noise and a more steady output signal owing to a digital PI controller. Furthermore, a user-friendly PC interface named "POTCON" controls data collecting, display, and filtering. In [3], the fabrication and design of a simple potentiostat that is capable of resolving a current of the order of a few microamperes (μA). The device when compared to commercial equipment, makes it a viable alternative for places where electrochemistry experiments are conducted using computer software or web-based simulators. In [4], the potentiostat designed is used for determination of pH, which is an important parameter for the initiation of any electrochemical experiment. To correctly measure the voltage between a pH sensor electrode and a reference electrode, a potentiometric apparatus with extremely low input bias current is required. An open-source potentiometric apparatus with bluetooth wireless connectivity for pH determination investigations. The hardware consists mostly of an Arduino Nano microcontroller, a 16-bit analog-to-digital converter, two electrical buffer amplifiers, a temperature sensor, and a bluetooth module, all of which cost roughly \$50. The device was tested against a commercial pH metre using a regular glass electrode and a bespoke palladium/palladium oxide pH detecting electrode. The accuracy and precision of the developed device were found to be adequate for industrial purposes. In [5], the paper demonstrates a unique gadget made by combining a miniature potentiostat with an

electronic micropipette in this work. The micropipette battery powers the mini-potentiostat, which is operated by a smartphone through bluetooth wireless connection. With the help of an adapter, a set of three electrodes is inserted into the tip of the micropipette, allowing electrochemical measurements to be performed without impairing the precision and authenticity of treating slight amounts of liquid. The device has shown to improve portability, versatility, agility, and analytical techniques in studies. This process needs a minimal number of samples and reagents, as well as the possibility of recovery after analysis. In [6], the KAUSTat is a wireless, wearable, open-source potentiostat. It enables the use of cyclic voltammetry for a variety of solutions, as seen above. The MIT App Inventor interface was used to create the app. The user-friendly interface makes parameter definition simple. Wireless connection and a testing distance of up to 16-20 metres are available with the BLE. This allows for easy access to the user's database and error-free point-to-point examination. With a high current ($10 \mu A$), the gadget has been proved to work more efficiently. Experiments suggest that the KAUSTat can work at $500 \mu A$ and could be a decent commercial potentiostat for use in laboratories.

5.2. Objective of the work

The objective of our invention is the development of a Raspberry pi based low cost, portable quality assessment electronic device for food and beverages which substitutes the conventional potentiostat devices. Further, the present invention can be implemented for food quality assessment based on specifically developed sensors.

5.2.1. Illustration of hardware

5.2.1.1. Function generator and Filter circuit

This component is used to generate a triangular wave of variable scan rate (user selectable) from $-0.5V$ to $+0.5V$. The generated triangular wave is fed to the potentiostat circuit (acts as the input of the circuit). Arduino UNO is selected to realize this component. Since UNO does not have a Digital to Analog Converter (DAC), we cannot directly output triangular waves from any UNO Pin. Instead, we use UNO to generate PWM waves of variable duty cycle (varying from 0 to 20%) and use a 2nd Order Low pass filter to get the low frequency DC component (which is proportional to the duty cycle). As the PWM duty cycle can be easily controlled and varied from the UNO, so will the filter output vary in a controlled way. UNO is also incapable of generating negative

voltages, so we achieve the required negative half of the triangular wave by shifting the filtered wave output. From UNO, we generate: 0 to ($V_+ - V_-$); So, shifting down of the filtered output required is V_- . Step duration is the time for which the system lasts at a given step n . Using above step size,

$$\Delta V_{step} = 2.5mV$$
$$\Rightarrow Scan\ rate = \frac{\Delta V_{step}}{T_{step}} = \frac{2.5}{T_{step}}$$
$$\Rightarrow T_{step} = \frac{2.5}{Scan\ rate}$$

We need to filter out the higher frequencies from the output PWM to get the low frequency components (average DC value) of the signal. We first used a first order filter with response time comparable to the highest step duration required, that is, $2.5/50\text{ mV/sec} = 50\text{ msec}$. But the ripples observed in the above circuit were in the order of 100 mV which is way beyond our required voltage resolution of 2.5 mV. The response time for 1st order filter with ripples around 2.5 mV is in the order of seconds, which is slower by many orders than required for generating the scan rates. So, a second order filter was used.

5.2.1.2. Potentiostat circuit

The $V_{applied}$ signal by Arduino is fed to the control amplifier of the potentiostat circuit as shown in fig5.1. The main function of the control amplifier is to shift the reference electrode (RE) potential 180° with the applied potential. Using negative feedback, the control amplifier sense the RE potential and then makes the difference between applied potential and RE potential to be applied by forcing current through an auxiliary or counter (CE). The voltage buffer is used mainly to overcome the current loading effect without changing the input voltage. It also provides a very high input impedance. As the Arduino cannot measure current directly, it can only measure voltage as an input, so we also need a current to voltage (I to V) converter.

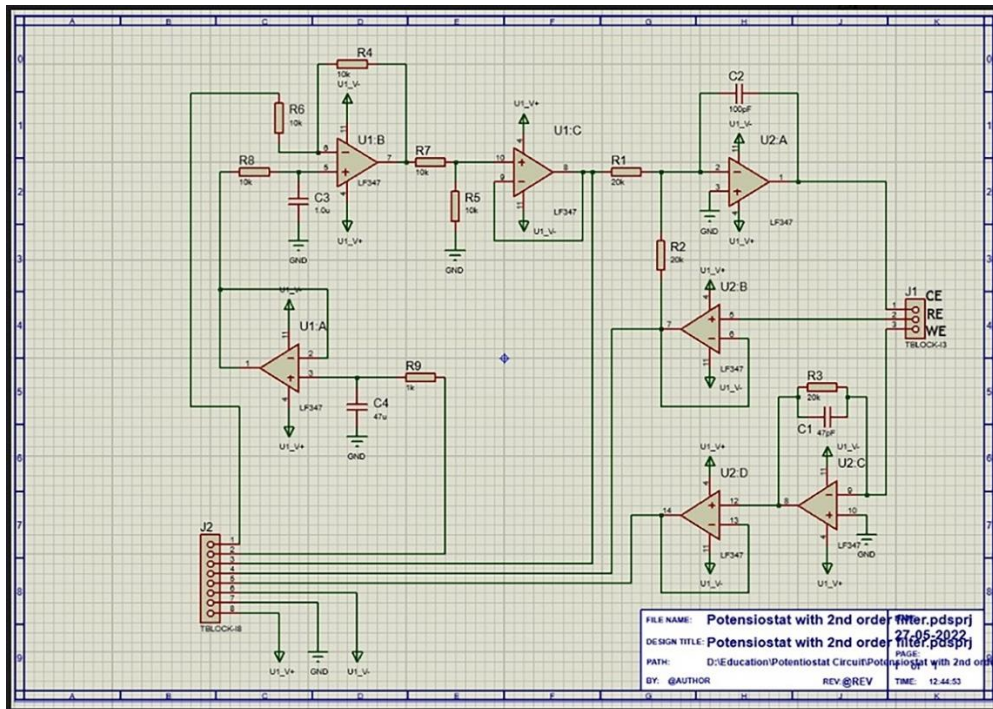


Fig.5.1 The circuit design comprising filter and potentiostat circuit.

5.2.1.3. Response sampler

The response of the Potentiostat circuit is measured by this component. This is implemented by an Arduino NANO. The functions of this component is two folds:

- 1) Sampling the output signal and input(triangular) signal
- 2) Encoding the output signal and input signal values in a suitable format and communicate it with the Raspberry pi

Inferring input signal

The idea is based on the fact that information regarding the input signal is available with Arduino UNO (function generator component). So an algorithm was developed to digitally transfer this information from the UNO to the NANO avoiding the need for analog measurements of the input signal, thus, freeing the ADC exclusively for the output signal measurements.

Signals (controlled by the function generator component)

- 1) *fsyncclock* – Function sync. Protocol clock signal. It transitions from low to high at the middle of each step (assuming steps are of equal width, as in our case). The transition is done at the middle, after the occurrence of a step, because the output transients is expected to settle by

then and the filtered output measurement is stable. Also, this strategy spaces out the *fsyncclock* and *fsyncrate* transitions which would otherwise lead to race conditions in the NANO interrupt handling

It transitions back from high to low at the occurrence of the next step.

2) *fsyncrate* – Function sync. Protocol rate signal. It is high or low depending on which half of the input signal (increasing or decreasing) is being generated at the present. It is inverted at the beginning of the first step of a period and at the beginning of the half of the total no of steps of a period (note: since number of steps_increasing is same as number of steps_decreasing, total number of steps in a period is always even)

This functionality is jointly implemented with the Raspberry pi. The Response sampler just passes the information regarding *current_step*, *current_rate*, and *total_steps* as part of the control protocol

1) Calculation of *total_steps* : First the total number of steps in the increasing (or decreasing) half wave is calculated. This is done by counting the number of low to high transition of the *fsyncclock* (D3) between one inversion of the *fsyncrate*(D2). The counting starts once the *fsyncrate* inversion is observed and ends when the next inversion in *fsyncrate* is observed

2) The NANO now enters the acquisition state, it keeps track of the *current_step* number (which begins at 0 since the above counting ends either at the beginning or at the half of a period, hence the next step number is 0) and increments it at the occurrence of *fsyncclock* rising transition (by interrupt of digital pin)

3) Similarly, it also keeps track of *current_rate* by attaching an interrupt to the *rate_pin* in both rising and falling transitions

4) The input wave signal is calculated as follows:

If *current_rate* is increasing,

$$\text{Input wave} = \left(\frac{\text{current_step}}{\text{total_steps}}\right)V_{\max}$$

If *current_rate* is decreasing,

$$\text{Input wave} = \left(1 - \frac{\text{current_step}}{\text{total_steps}}\right)V_{\text{max}}$$

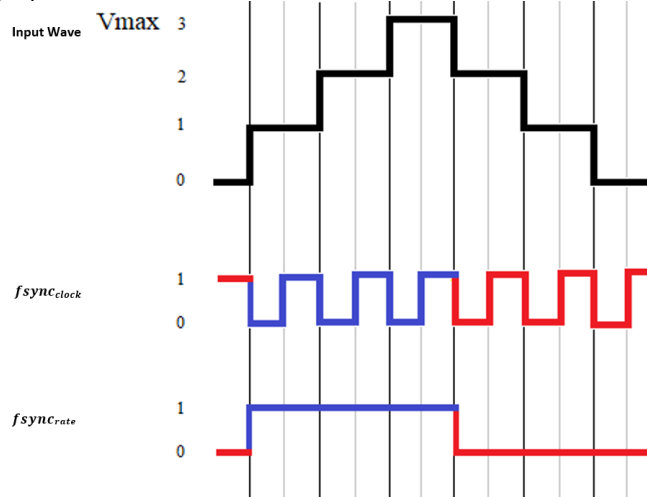


Fig.5.2 Timing diagram of protocol signals assuming the input triangular wave is generated in 3 steps.

Output signal measuring

As pointed above, the ADC is free for exclusive measuring of the output signal. Arduino has an inbuilt method `analogRead()` for the purpose. But this function takes around $110 \mu\text{s}$ for completion, and during this time the microcontroller cycles are wasted (just waiting for the ADC to complete the conversion). Since the ADC is noisy we also need multiple readings to arrive at a stable value, which will further multiply the delay. Instead, we use ADC in continuous mode with the help of interrupts. The output is measured continuously (as soon as a conversion is complete, the next conversion is immediately setup in the ISR for the ADC). The measurement is run in parallel and independently to all protocols of the Response sampler. The continuous ADC measurements are accumulated using a moving average filter, and implemented using a circular queue.

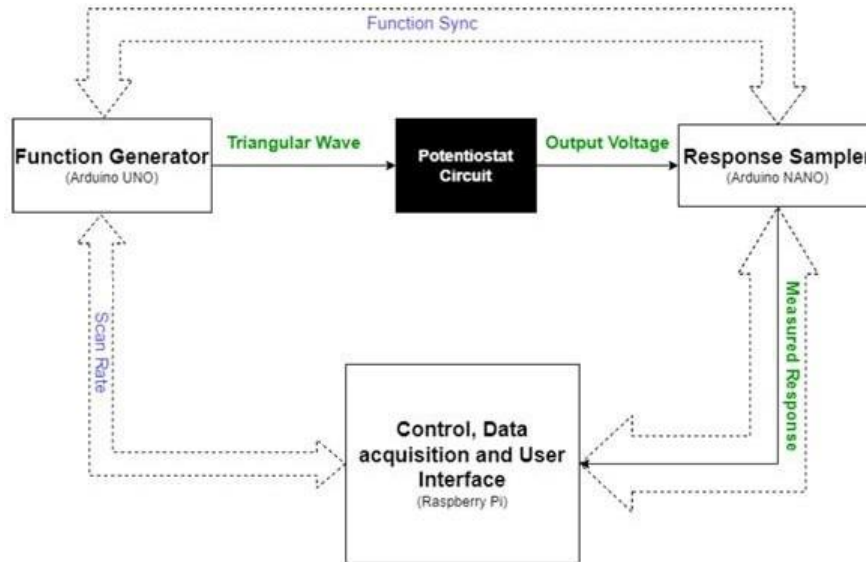


Fig.5.3 Schematic diagram of the system.

5.2.1.4. Control, user interface

This is the protocol used for encoding the current_step, total_steps, measured output_signal etc. as well as sending control information regarding the state of the Response Sampler. This protocol is implemented by the Arduino NANO and the Raspberry pi. This is a one way protocol, from the NANO to the Pi. Data is exchanged over UART and is transmitted in fixed length packets of size 4bytes, with a definite structure. The GUI (graphical user interface) components comprise overall window layout. It allows the user to select desired scan rate within limits. It uses the selected scan rate and handles the connection with the arduino UNO based function generator. Overall connection status is displayed along with the plots the data in three different modes using the functionality.

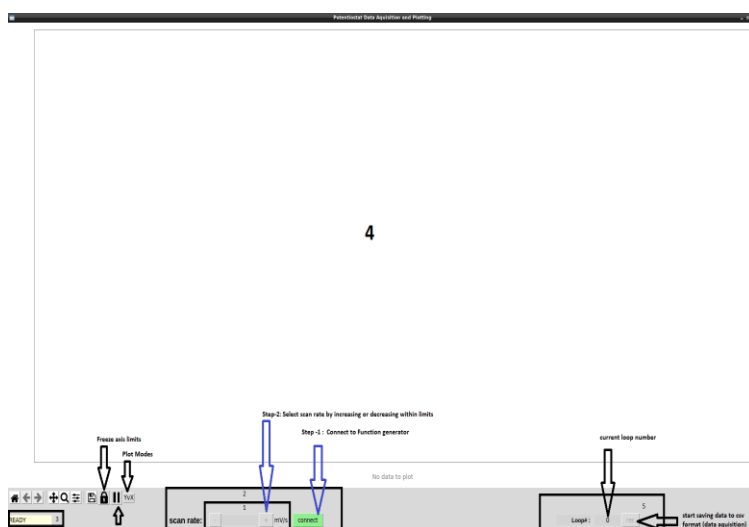


Fig.5.4 Raspberry pi GUI.

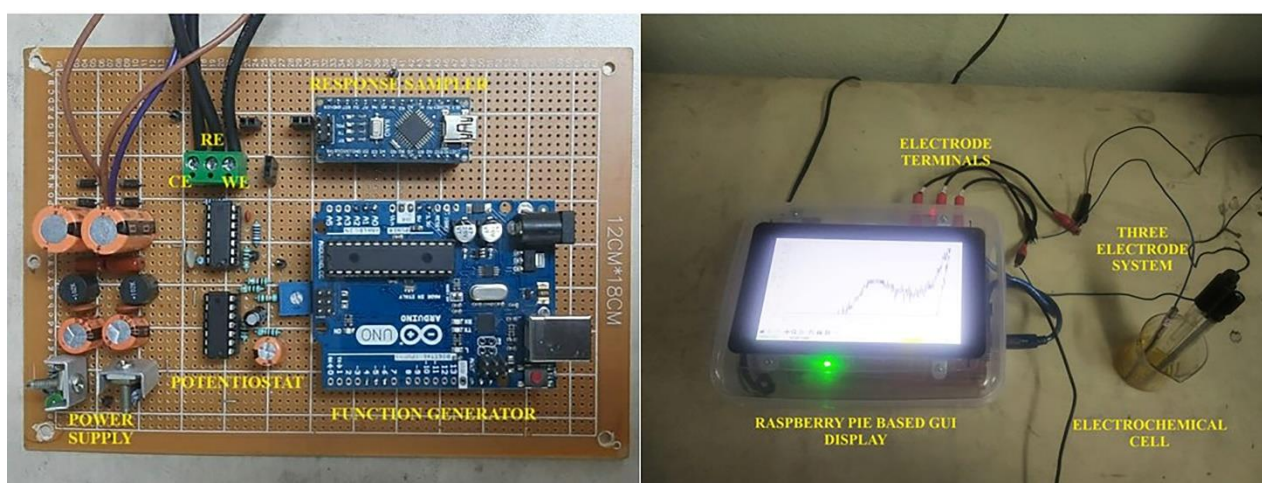


Fig.5.5 The proposed experimental setup.

5.3. Brief description of the device

A low-cost, portable food quality assessment device has been developed based on Raspberry pi which is capable to detect specific target analytes in food and beverage samples. The system setup comprises of a) the specifically developed molecular imprinted (MIP) electrochemical sensors for target analytes as working electrode (WE), Ag/AgCl based RE, Pt based CE and b) the quality assessment instrumentation interface based on a Raspberry pi. The system comprises of a power supply, Arduino UNO-based function generator (1V peak to peak) with a signal conditioning unit, a potentiostat circuit, Arduino Nano-based output response sampler, a data acquisition, and a display through a Raspberry pi user interface.

The system comprises of a 12 V portable power supply developed, an Arduino Uno based function generator for triangular waveform generation for the voltammetry input signal, and a function generator designed to produce a triangular waveform with wide range of variable scan rates 50 to 1250 mV/s. The system also comprises of a graphical user interface (GUI) developed using Raspberry pi with the following components:

- Overall window layout
- Scan rate selection
- Connection status
- Plot data in three modes
- Save data as csv file

5.4. Summary

A low-cost, portable food quality assessment device developed based has been Raspberry pi. The system is capable to detect specific target analytes in food and beverage samples. The system setup comprises of a) the specifically developed molecular imprinted (MIP) electrochemical sensors for target analytes and b) the quality assessment instrumentation interface based on a Raspberry pi. The system comprises of Arduino UNO-based function generator with a signal conditioning unit, a potentiostat circuit, Arduino Nano-based output response sampler, a data acquisition, and a display through a Raspberry pi user interface.

References

- [1] M. D. Dryden and A. R. Wheeler, "Dstat: A versatile, open-source potentiostat for electroanalysis and integration," *PloS one*, vol. 10, pp. 0140349, 2015.
- [2] K. Kellner, T. Posniecek, J. Ettenauer, K. Zuser, and M. Brandl, "A new, low-cost potentiostat for environmental measurements with an easy-to-use pc interface," *Procedia engineering*, vol. 120, pp. 956-960, 2015.
- [3] G. N. Meloni, "Building a microcontroller based potentiostat: A inexpensive and versatile platform for teaching electrochemistry and instrumentation," *Chem.Educ.*, vol.93, pp. 1320-1322, 2016.
- [4] H. Jin, Y. Qin, S. Pan, A. U. Alam, S. Dong, R. Ghosh, and M. J. Deen, "Low-cost wireless potentiometric instrument for ph determination experiments," 2018.
- [5] J. T. Barragan and L. T. Kubota, "Minipotentiostat controlled by smartphone on a micropipette: A versatile, portable, agile and accurate tool for electroanalysis," *Electrochimica Acta*, vol. 341, pp. 136048, 2020.
- [6] R. Ahmad, S. G. Surya, J. B. Sales, H. Mkaouar, S. Y. C. Catunda, D. R. Belfort, Y. Lei, Z. L. Wang, A. Baeumner, O. S. Wolfbeis et al., Kaustat, "A wireless, wearable, open-source potentiostat for electrochemical measurements," *IEEE Sens. J.*, pp.1-4, 2019



Conclusions and future scopes

This chapter shows a general outline of the work done and highlights the finishing up comments with certain suggestions and a few proposals are presented which may be taken up later.

Chapter 6

Conclusions and future scopes

6.1. Introduction

An additive is a chemical substance added to food to produce a specific desired effect. To preserve and enhance the taste of foods, ancient cultures used ingredients such as salt, spices, and sulfites. Food additives became more necessary during the 20th century as the processing of foods increased. The use of food additives is essential to the development of modern products, such as low-calorie snacks, ready-to-eat foods, and snack foods. A food additive can either be nutritional, a processing agent, a preservative, or a sensory additive. There are many additives that fall into more than one category, so this is not a strict classification. Emulsifiers, food coloring, nutritional supplements, and preservatives are some examples of additives. The effects of the chemicals on behavior, growth, mortality, blood chemistry, organs, reproduction, and tumor formation in test animals are observed in these investigations over a period of 90 days to two years. The no-effect level is the lowest concentration of an additive that has no toxicological effects (NOEL). The NOEL is often divided by 100 to get the maximum daily consumption (ADI). The effectiveness of food safety in terms of quality has led to an increase in interest in them. Today, researchers from all around the world are approaching the food quality improvement parameters leading to the development of novel procedures. In order to determine the concentration of food quality parameters, the safety parameters are often assessed in laboratories utilizing pricey equipment like HPLC and GCMS. In parallel, work is being done to create low-cost sensor probes that can evaluate the quality of food products without causing damage. These sensors can be utilized in the fields, but there are currently very few of them on the market. This thesis study was undertaken to create functionalized electrodes for a few food samples with this background in mind. Electrochemical sensors were created as part of this thesis study, and they were used in a variety of tests. The development of the sensor materials was done using the metal oxide and MIP approach. The MIP method makes use of the idea of an engraved polymer-based approach, where

the engraved holes are similar to the target molecule in terms of size and other characteristics. The following reasons make this strategy effective for the agro-industrial industries:

- a) The created electrodes will be very beneficial in replacing the expensive existing equipment. Unlike noble metals or other electrodes, all of the precursors utilized in MIP synthesis are readily accessible and inexpensive.
- b) The electrodes are particularly practical and beneficial for real-time applications because of their easy fabrication method and quick response-recovery capabilities.

In order to evaluate the number of important food additives, such as formalin, metanil yellow, and vanillin in food products, specific sensors have been conceived and constructed as a part of this thesis work.

6.2. Summary of findings

Many studies that concentrated on the distinct electrochemical detection of FAL, MY, and VNL were found in the literature after we conducted our search. The results of this thesis's study are shown in Table 6.1. As compared to the outcomes achieved by earlier authors, the detection limit has raised dramatically in each of the three cases. The metal oxides and MIP strategy, which were used to make all the electrodes, were proven to result in a lower LOD value than certain electrochemical methods. Also, the procedures needed in making the electrodes are time-consuming or expensive in terms of the precursors used. Moreover, some papers do not provide a thorough discussion of the electrodes' selectivity. The MIP electrodes were made stable, biocompatible, and environmentally benign because of the affordable precursors utilized in this research. These electrodes can therefore function as effective, environmentally friendly sensors for the detection of FAL, MY, and VNL in actual samples.

The results of the thesis project are outlined below.

- a) The learning process for the current study's three alternative methods to the quick electrochemical detection of the hazardous food ingredient formalin is covered in Chapter 2. First off, substantial linearity was shown in voltammetry responses carried out in formalin using a noble metal Pt electrode. With the use of PCA, effective data clustering was accomplished, yielding a high separability index. Additionally, the PLSR and the PCR regression models offered highly

accurate predictions. Noble metal electrodes produced good analytical findings despite their high cost and lack of molecular selectivity. So, to improve electrode effectiveness, the carbon paste's metal oxide modification was used in the study that followed. CeO₂ nanocomposites over graphite were thought to be able to detect formalin with superior electroanalytical features due to their extraordinary qualities. Moreover, with time, the CeO₂@GP electrode exhibited relatively positive electroanalytical properties. The electrode performed exceptionally well when tested against mushroom compounds. The limitations of the prior study were a constrained linear range of operation, a constrained detection limit, and a constrained capacity to identify certain template molecules. As a result, low-cost polymers containing recognition cavities served as a remedy for selective electrocatalytic activities. So, to improve electrode effectiveness, the carbon paste's metal oxide modification was used in the study that followed. CeO₂ nanocomposites over graphite were thought to be able to detect formalin with superior electroanalytical features due to their extraordinary qualities. Moreover, with time, the CeO₂@GP electrode exhibited relatively positive electroanalytical properties. The electrode performed exceptionally well when tested against mushroom compounds. The limitations of the prior study were a constrained linear range of operation, a constrained detection limit, and a constrained capacity to identify certain template molecules. As a result, low-cost polymers containing recognition cavities served as a remedy for selective electrocatalytic activities. As a potential remedy, a molecularly imprinted acrylonitrile polymer (MIP) based electrochemical sensor was investigated. As compared to earlier investigations, this MiPAN@GP electrode performed significantly better in terms of linear range and LOD thanks to its reasonable selectivity and steady behavior. In comparison to HPLC technology, the electrode also demonstrated very accurate actual sample analysis in extracts of fish and mushrooms.

b) The two separate methods employed in the current study's investigation of the quick electrochemical detection of the food additive metanil yellow are presented in Chapter 3. In order to improve electrode efficacy, we first examined the voltammetry responses in metanil yellow while changing the carbon paste with metal oxides. Due to their outstanding qualities, NiCo₂O₄ nanocomposites over graphite are regarded as having good electroanalytical features. Also, with time, the NiCo₂O₄@GP electrode showed average electroanalytical characteristics. Moreover, the electrode was effective against turmeric powder. The linear range of operation, the detection limit,

and the capacity to identify certain template molecules were constrained by earlier studies. Hence, cheap polymers containing recognition holes were discovered to provide a solution to selective electrocatalytic activity. As a potential remedy, electrochemical sensors based on molecule-imprinted methacrylic acid polymer (MIP) were studied. This MIP electrode showed good selectivity and consistent behaviour in comparison to the earlier studies, greatly enhancing linear range and LOD. The electrode also displayed extremely accurate measurements of turmeric powder and pigeon pea extracts when compared to HPLC method.

c) A MIP-based sensor for vanillin estimation in deserts is shown in Chapter 4. For the production of a particular vanillin sensor in this instance, a monomer, EGDMA as a crosslinker, and benzoyl peroxide as an initiator were all utilized. The MIP material has been examined using ultraviolet-visible (UV-Vis) spectroscopy both before and after the template molecule has been eliminated. This chapter has offered a comparison analysis with other research reports on vanillin determination.

Table 6.1. Major findings of the thesis

Sl. No.	Target compound	Electrode	Precursors	Performance parameters of the proposed sensors		Ref
				Linear range (μM)	LOD	
1	Formalin	Pt	Platinum	100 to 1000 μM	5 μM	[1]
		CeO ₂ @GP	Cerium oxide Nanoparticles	25 – 120 – 1000 μM	1 μM	[2]
		MiPAN@GP	Monomer: Acrylonitrile Crosslinker: EGDMA	10-100-1000 μM	0.63 μM	[3]
2	Metanil yellow	NiCo ₂ O ₄ @GP	Nickel cobalt oxide nanoparticles	5 – 1000 μM	100nM	[4]
		MIP	Monomer: Methacrylic acid Crosslinker: EGDMA	0.001 to 1000 μM	0.67nM	[5]
3	Vanillin	MIPAM/GP	Monomer: Crosslinker: EGDMA	0.1-50-1000 μM	0.00143nM	[6]

6.3. Recommendations

The following technologies are suggested for use in agro-industries based on the findings of the produced electrodes listed above:

- a) These electrodes can be used by those in the agro industries, overcoming the limitations of traditional methods in terms of cost and exportability.
- b) Formalin, metanil yellow, and vanillin quantities present in actual samples may also be measured in-situ using these electrodes.
- c) The developed sensors may be used profitably in the business and health sectors due to the numerous influences of the test compounds taken into consideration here, and there are a huge number of opportunities for value addition to products.

6.4. Future scopes of research

Here are some more enhancements to the suggested sensing approaches for expanding the study in the same field. Here is a list of them:

- a) The discussion that came before led to the conclusion that the sensors needed to be made more economically viable for easier deployment in the industrial and agricultural sectors. It may be done with screen-printed electrodes or disposable paper electrodes. The use of disposable electrodes can improve the sensors' accuracy. This will make it unnecessary to repeatedly wash the sensor surface, ensuring the sensors' great repeatability.
- b) Advanced methods like deep learning and convolution neural networks may be employed for higher accuracy when designing the prediction model to quantify the relevant food additives.
- c) Only FAL, MY, and VNL-specific sensors have been created for this project. In a similar manner, other substantial food additives that contribute to the greatest health impacts can be created.

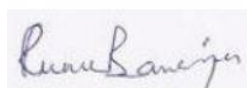
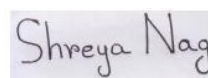
- d) As discussed in Chapter 5, an approach towards the development of a portable, low-cost tool for evaluating the quality of food has been taken as future research scope. The device has the ability to identify particular target analytes in samples of food and drink. The molecular imprinted (MIP) electrochemical sensors for the target analytes and the quality evaluation instrumentation interface based on a Raspberry Pi make up the system setup. The system consists of an Arduino Nano-based output response sampler, an Arduino Nano-based function generator with a signal conditioning unit, a potentiostat circuit, a data acquisition, and a display through a Raspberry pi user interface. Such a portable potentiostat-based E-tongue based on smart phone application can help to fulfil commercial demands based on the suggested investigations and potential improvements that were addressed before. An array-based customized electrode module with an integrated potentiostat may be shown to get a reliable prototype. The user is then able to obtain an overall fingerprint of any food product being researched. Using appropriate modelling approaches, the customized E-tongue will process the total data acquired from the particular electrodes and produce values for the food products.

6.5. Conclusion

This thesis introduces the electrochemical sensor technology for the quantitative assessment of several food additives (FAL, MY, and VNL) in food products. Despite the fact that the study described here is still in its early stages, there is no dispute that it has added a new dimension to the approach for evaluating various food samples. The sensor electrodes are lightweight, inexpensive, and small enough to be utilised out in the fields. Consequently, it would be feasible to utilise these tools widely, which would benefit both the producers who would be able to maintain the food quality as well as the final consumers who would be able to assess the product's quality before to purchase. Overall, the manufacturing process for the sensors described in this thesis shows effectiveness with three different food additives, has promise for usage with molecules of a similar kind, and is anticipated to usher in a new approach to quality control for food products.

References

- [1] S. Nag, H. Naskar, S. Pradhan, R. Chatterjee, V. Sharma, B. Tudu and R. B. Roy, “Formalin Detection using Platinum Electrode-Based Electrochemical System”, *Journal of The Institution of Engineers (India): Series B*, vol. 103, pp. 1159-1165, 2022.
- [2] S. Nag, S. Pradhan, H. Naskar, R. B. Roy, B. Tudu, P. Pramanik, and R. Bandyopadhyay, “A simple nano cerium oxide modified graphite electrode for electrochemical detection of formaldehyde in mushroom,” *IEEE Sens. J.*, vol. 21, pp. 12019 – 12026, 2021.
- [3] S. Nag, S. Pradhan, D. Das, B. Tudu, R. Bandyopadhyay, and R. B. Roy, “Fabrication of A Molecular Imprinted Polyacrylonitrile Engraved Graphite Electrode for Detection of Formalin in Food Extracts,” *IEEE Sens. J.*, vol. 22, pp. 42–49, 2022.
- [4] S. Nag, D. Das, H. Naskar, B. Tudu, R. Bandyopadhyay, and R. B. Roy, “Detection of Metanil Yellow Adulteration in Turmeric Powder Using Nano Nickel Cobalt Oxide Modified Graphite Electrode,” *IEEE Sens. J.*, vol.22, pp. 12515-12521, 2022.
- [5] S. Nag, D. Das, H. Naskar, B. Tudu, R. Bandyopadhyay, and R. B. Roy, “A Novel Molecular Imprinted Polymethacrylic Acid Decorated Graphite Electrochemical Sensor for Analyzing Metanil Yellow Adulteration in Food,” *IEEE Sens. J.*, vol.23, pp. 20951-20958, 2023..
- [6] S. Nag, D. Das, and R. B. Roy,” Voltammetry application of molecularly imprinted polyacrylamide as vanillin receptor in desserts,” *IEEE Sens. J.*, vol.23, pp. 3446-3452, 2023.



Professor
Dept. of Instrumentation & Electronics Engg
Jadavpur University
Saltlake, 2nd Campus
Kolkata-700 108

